UNIVERSITEIT VAN PRETORIA
UNIVERSITY OF PRETORIA
YUNIBESITHI YA PRETORIA

The effect of filler metal on the corrosion resistance of stainless steel weldments in a hot organic acid environment

Charles Petrus Marais Orsmond

Submitted in partial fulfilment of the requirements for the degree

Masters of Engineering

(Metallurgical Engineering)

In the Faculty of Engineering, Building and Information technology,

University of Pretoria,

PRETORIA

29 October 2009

ACKNOWLEDGEMENTS

I would like to thank our Heavenly Father for giving me the opportunity and ability to perform this study.

I express my sincere gratitude to Prof. Chris Pistorius for his support and guidance during this study.

I which to thank MegChem Engineering and Drafting Services and SASOL Synfuels for sponsorship for this study.

SYNOPSIS

Selective corrosion of type 316L austenitic stainless steel welds during the production of organic acids resulted in losses in production due to unscheduled downtimes to perform repairs. Estimated corrosion rates of type 316L filler material welds were an order of magnitude higher than that of the base material. Alternative higher alloyed commercial filler materials were evaluated under actual production conditions. The evaluated filler materials were types 316L, 317L, 309L, 309MoL, 2205, 2507, 625, 825 and 904L. The effect of nitrogen on the corrosion properties of type 309L filler material was evaluated by manipulating the nitrogen concentration of the shielding gas during MIG welding. These changes in nitrogen concentration did not influence the corrosion resistance of the type 309L filler material.

No correlation could be established between the corrosion rates, analysed chemical composition of the product and operating temperature during production. In almost all the cases where the chemical composition of the filler material was comparable with that of the base material the corrosion rates of the filler materials were higher than that base material.

It might be expected that the ferrite phase with higher molybdenum and chromium should be more corrosion resistant while the austenite should be less resistant. This was, however, not the case with the corrosion of type 309L filler material. It would thus appear that in this case nickel enrichment of the austenite phase had a larger influence on the corrosion resistance of the austenite phase than the chromium and molybdenum had on the corrosion resistance of the ferrite phase. It appears that nickel and molybdenum had the largest contribution to the corrosion resistance of stainless steels welds under these operating conditions. It is, however, believed that a certain minimum concentration of chromium is also required to provide corrosion resistance to these alloys in hot organic acid environments.

In contrast with the fact that a substantial alloying content is required to improve corrosion resistance of the filler material, the small difference in composition between ferrite and austenite phases, due to micro segregation, appeared to affect the corrosion resistance on micro scale. This is illustrated by the micrographs, which show corrosion to etch out the dendrite structure. Since the morphology of the austenite and ferrite phases is so similar, it could not always be conclusively established which one of the two phases corroded selectively.

Analyses performed on the austenite and ferrite phases did not indicate a concentration difference within the phases itself. However, there were significant differences in the concentration of elements between the phases, with the austenite stabilising elements reporting to the austenite phase and the ferrite stabilizing elements reporting to the ferrite phase, in line with thermodynamic predictions.

In the case of the filler materials following the austenite mode of solidification, no significant concentration differences were detected within the matrix. Although all highly alloyed high nickel alloyed filler materials (types 904L, 825 and 625) corroded at a lower rate than the type 316L base material, type 625 filler material was the filler material of choice due to the lack of any pitting of the weld. Pitting was detected in both the 825 and 904L filler materials. Galvanic corrosion was not noted at any of the weld/HAZ interfaces and in no case did the type 316L parent metal adjacent to the weld corrode preferentially to the material further away from the weld.

Keywords:

Weld solidification, dendrites, segregation, weld corrosion, hot organic acid, formic acid, acetic acid, stainless steel, alloying.

The effect of filler metal on the corrosion resistance of stainless steel weldments in a hot organic acid environment

Table of contents

1. Background.

1.1. Practical background:

In the production unit where the tests were performed mixed organic acids are removed from reaction water by a reaction of the water with a solvent. The complex formed between organic acid and solvent enables effective density separation between the acids and water. The solvent-organic acid complex is then heat stripped in a subsequent column (column A). This mixed acid mixture contains acetic acid (CH_3COOH), propionic acid (CH_3CH_2COOH) and butyric acid ($CH_3CH_2CH_2COOH$) and possibly small quantities of formic acid (HCOOH). These acids are separated from one another in distillation columns by making use of their relative boiling point. In the first distillation column, column B, the heavier acids (C4 and C4+, that is, containing four or more carbon atoms in the compound) are separated from the lighter (C3 and C3-) acids. The lighter acid mix is transported to column C where the propionic acid (CH_3CH_2COOH) is distilled out of the C3 and C3- acid mixture. The lighter product (C2 and C2-) is then again pumped to column D where the final distillation is performed to produce high grade acetic acid (C2 acid).

Type 316L austenitic stainless steel is regarded as a suitable alloy for the construction of equipment for the production of acetic and propionic acid. [1, 2] Published corrosion rates for type 316L material in acetic acid distillation environments range between <0.0025 mm/y and >1.25 mm/y under conditions ranging between 10% acetic acid to concentrated acetic acid at temperatures ranging between 20°C to 212°C.[1] Table 1 lists typical measured corrosion rates of austenitic NiCrMo stainless steels similar to type 316 and 317 stainless steels exposed to various formic-, acetic- and propionic acid environments at various temperatures[1]. Experience under plant conditions indicated that corrosion in organic acid media is expected to be predominately of an intergranular nature. It is also further expected that the corrosiveness of the acid is highly dependent on the number of carbon atoms in the compound and that corrosiveness of these acids decreases as the chain length increases.[3] Of all the organic acids, formic acid is hence expected to be the most corrosive.[5] It is

further also expected that the corrosiveness of the organic acid will increase with temperature with the acids being the most corrosive near/at the relative boiling point of organic acid. Impurities like chloride are known to increase the corrosion rate significantly.[1, 2, 21] It was also reported that contamination by elements such as Cl^- ions can have a significant influence on the passivation behaviour of type 316L austenitic stainless steel.[4] The concentration of the organic acid may have a significant influence on the effect of such contaminants: steels in a medium containing 70 % of acetic acid experienced a step change in the corrosion potential with Cl^- additions, but this change in the corrosion potential was not seen in solutions containing 90% acetic acid.[4]

It has been reported that laboratory tests can be misleading.[5] Testing can yield variable results depending on the behaviour of the test medium and interaction of this medium with the environment, whether being depleted or contaminated with air (oxygen). The mode of corrosion in organic acids may vary from highly localised intergranular corrosion to severe general corrosion, pitting and crevice corrosion. Organic acids are reducing acids, but contamination by air (oxygen), ferric and cupric irons might shift the redox potential to such a degree that the acid might become oxidising and the presence of small amounts of these elements might also improve passivation and overall corrosion resistance.[21] It was also reported that warm organic acids can cause intergranular corrosion in the highly stressed heat affected zones [HAZ] of stainless steel weldments.[1]

Table 1: Corrosion behaviour of type 316L stainless steel exposed to acetic environments at various concentrations and temperatures. [1]

Material description	Acetic acid %	Temp °C	Corrosion rate mm/y	Special conditions
AISI 316 19Cr, 12Ni, 3Mo, 0.06C	24	35	<0.0025	Storage test – 115 days
	98	35	<0.0025	Storage test – 157 days
	99	Boiling	0.015	Operational tests – 11,12,21 days
CrNiMo 18 8	10 – conc.	20	<0.1	
		Boiling	<0.1	
	Conc.	200	<1.0	0.10 MPa
CrNiMo 18 10	50	102	<0.025	Without heat transfer (heat exchanger)
	50	110	<0.025	With heat transfer (heat exchanger)
	50	125	<0.025	
	50	140	<0.025	
	99.6	118	<0.025	Without heat transfer (heat exchanger)
	99.6	110	<0.025	With heat transfer (heat exchanger)
	99.6	125	0.33	
	99.6	140	0.25	

Table 1: Continued…

Material description	Acetic acid %	Temp °C	Corrosion rate mm/y	Special conditions
AISI 316 317	10 – 50	100	<0.05	Air free
	60-100	100	<0.5	Air free, intergranular corrosion
	100	212	>1.25	Air free, stress corrosion cracking
	10-100	25	<0.05	Aerated, no HCl, H2SO4, NaCl
	10-40	100	<0.05	
	30	125	<0.5	
	50-100	75	<0.5	
	50	100	<0.5	
	60-100	100	0.5-1.25	
	30	212	>1.25	
	40	212	>1.25	
	30	100	<0.5	Acetic acid vapour, intergranular corrosion
	100	100	<0.5	
	99	120	0.075	Acetic acid vapours operational test, 82 days
	30	50	<0.05	90% acetic acid with acetaldehyde + 7% water
	0	100	<0.05	
	90	100	0.5-1.25	
	100	100	0.03	90% acetic acid with 7% acetaldehyde + 2% water + 1% formic acid
AISI 316	10	100	<0.05	Acetic acid + formic acid
	60	100	0.5-1.25	
	100	79	<0.5	
	100	100	0.5-1.25	
	56	100	0.0025	Condensate of 6 parts 56% acetic acid and 1 part 90% formic acid
	56	104.6	0.0025	
	100	100	<0.5	95% acetic acid + 5% propionic acid, stress corrosion cracking

Table 1: Continued…

Material description	Acetic acid %	Temp °C	Corrosion rate mm/y	Special conditions
AISI 316 (18Cr,10Ni, 2Mo, 0.07C)	25	104	0.025	25% Acetic acid + 1.5% formic acid operational test 129 days
	25	104	0.0825	25% Acetic acid + 4% formic acid operational test 129 days
	30-50	104	0.5	30-50% Acetic acid + 2-10% formic acid operational test 129 days
AISI 316 (18Cr,13Ni, 2Mo, 0.07C)	50	118	0.018	50% acetic acid + 2% formic acid
	25	110	0.08	25% acetic acid + 4% formic acid
	30	135	0.11	30% acetic acid + 8% formic acid

Typical process conditions are indicated in the experimental procedure in chapter 2.1.5. For the construction of the production plant only type 316L austenitic stainless steel material was used. Experience with current production system indicates that the corrosion rate of un-welded plate varies between 0.06 mm/y and 0.8mm/y depending on the temperature and concentration during the distillation process. Measured corrosion rates of the original type 316L material, as determined with ultrasonic wall thickness measurements are indicated in table 4.

Table 2: Actual measured corrosion rate [mm/y] as determined with ultrasonic wall thickness measurements, at different positions in the plant; see table 4 for solution compositions and temperatures.

Measured corrosion rate [mm/y]				
A	**B**	**C**	**D**	**E**
0.29 – 0.42	0.14 - 0.19	0.10 - 0.17	0.21 - 0.29	0.09 - 0.17
F	**G**	**H**	**I**	**J**
0.06 - 0.12	0.11 - 0.21	0.1-0.4	0.2-0.8	0.2-0.3

This was not the case for welds. Figure 1 shows a Scanning Electron Microscope (SEM) photograph of type 316L weld exposed to the organic acid environment for a period of approximately 5 years at temperatures exceeding 125 °C. The estimated corrosion rates of the filler material were an order of magnitude higher than that of the base material. Some weld repairs were performed, but, eventually material loss during the distillation of acetic and propionic acid necessitated the replacement of two of the columns in the production plant.

Figure 2 shows a comparative photograph of the type 316L base material exposed to the same conditions as that of the filler material. Note the difference in corrosion characteristics between the filler and base material. The fundamental causes why weld materials corrode at a different rate than the base material is not fully understood, but in carbon steel, it is believed that the complexity of the microstructure and the redistribution of sulphur and sulphur species has a influence on this.[6] Work performed by Otero[7] indicated that cavities produced during the production of type 304L and type 316L via powder metallurgy techniques might generate minute crevices enhancing the corrosion of these materials during the exposure to organic acids. It is also believed by this researcher that the interdendritic nature of weld filler materials may also act in a similar way and that this can contribute to the differences in corrosion rates

observed between the weld metal and the base metal of material exposed to organic acid environments.

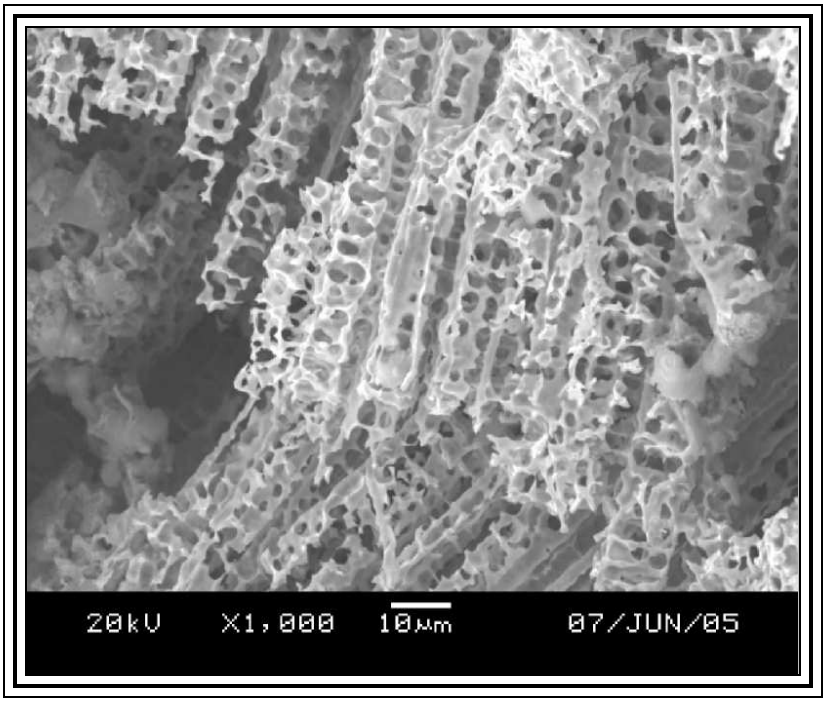

Figure 1: An SEM micrograph indicating the corrosion on the type 316L filler material at the end of the service life of the equipment.

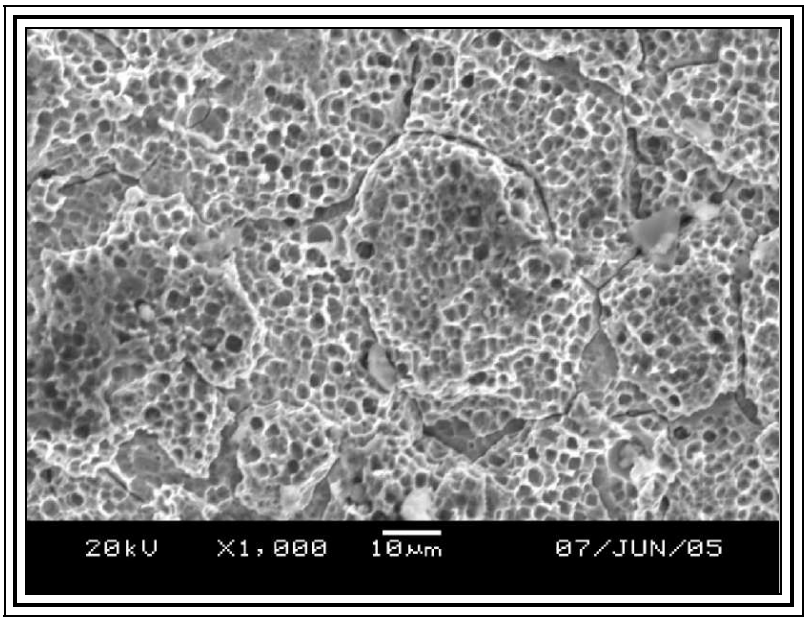

Figure 2: A comparative SEM photograph indicating the corrosion of the type 316L base material exposed under the same conditions as figure 1.

Plant experience has shown that corrosion of welds was mostly interdendritic, as indicated above in Figure 1. Prolonged exposure of the welds resulted in preferential corrosion of the weld to such an extent that welds separated at the fusion line. Observation of welds during periodic inspections suggest that the corrosion rate increases after some initial attack: Welds which were inspected in one year appeared to be intact (though with a heavily etched surface), but were nearly completed corroded away at the next inspection. This may be related to corrosion attack along dendrites. Upon initial solidification of the weld metal, dendrite growth is largely perpendicular to the fusion line. As the weld pool moves away, the solidification direction further from the fusion line tends to follow the direction of welding, so that the cap solidifies with dendrite growth almost parallel to the welded plane. This change in dendrite direction may contribute to more rapid attack as corrosion proceeds along to the dendrites.

1.2. Structure of stainless steel welds and the influence of partition of elements.

The major alloying elements in stainless steels are chromium and nickel. It is thus of great importance to understand the effect that these alloying elements have on the phase balance and solidification nature of the welds; these are briefly reviewed below.

1.2.1. Influence of chromium (Cr).

A generally accepted definition of a stainless steel is steel containing more than 12% Cr. Looking at the Fe-Cr phase diagram as published by Folkhard [8] (Figure 3, based on work performed by Kubaschewski [9]), it can be seen that the austenite phase (γ) is only stable up to 12 % Cr. This indicates that at Cr concentrations of more than 12% the austenite (γ) to ferrite (α) phase transformation is absent. It is known that primary ferrite precipitating from the melt is coarse. Thus, a common problem in ferritic stainless steels is unwanted mechanical properties of heat affected zone (HAZ) properties due to the lack of phase transformation during welding.[10] Chromium promotes ferrite formation.[8] At higher chromium

concentrations it can also contribute to the formation of an intermetalic sigma (σ) phase containing 45% Cr and 55% Fe. This intermetalic phase is known to be very brittle below 600°C and can result in brittle failure of materials at room temperature.[8] There are also reports that this might have negative effects on the corrosion properties due to the depletion of Cr in the vicinity of the σ phase.[8]

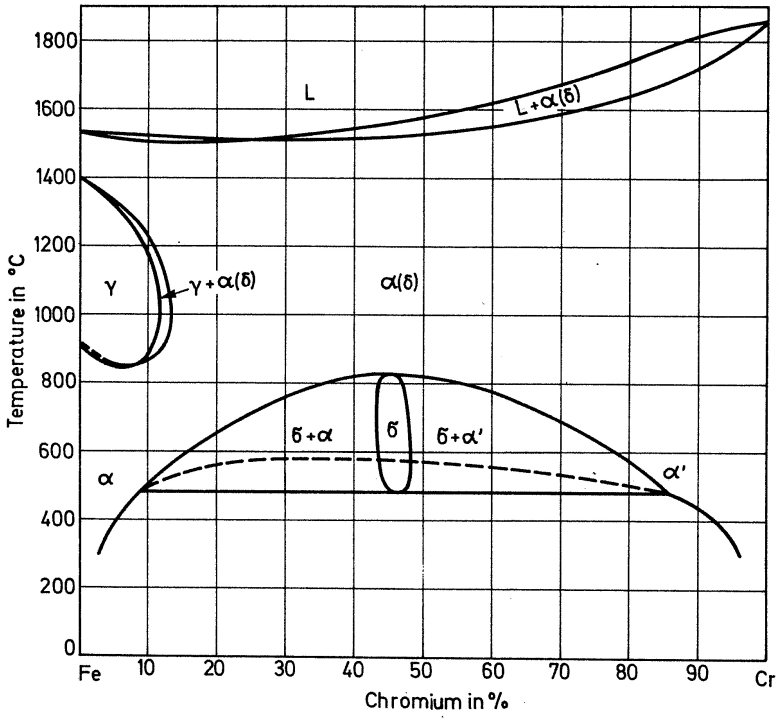

Figure 3: Iron Chromium diagram as published by Folkhard.[8]

1.2.2. Influence of nickel (Ni).

Looking at the iron-nickel phase diagram as published by Folkhard [8] (Figure 4, based on work performed by Kubaschewski [9]), it can be concluded that nickel (Ni) has the opposite effect to chromium (Cr) on phase stability: Ni stabilises the austenite (γ) phase. It can be also be seen that the ferrite region is suppressed, resulting in the lack of formation of primary and secondary ferrite at Ni concentrations higher than 5%. There is only a small region on this phase diagram where ferrite solidifies directly from the melt at temperatures between 1400°C and

1450°C. This diagram also indicates that the transformation from primary ferrite (δ) to austenite (γ) is a peritectic phase transformation.

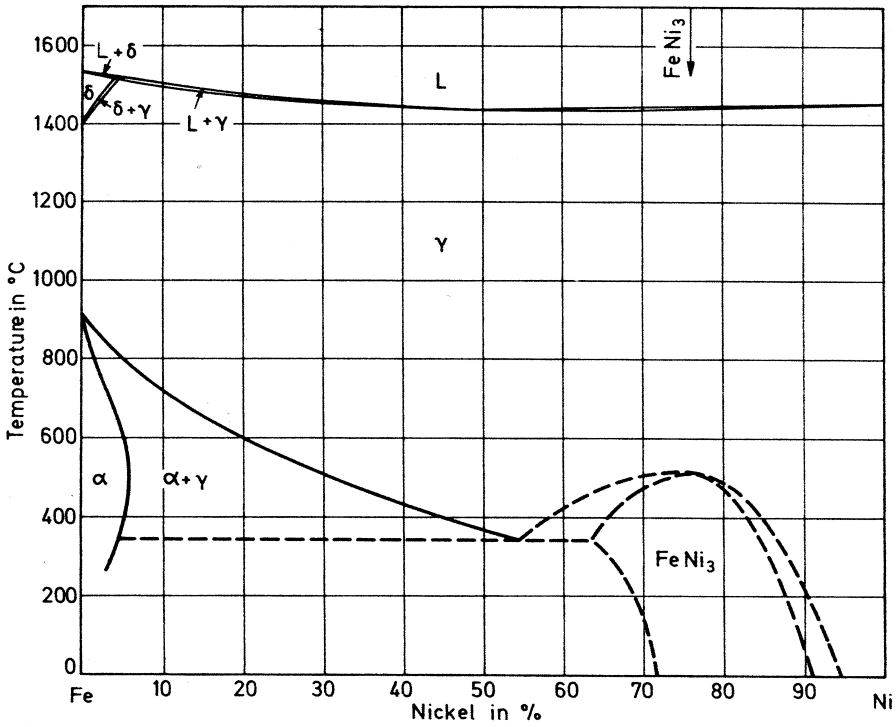

Figure 4: Iron nickel phase diagram as published by Folkhard. [8]

In the chromium-nickel phase diagram as published by Folkhard [8] (Figure 5) it is indicated that alloys with approximately equal amounts of Cr and Ni solidify eutectically.

These binary phase diagrams do provide some insight into the solidification and high temperature phase relationships in ternary alloy iron-chromium-nickel alloys. It is more difficult to depict the solidification of ternary melts; see Figure 6.[8] Due to this difficulty numerous authors [8,17,19,24] have made use of pseudo binary phase diagrams. Figure 7 presents the pseudo binary diagrams for the iron-chromium-nickel system at 60% and 70% iron.[8] Due to the additional alloying element, which generally imparts an additional degree of freedom to this system, invariant eutectic solidification as observed in the Cr-Ni binary ($L \rightarrow \alpha + \gamma$) changes to the coexistence of the three phases ($L + \alpha + \gamma$) over a temperature and composition range.

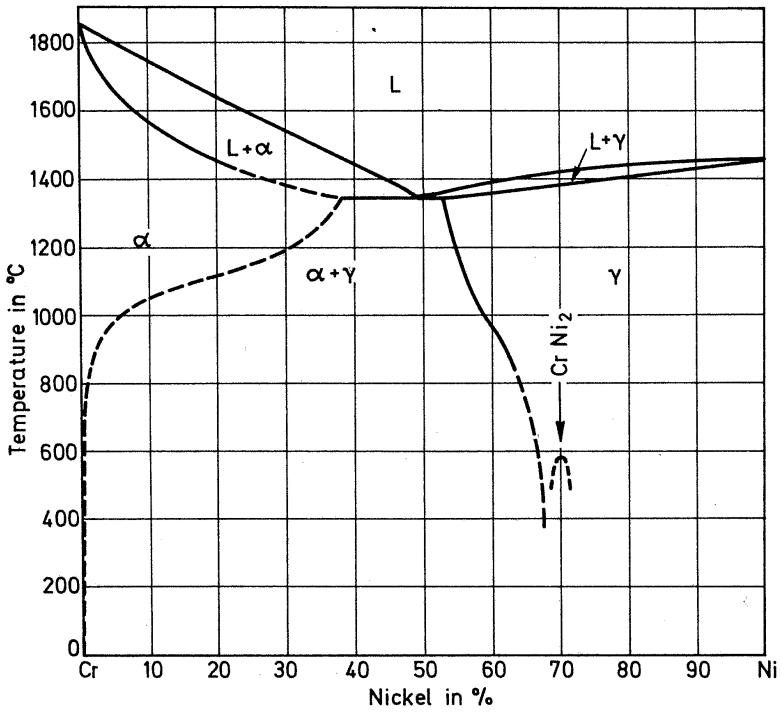

Figure 5: Chromium-nickel phase diagram as published by Folkhard.[8]

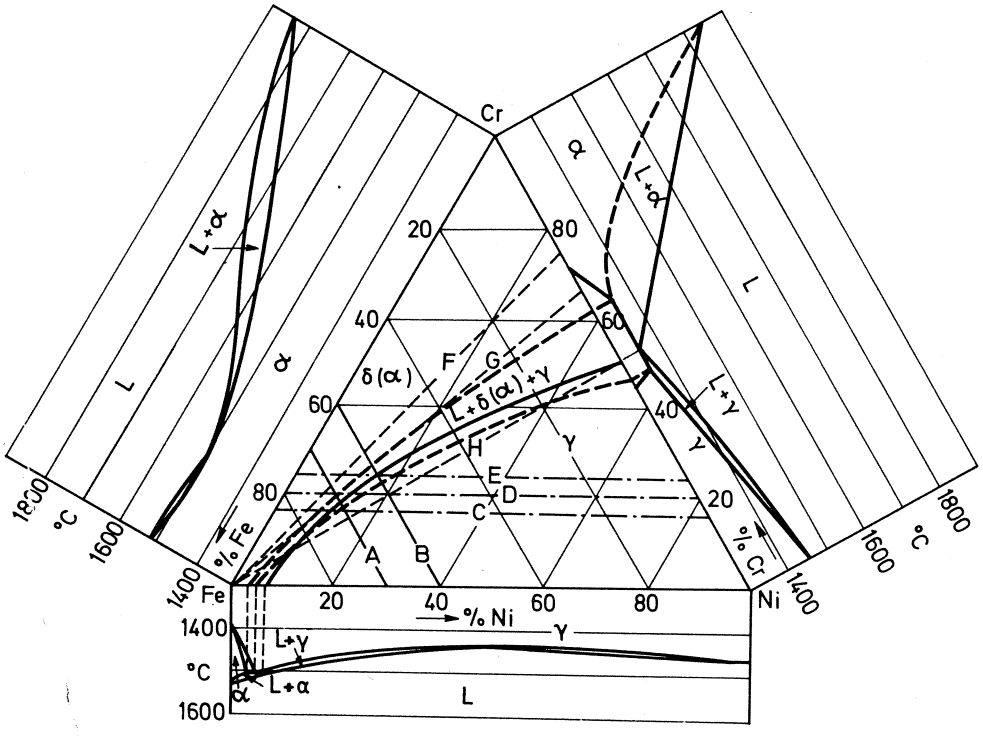

Figure 6: Iron-chromium-nickel phase diagram.[8]

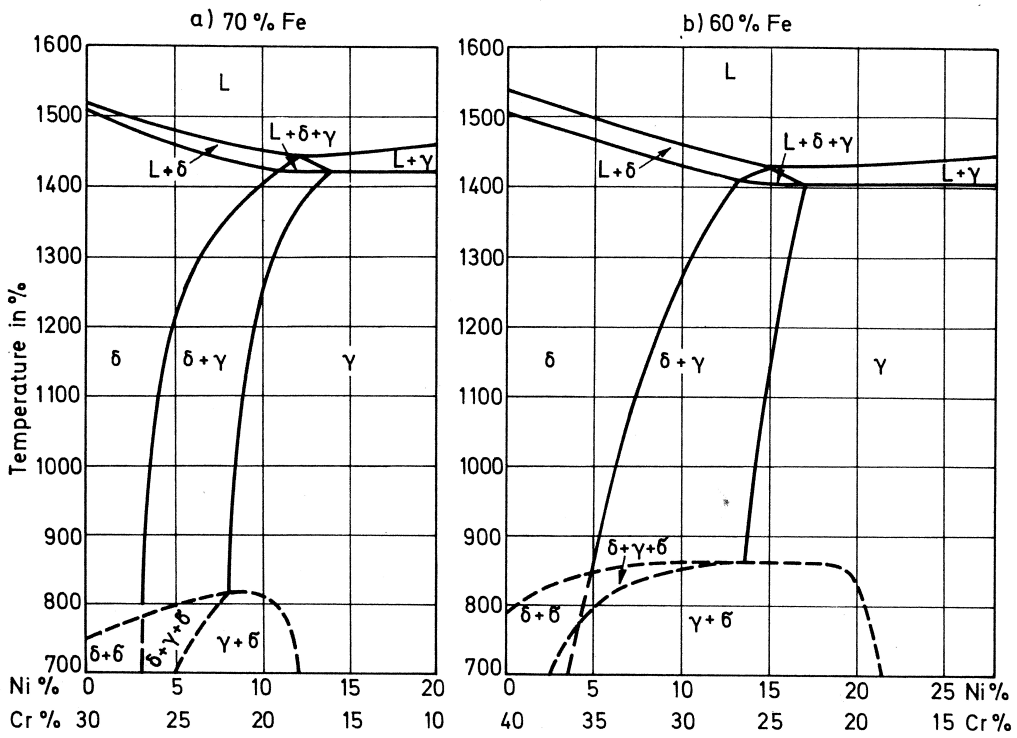

Figure 7: Pseudo-binary sections through the Fe-Cr-Ni system at 70% and 60% Fe.[8]

1.2.3. Influence of other alloying elements.

Another alloying element that is used in certain stainless steels for its positive influence on the corrosion behaviour is molybdenum (Mo).[8] Depending on the type of alloy the Mo concentration may differ, but in the case of type 316 it is 2-3%. Similar to Cr, Mo has a stabilising effect on the ferrite phase. Carbon (C) is another alloying element that is always present in steel alloys. The concentration of this alloying element is carefully controlled due to its influence on carbide precipitation. Figure 8 indicates the influence of both Mo and C on the phase stability of austenite. From this diagram it can be seen that these elements have opposite influences on the stability of austenite. With increasing C concentration, the austenite phase region is increased but with increasing Mo concentration the stability of the austenite phase region is decreased.

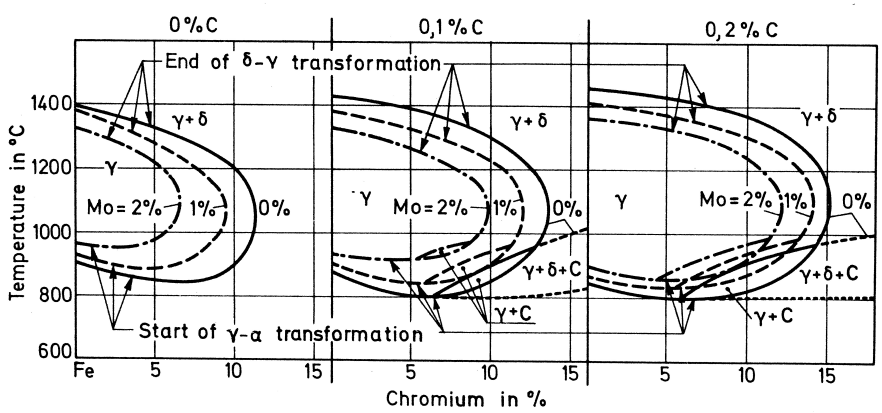

Figure 8: Influence of Mo and C on the stability of the austenite. [8]

In the recent past, much research has gone into the effect of nitrogen on the phase stability and corrosion properties of various stainless alloys.[8, 19] In contrast with its effect in low alloy steels, N can be a beneficial alloying element in stainless steel.[8] Cr and Mo are known to improve the N solubility in stainless steels. Worked performed by Kohl,[11] as referenced by Folkhard,[8] indicates that N solubility increases from 0.2% N in a 17% Cr-Ni alloy to 0.5% N in a 25% Cr-Ni alloy ingots. Nitrogen is a strong austenite stabiliser as indicated in Figure 9.

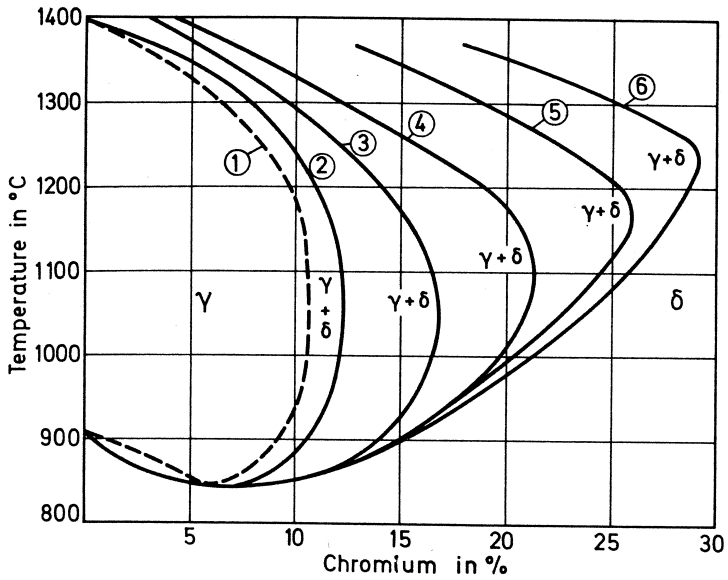

Figure 9: Influence of the addition of nitrogen on the austenite phase stability.[8]

Nitrogen is known to improve the pitting corrosion resistance of materials. Previous authors [22,12,13] have indicated that increasing the nitrogen content may also be beneficial for the general corrosion resistance of the material. Work done by Schmidt-Rieder et al [22] indicated that there is an increase in the nitrogen content up to 5 atom %, 0 to 60 monolayers underneath the passive surface of a duplex stainless steel. Schmidt-Rieder et al.[22] also indicated that the nitrogen increase was limited to the nobler austenite phase of the duplex material. Schmidt-Rieder et al.[22] concluded that nitrogen contributed to the enhanced corrosion resistance of the austenite phase of this duplex material.

Work done by Du Toit and Pistorius[12] and Gruszczyk[13] indicated that the nitrogen content of the weld filler material can be manipulated by variating the nitrogen concentration in the shielding gas. Using this as a basis, corrosion coupons were prepared, welding type 309L filler material on a type 316L base material and varying the nitrogen composition of the shielding gas. This variation of the shielding gas was sufficient to produce welds with varying amounts of nitrogen in the deposited filler material.

The arc takes up nitrogen during the welding process. Factors that influence the amount of nitrogen taken up include the following:

- The arc length during welding.
- The alloying composition of the filler material.
- The concentration of nitrogen in the shielding gas.

One of the elements that have a major influence on the amount of nitrogen solubility in the weld pool is chromium. The higher the chromium content in the filler material, the higher the solubility of nitrogen in the weld. According to Folkhard[8], the solubility limit of nitrogen during solidification increases linearly from 0.20% N in austenite with a chrome

content of 18% to 0.50% for austenite with a chrome content of 26%. Above these nitrogen concentrations, porosity is normally visible. This corresponded with the porosity seen in the 0.24% nitrogen sample.

Nickel has a negative influence on the nitrogen solubility, but the effect of that is not as noticeable as seen with chromium. Nitrogen is a strong austenite stabiliser that also has a negative influence on the precipitation rate of precipitates in which nitrogen is not soluble. Among these precipitates are $M_{23}C_6$, Chi and Laves phases. On the other hand, M_6C is a precipitate that does dissolve nitrogen in its matrix and formation of this precipitate is promoted by the presence of nitrogen.

It can be concluded that certain elements have similar effects on the stability of ferrite and austenite. This effect was thoroughly researched and documented by Schaeffler and Delong, and used to draw up diagrams which predict the structure after solidification.[14] Development and use of duplex stainless steels indicated inaccurate delta ferrite predictions from these diagrams, and resulted in the development of the WRC-92 diagram as shown in Figure 10.[15]

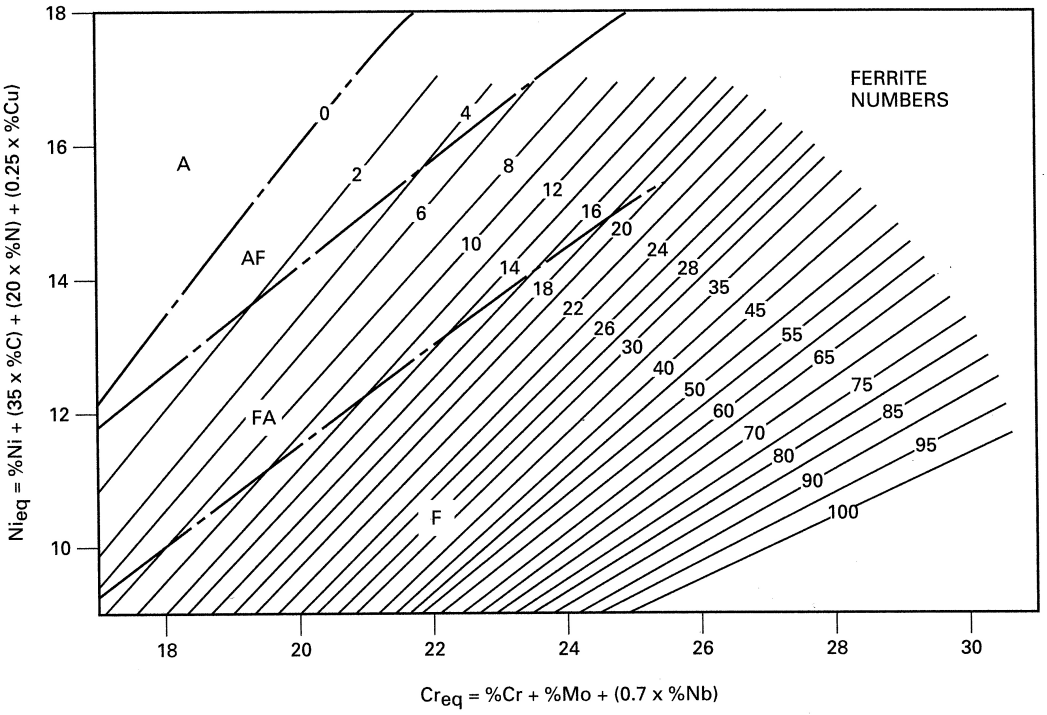

Figure 10: WRC-92 diagram.[16]

The latest WRC diagram plots the expected phases in welds after cooling to room temperature for different chemical compositions. For this purpose alloying elements are divided in two groups; elements that behave similarly to Cr in stabilising the ferrite phase and, elements that behave similarly to Ni in stabilising the austenite phase.[16] The relative effects of the different elements are given in equations 1 and 2 (the Cr and Ni equivalents). Previous authors [7,8,17] indicated that four different solidification modes are found, depending on the Cr_{eq}:Ni_{eq} ratio of the steel, where the Cr_{eq} and Ni_{eq} are calculated with equations 1 and 2.[17]

$$Cr_{eq} = \%Cr + \%Mo + 1.5\%Si + 0.5\%Nb \quad \text{.....1}$$

$$Ni_{eq} = \%Ni + 30\%C + 0.5\%Mn \quad \text{.....2}$$

1.2.4. The four modes of solidification

- **The Austenite mode: [A-mode]**

The reaction sequence $L \rightarrow [\ L+ \gamma\ ] \rightarrow \gamma$

is limited to steels with $Cr_{eq} : Ni_{eq} < 1.25$. [17]

Figure 11a indicates the effect of this solidification mode on the microstructure. In this mode, there is an absence of any other transformation reactions during cooling and the solidification structure is retained. Due to the segregation during solidification, as indicated in Figure 12b, the cell/dendrite cores will be relatively low in the ferrite formers Cr, Mo, Si, Ti and Al, while being high in the austenite formers Ni, Mn, Cu, N and C. [18] Marshall et al. similarly indicated that there might be some segregation of Mo and Cr.[19]

- **The Austenite-Ferrite mode: [AF mode]**

The reaction sequence $L \rightarrow [\ L+ \gamma\ ] \rightarrow [\ L+ \gamma + \delta\ ] \rightarrow [\ \gamma + \delta\ ]$

is limited to steels where $1.25 < Cr_{eq} : Ni_{eq} < 1.48$. [17]

In this solidification mode, see Figure 11b, there will be some ferrite present interdendritically. As indicated in Figure 12c, the interdendritical ferrite will be richer in ferrite stabilisers, like Cr and Mo.

- **The Ferrite-Austenite mode: [FA mode]**

The reaction sequence $L \rightarrow [\ L+ \delta\ ] \rightarrow [\ L + \delta + \gamma\ ] \rightarrow [\ \delta + \gamma\ ]$

is limited to steels where $1.48 < Cr_{eq} : Ni_{eq} < 1.95$.[17]

In this solidification mode, see Figure 11c, there will be some untransformed ferrite present in dendrite cores. The segregation in this mode (Figure 12d) will be different from the AF mode in the sense that the first material to solidify [cores] will be rich in ferrite stabilizers, and the interdendritical regions will be rich in austenite stabilizers. According to Rajasekhar et al.[17] some of the liquid solidifies as ferrite, but as the sample cools down solid state transformation takes place, from ferrite to austenite, altering existing partitioning profiles. In the end, this leads to a complex structure.

- **The ferrite mode: [F mode]**

The reactions sequence $L \rightarrow [\ L+ \delta\ ] \rightarrow\ \delta\ \rightarrow [\ \delta + \gamma\ ]$

Is limited to steel where $Cr_{eq} : Ni_{eq} > 1.95$.[17]

In this solidification mode (Figure 11d) Widmanstätten type austenite can be seen in the ferrite matrix. The segregation will be similar to that for the FA mode (Figure 12a&c): the first material to solidify [cores] will be rich in ferrite stabilizers, and the interdendritical regions will be rich in austenite stabilizers. According to Rajasekhar et al.[17] all of the liquid solidifies as ferrite, but as the sample cools down solid state transformation takes place, from ferrite to austenite, altering existing partitioning profiles. In the end, this leads to a complex structure.

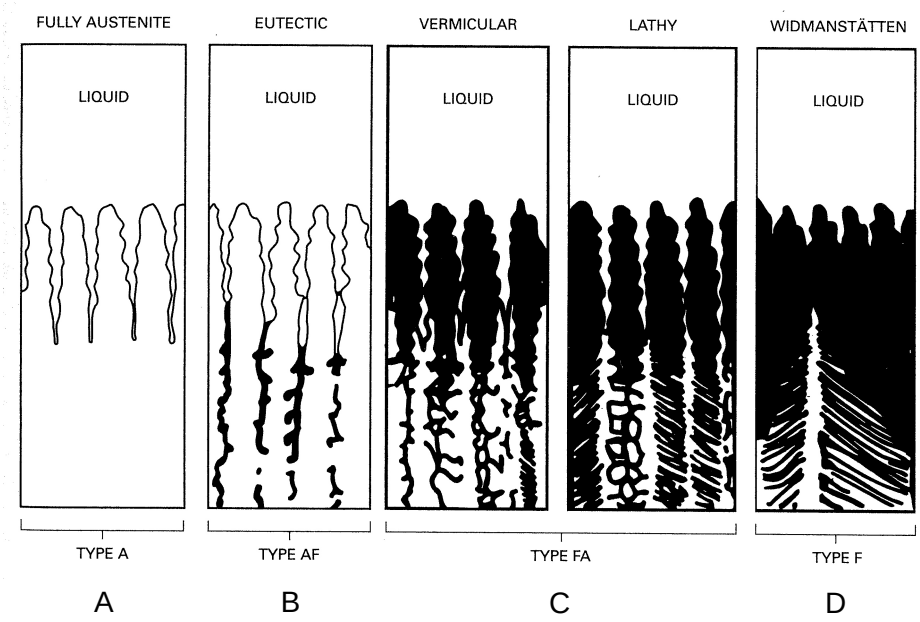

Figure 11: Difference in solidification structure because of compositional differences. [16]

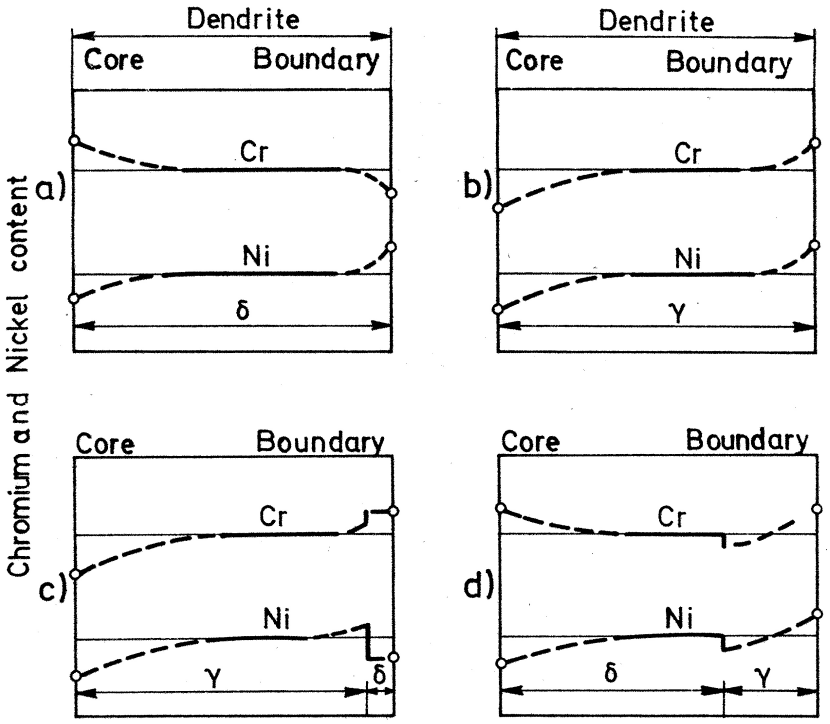

Figure 12: Segregation of elements during solidification.[8]

1.2.5. Segregation during cooling

It is also believed that this partitioning of elements during solidification contributes to the inferior corrosion properties of welds. It is known that sensitization and precipitation of intermetalic phases depletes the adjacent matrix of corrosion resistant Cr.[8] This can result in intergranular corrosion and pitting of the depleted matrix. It is believed that the partitioning of elements during solidification and subsequent cooling can have similar effects. Due to the high cooling rates during welding, time for diffusion in the solid state is limited. Therefore, much of the chemical partitioning which arises during solidification is frozen into the final microstructure.

A way to capture and compare alloys in terms of their localised-corrosion properties is by way of the Pitting Resistance Equivalent Number (PREN). This is given by:

$$PREN = Cr+3.3\ (Mo+0.5\ W)+16\ N\ (wt\%)$$

From this, it can be seen that alloying elements influence the localised corrosion of stainless steel, so local decreases in the concentrations of these elements (due to segregation) would have a detrimental effect on corrosion resistance.[20] Kangas and Newman similarly indicated that nickel (Ni) and molybdenum (Mo) also have a significant influence on the passivation behaviour of alloys in organic acid service.[21] This was also reported in work performed by Schillmoller.[5]

Schmidt-Rieder et al.[22] indicated that N has a large effect on the stability of the passive film of the austenite phase in duplex stainless steels, adding to the superior corrosion properties of the austenite. Raja et al.[23] also indicated that nitrogen can be used to manipulate the phase balance of alloys and their pitting resistance in certain environments. Nitrogen may also be expected to have an influence on the general corrosion resistance of stainless steels, but this is not supported by evaluations performed by Weber and Uggowitzer[24], who found that significant quantities of molybdenum are required for increased corrosion resistance.

2. Experimental procedure.

2.1. Sample preparation.

2.1.1. Commercial filler materials.

The ultimate aim of the study was to identify the best suitable commercial weld filler to increase the service life of weld repairs for columns in organic acid distillation. Plant experience has shown that a chemically matching filler material has lower corrosion resistance than the base material (parent metal). To evaluate different filler materials, corrosion coupons were, therefore, prepared using commercial type 316L plate. As indicated above, literature indicated that an increase in Mo, Cr and Ni could have beneficial effects on the corrosion resistance of alloys in an organic acid environment. Commercial filler materials with higher alloying contents of these elements were therefore selected to be evaluated under production conditions. The commercial filler materials which were used are listed in Table 3. Field conditions would be repairs to fillet and butt welds and might consist of only a single bead repair in some cases. To simulate this, the plate was therefore grooved using a 5mm cutting disk to generate a square groove approximately 5mm wide by 5mm deep. During welding in this groove the square section of the preparation was melted resulting in a slightly higher dilution of the filler than would be expected from a normal bead on plate. This was done to simulate the worst-case scenario where only single beads of weld overlay are deposited on corroded field welds. Using the different commercial filler materials, as listed in Table 3, single bead strips were welded on the plate with a SMAW process. Cross sections indicated a typical welding profile, protruding slightly less than what would be expected from a bead on plate weld. Spectrographic chemical analyses were performed on the filler materials to determine their chemical composition. Due to dilution during welding, the chemical composition of the welds did not always fall within the specified chemical composition of the filler materials.

Table 3: Typical nominal chemical composition in mass percentage of commercial filler materials used for this evaluation.

Filler material type	Elements [w%]					
	Cr	Ni	Mo	C	Si	Mn
625 (ENiCrMo3)	20.0	55.0	8.0	0.05	0.75	1.0
825 (ENiCr28Mo)	27.0	31.0	3.5	0.025	0.80	1.0
904L (E 20.25.5LCuR2)	20.0	25.0	5.0	0.030	0.5	1.0
316L (E316L)	18.0	12.0	2.8	0.03	0.7	1.0
317L (E317L)	19.0	13.0	3.7	0.03	0.7	0.7
309L (E309L)	23.0	13.0	-	0.03	0.8	0.8
309MoL (E309MoL)	23.0	13.0	2.7	0.03	0.7	0.7
2205 (E2209)	22.0	9.0	3.0	0.03	0.8	0.8
2507 (SANDVIK 25.10.4LR)	25.0	9.5	4.0	0.03	0.5	0.7

2.1.2. Nitrogen manipulation in 309L filler material.

To test the influence of nitrogen on the corrosion properties of the filler material, the nitrogen concentration of the filler material was manipulated using shielding gas with different nitrogen concentrations. Four bead on plate welds using 1.2mm type 309L filler material were welded using GMAW. By varying the nitrogen content of the argon shielding gas, it was possible to manipulate the nitrogen content of the welds. One noticeable effect of the higher nitrogen content of the shielding gas was the deterioration of the arc stability with higher nitrogen content in the shielding gas. The wire feed rate and travel speed were kept constant during the tests. More detail of these results is given in paragraph 3.1.2.

2.1.3. Passivation.

It is a normal recommended practice to pickle and passivate all stainless steel welds. This was also done for all welds tested under these conditions. A commercial pickling and passivation solution was used on all samples prior to installation in the columns. However, to test the effect of passivation on the corrosion rate in this environment, commercial corrosion coupons were selected for testing. The samples were split into two groups. Both sets of samples were ground to a 220 grit finish with silicon carbide paper. One group was passivated under lab conditions with a 30 % nitric acid solution, while the other group was not passivated. Both sets of samples were welded. Examination of the samples after subsequent corrosion exposure indicated that passivation did not significantly contribute to the corrosion properties of stainless steels in these environments. This is possibly due to the fact that considerable time elapsed between the time of sample preparation and exposure to operating conditions allowing passivation to take place in atmosphere. The effects of the removal (or not) of high temperature oxide by pickling were not evaluated, however.

2.1.4. Chemical analyses.

To determine the chemical composition of the filler materials after welding, samples were subjected to spectrographic chemical analyses by a certified commercial laboratory. Nitrogen concentrations were determined by inert gas fusion analysis from drillings taken from the filler material.

The chemical composition of the operating medium was determined by standard plant procedures using standard plant techniques conforming to international standards.

2.1.5. Exposure.

Samples were installed in production columns and tested under production conditions. Figure 13 indicates a typical coupon as inserted within a production column. For the purpose of this study the production system was divided into 10 subsystems, numbered A to J. Typical chemical compositions of the operating medium in the different sub-systems are listed in Table 4. Table 5 lists the typical operating temperature at the various points where coupons were inserted. Exposure times depended on production runs. The exposure times ranged between 120 to 214 days. Samples were used in an as-welded condition and no additional surface preparation was performed, except in the cases where the influence of passivation was evaluated. All samples were pickled and passivated before exposure.

For these mediums, electrochemical tests could not be conducted since the mediums, being organic, have a very low electrical conductivity, making electrochemical corrosion testing difficult. Due to the possible influence that elements commonly used to increase the conductivity of media, such as Br^- and Cl^- , could have on the corrosion reactions, addition of these as a background electrolyte could not be used. In addition, during some trial potentiodynamic measurements "masking" redox reactions were identified, with higher current densities that the actual corrosion reactions. These were presumed to originate from

oxidation of the organic components in the electrolyte, and precluded electrochemical quantification of the rates of the corrosion reactions. Also, given that the attack is localised (and generally concentrated on specific phases in the weldments), the average electrochemical behaviour – even if this were measurable – would have been of limited use in any case.

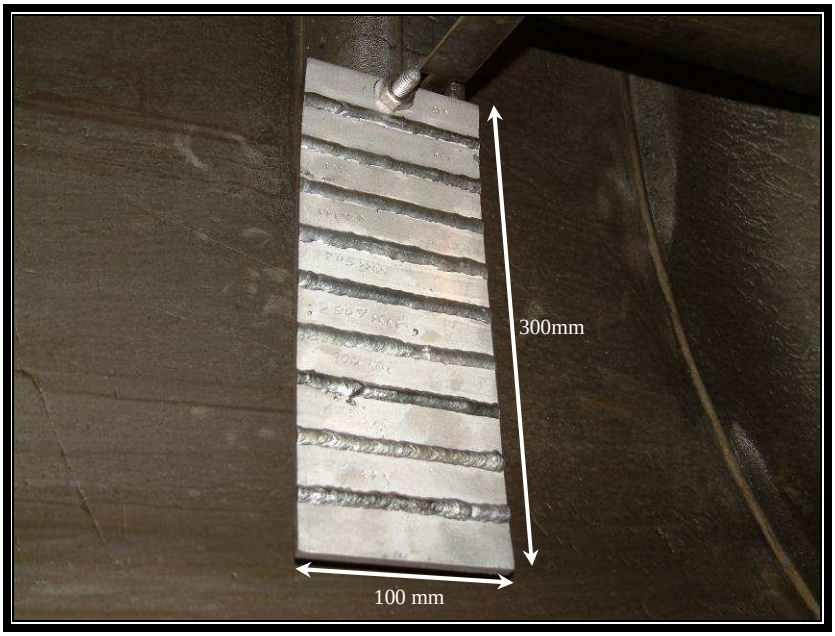

Figure 13: A photograph indicating a typical coupon as inserted within a production column.

Table 4: Typical chemical composition of the operating medium to which samples were exposed.

Component	Exposed Condition Composition mass%									
	A	B	C	D	E	F	G	H	I	J
Acetic acid	37-41	<0.1	37-41	54-60	<0.1	54-60	99.96	99.98	99.96	99.68
Propionic acid	29-32	2-4	29-32	41-45	99.9	41-45	<0.1	<0.1	<0.1	<0.1
Isobutanoic acid	4-6	13-16	4-6	<0.1	<0.1	<0.1	<0.1	<0.1	<0.1	<0.1
Butanoic acid	13-15	40-44	13-15	<0.1	<0.1	<0.1	<0.1	<0.1	<0.1	<0.1
Isopentanoic acid	2-4	8-11	2-4	<0.1	<0.1	<0.1	<0.1	<0.1	<0.1	<0.1
Pentanoic acid	3-5	12-15	3-5	<0.1	<0.1	<0.1	<0.1	<0.1	<0.1	<0.1

Table 5: Typical operating temperatures to which samples were exposed.

Exposed Temperature °C									
A	B	C	D	E	F	G	H	I	J
140-142	178-180	124-126	118-120	155-157	153-155	110-112	129-131	125-127	85-87

2.1.6. Evaluation.

2.1.6.1. Visual.

After exposure all samples were evaluated visually for any inconsistencies, pitting and galvanic corrosion. Polished cross sections of the exposed samples were also prepared and comparisons drawn between relative corrosion rates of the filler material vs. the corrosion rate observed on the base material at the toe of the welds. More detail of this evaluation is given in paragraph 3.2.1.

2.1.6.2. Scanning electron microscopy

All exposed samples were also evaluated using a JEOL JSM-6360LV scanning electron microscope (SEM). The exposed surfaces were evaluated in terms of corrosion characteristics. Cross sections of the samples were also evaluated for selective (e.g. interdendritic) corrosion. Using the EDS (Energy-dispersive X-ray spectroscopy) facility of the SEM surface analyses of the corroded surfaces were performed. Attempts were also made to evaluate the chemical compositions of the phases present. Depending on the acceleration voltage and atomic number of the sample, the interaction volume – from which characteristic X-rays (as used for EDS) are emitted - extends to 1-6 μm below the surface of the sample, as indicated in Figure 14. Given that the phases in the weld microstructure were often finer than this, accurate phase compositions could not be obtained by this method and transmission electron microscopy (TEM) was used for microanalysis of the phases.

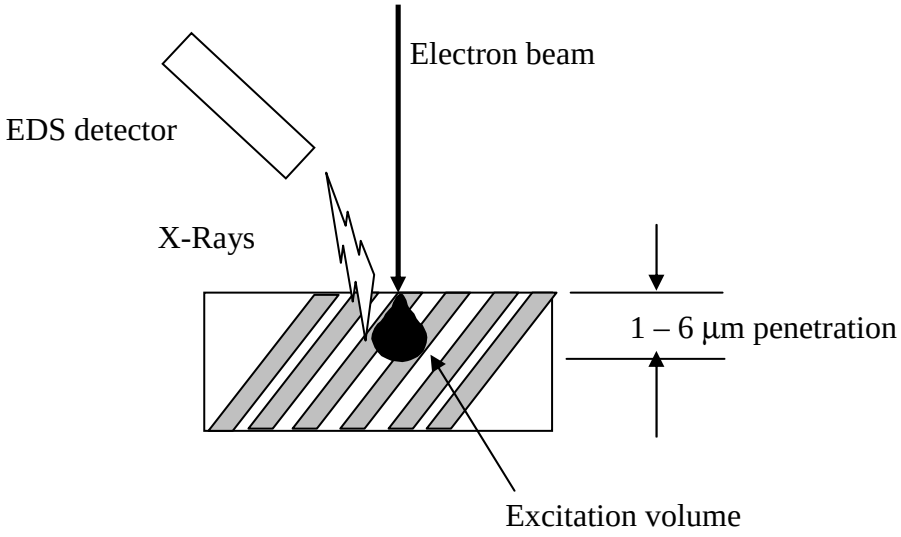

Figure 14: Schematic representation of the interaction volume during EDS analysis

2.1.6.3. Transmission electron microscopy

To determine the extent of chemical segregation within weld metal, the EDS facility of the TEM was used. Samples were removed from the caps of three unexposed filler materials. These were machined down to 3mm rod sections after which disks were sectioned from these rods. These disks were mechanically thinned to about 100 microns and then subjected to chemical polishing up to a point where a hole was polished through the sample. The aim was to create sections of filler material around the hole that are electron transparent.

Using selected-area diffraction patterns, it was possible to identify the phases which were analysed by EDS. As examples, Figure 15 and Figure 16 show [110] diffraction patterns of ferrite and austenite.

In determining the chemical composition of thin samples with the EDS function of the TEM, the Zaluzec [25] correction factor is used.

The Zaluzec correction factor is given as:

$$I_A = \varepsilon_A k_A N C_A \eta_A t_A$$

Where:

I_A	=	measured intensity
ε_A	=	detection efficiency
k_A	=	constant for element A (a function of the ionisation cross section, fluorescence and atomic weight)
N	=	Avogadro's constant
C_A	=	Concentration of A
η_A	=	number of electrons
t_A	=	thickness

From this, it can be seen that one of the factors effecting the concentration measurement of elements is the thickness of the sample, but this is not easily determined. Chemical analyses were hence performed at positions which were a constant distance from the edge of the hole. This yielded analyses that were comparable. Because thickness measurements were not performed, the absolute chemical composition is not accurate, but comparative results were obtained. By the nature of the EDX analysis, the nitrogen concentrations could not be determined.

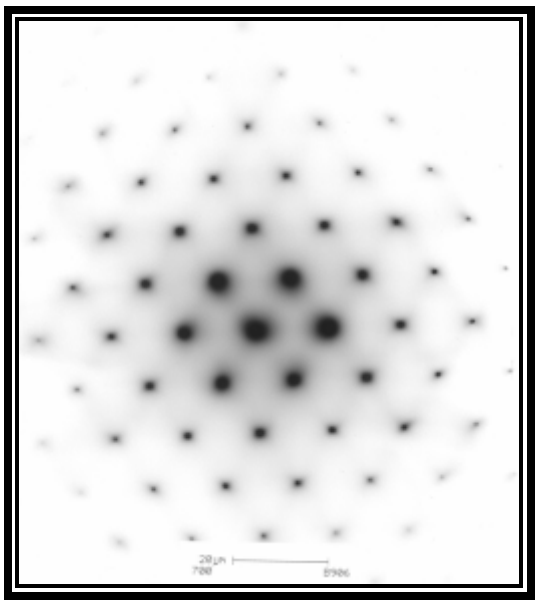

Figure 15: A [110] electron diffraction pattern of austenite (face centred cubic).

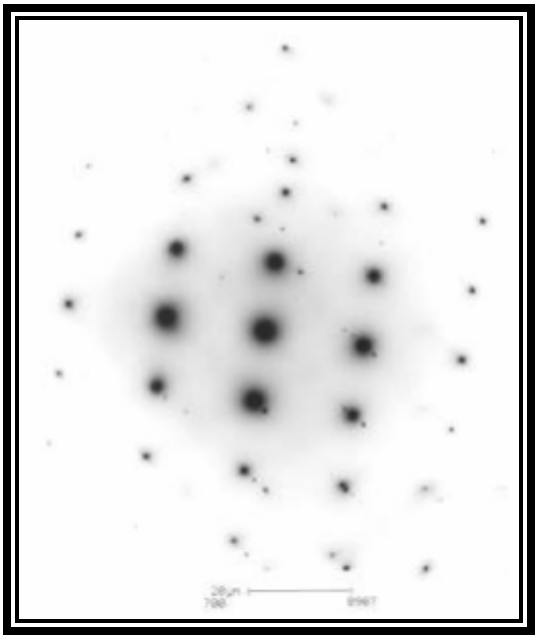

Figure 16: A [110] electron diffraction pattern of ferrite (body centred cubic).

3. Results and discussion.

3.1. Steel compositions

3.1.1. Chemical composition of filler materials

The filler materials varied in Cr, Ni, and Mo concentrations, among others. These elements are known to have the largest influence on the corrosion resistance of stainless steel alloys. Spectrographical chemical analyses were performed on all the deposited filler materials used in the test. To be able to perform the chemical analyses, a 3-5mm section of the weld bead cap was removed by milling. This provided a large enough surface to be able to perform the spectrographic analyses on the filler materials. The results of the chemical analyses are reported in Table 6. From comparison with the nominal filler compositions (Table 7) it can be seen that a certain amount of dilution occurred during welding. The chemical compositions that fell outside the specified range of the filler materials are indicated in bold in this table.

Table 6: Chemical compositions of the as-deposited weld beads for different fillers.

Filler material	Elements						Cr_{eq}	Ni_{eq}	$\frac{Cr_{eq}}{Ni_{eq}}$
	Cr	Ni	Mo	C	Si	Mn			
Type 625	19.03	39.78	5.71	0.022	0.33	1.07	25.24	40.98	0.6
Type 825	25.14	26.76	2.94	0.036	0.40	1.70	28.68	28.69	1.0
Type 904L	19.31	20.62	4.02	0.025	0.31	2.49	23.80	22.62	1.1
Type 316L	18.27	11.66	2.27	0.031	0.66	0.81	21.53	13.00	1.7
Type 317L	18.04	11.74	2.87	0.025	0.59	0.81	21.80	12.90	1.7
Type 309L	21.11	11.64	0.96	0.034	0.63	0.94	23.02	13.13	1.8
Type 309MoL	20.41	11.95	2.24	0.021	0.62	0.83	23.58	13.00	1.8
SAF 2205	20.91	9.62	2.90	0.027	0.55	1.05	24.64	10.96	2.2
SAF 2507	22.97	10.30	3.21	0.042	0.48	0.86	26.90	11.99	2.2
Base material	18.20	11.90	1.97	0.015	0.44	1.52	20.83	13.11	1.6

Table 7: Comparison of weld bead compositions (data of Table 6; listed as "Actual") with filler specifications.

Filler material	Cr		Ni		Mo	
	Specified	Actual	Specified	Actual	Specified	Actual
Type 625	**20.0-23.0**	**19.030**	**55 min typical 64**	**39.780**	**8.0-10.0**	**5.710**
Type 825	**27.0-31.0**	**25.140**	**35.0-40.0**	**26.760**	2.5-4.5	2.940
Type 904L	**19.5-21.5**	**19.310**	**24.0-26.0**	**20.620**	**4.2-5.2**	**4.020**
Type 316L	17.0-20.0	18.270	11.0-14.0	11.660	2.0-3.0	2.270
Type 317L	18.0-21.0	18.040	**12.0-14.0**	**11.740**	**3.0-4.0**	**2.870**
Type 309L	**22.0-25.0**	**21.110**	**12.0-14.0**	**11.640**	**0.75 max**	**0.960**
Type 309MoL	**22.0-25.0**	**20.410**	**12.0-14.0**	**11.950**	2.0-3.0	2.240
SAF 2205	**21.5-23.5**	**20.910**	8.5-10.5	9.620	2.5-3.5	2.900
SAF 2507	**24.0-27.0**	**22.970**	**6.5-8.5**	**10.30**	2.9-3.9	3.210

3.1.2. Chemical composition manipulation using shielding gas.

Table 8 indicates the parameters used during welding and the effect of these on the nitrogen concentration of the weldment. Shielding gases were not additionally analysed and their compositions were assumed to be accurate as per purchased specifications from a reputable local supplier. These results are presented graphically in Figure 18. The nitrogen concentration in the shielding gas was manipulated by adjusting the flow of commercially prepared gas from gas cylinders into a common header. Arc voltage was read from the meters on the welding power supply while current was measured using a clamp meter. Travel speed was controlled by variable speed trolley on which the welding head of the MIG machine was mounted. The speed of the trolley was determined by measuring the time it travelled over a set distance.

It is a commonly accepted fact, as indicated in the pitting resistance equivalent calculation, that nitrogen has a strong influence on the pitting resistance of stainless steels. However, there is no corresponding effect of nitrogen on active dissolution kinetics, except in highly concentrated hydrochloric acid (3-4M).[26] The influence of the nitrogen concentration on the corrosion resistance of type 309L filler materials is illustrated graphically in Figure 18. From this graph it is clear that the increase in the nitrogen concentration in the filler material did not have a significant effect on the corrosion resistance of the 309L filler material in this case.

The relative corrosion rate evaluation was performed as indicated below in Figure 17. Distance (**a**) represents the corrosion of the filler material during the exposed period and (**b**) represents the corrosion of the parent metal during the exposed period. Distance (**c**) represents the difference between these relative corrosion losses (a-b) and was physically detectable and measurable during the evaluation of the samples after exposure.

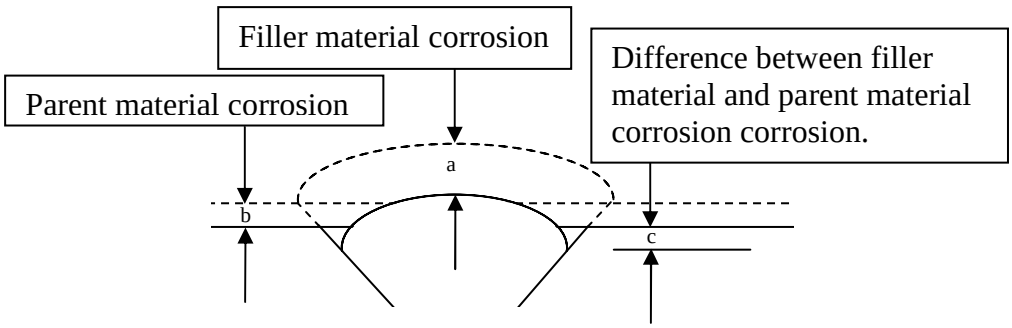

Figure 17: Schematic representation to illustrate the effect of the different corrosion rates between the weld and the base material and how this difference was interpreted during this study.

Table 8: Variation in chemical composition of the welds with variation in the shielding gas.

Weld nr.	Nitrogen in shield gas [vol. %]	Arc potential [V]	Arc current [A]	Travel speed [mm/s]	Heat input [kJ/mm]	Nitrogen in weld [mass %]
1	25	30	130	4.45	0.9	0.230
2	10	28	165	4.45	1.0	0.160
3	5	30	165	4.45	1.1	0.110
4	1	27	170	4.45	1.0	0.078

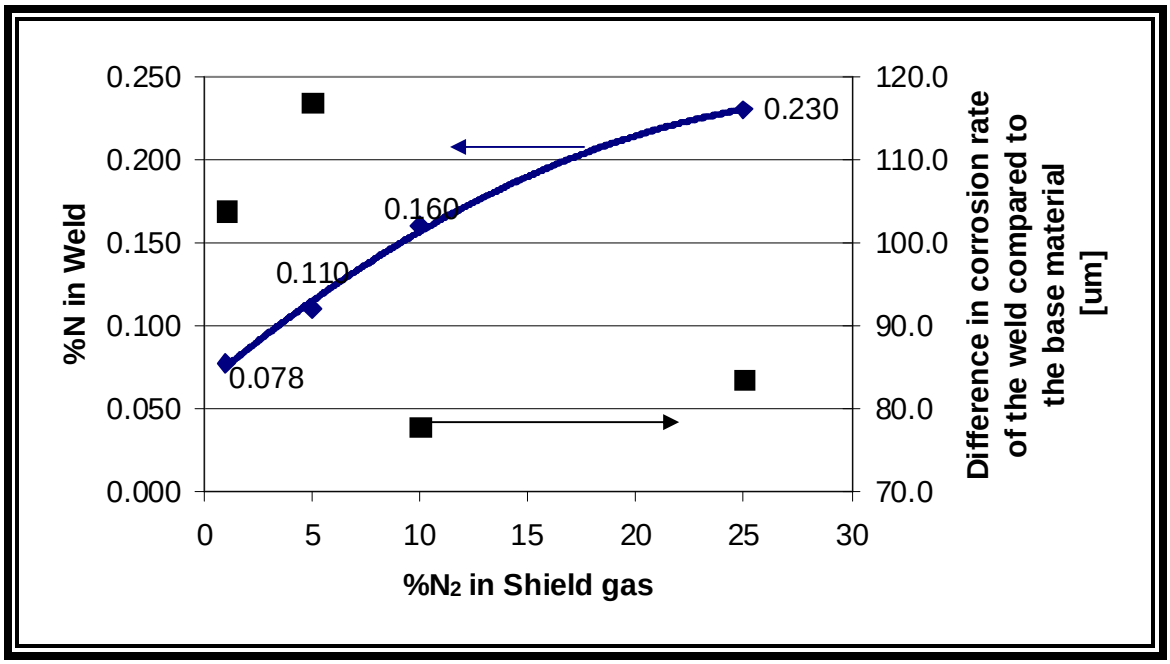

Figure 18: A graphical representation of the results of the variation of the nitrogen concentration in the shielding gas on the nitrogen concentration of the filler material and the corrosion resistance of the filler materials in organic acid media.

Results of the microstructural evaluation of the filler material are presented in Figure 19 to Figure 22. In these figures the influence of nitrogen as an austenite stabiliser is clearly visible. The absence of delta ferrite is visible in Figure 19 and Figure 20 (in which cases the nitrogen content was above 0.16 wt%). Microstructural evaluation of the dendritic nature also indicated that the solidification mode of these fillers differed from type 309L fillers with lower N concentrations and most probably followed the austenite mode of solidification. During this mode of solidification there is a risk of hot cracking due to the low solubility of S in the austenite matrix,[15] but no effect of this was observed during the evaluation. Evaluation of the sample containing 0.24% nitrogen in the filler material also revealed some porosity in the weld, suggesting that this is the limiting solubility of nitrogen under these conditions in type 309L filler materials.

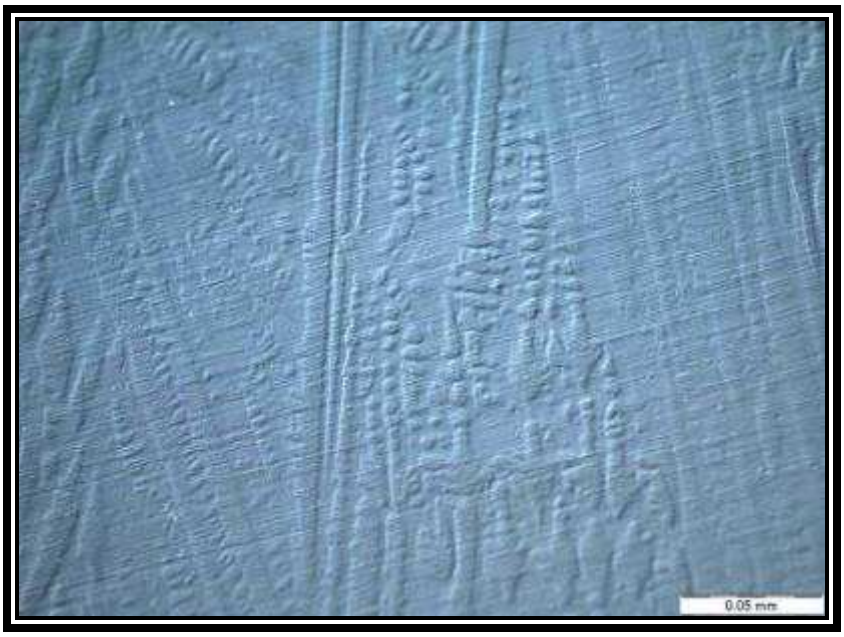

[Oxalic acid]

Figure 19: A photomicrograph showing the dendritic nature of the weld filler material containing 0.24% nitrogen. Note the lack of any delta ferrite in the filler material.

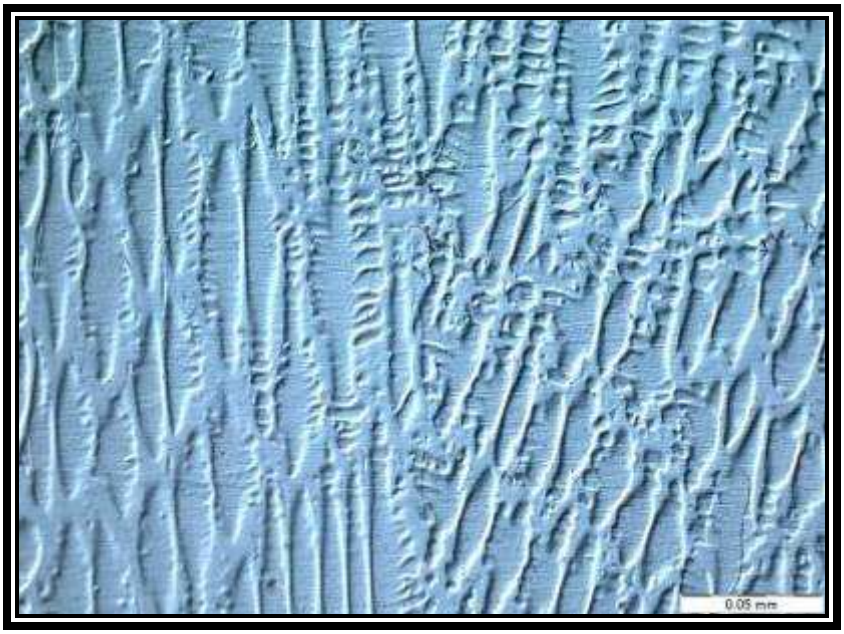

[Oxalic acid]

Figure 20: A photomicrograph showing the dendritic nature of the weld filler material containing 0.16% nitrogen in the weld. Again, note the lack of any delta ferrite in the filler material.

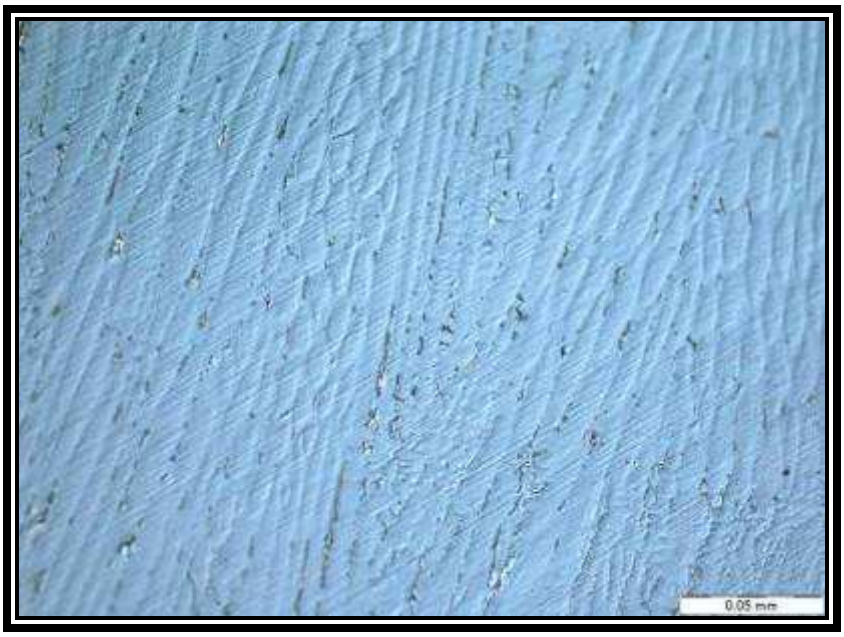

[Oxalic acid]

Figure 21: A photomicrograph showing the dendritic nature of the weld filler material containing 0.11% nitrogen in the weld. Note the presence a limited amount of dark-etching delta ferrite in the filler material.

[Oxalic acid]

Figure 22: A photomicrograph showing the dendritic nature of the weld filler material containing 0.078% nitrogen in the weld. Note the presence of dark-etching delta ferrite in the filler material, typical of P8 filler materials.

One noticeable effect of the higher nitrogen content of the shielding gas is the deterioration of the arc stability with higher nitrogen content in the shielding gas. The wire feed rate and travel speed were kept constant during the tests. From the results (Table 8) it can be seen that the arc current for the high nitrogen shielding gas was much lower than that for the lower nitrogen shielding gases. This is most probably due to the high ionisation energy that is required for the higher nitrogen shielding gases which contained less argon.

3.1.3. Chemical segregation.

3.1.3.1. Point analyses using EDS facility of SEM.

To determine whether the segregation in the filler material was measurable, point analyses were conducted on a cross section of the 625 weld near the surface of the weld. The analyses were performed at a very high magnification (100 000 x) at an acceleration voltage of 20kV (interaction volume approximately 1μm in diameter). The position analysed was moved by moving the sample 1 μm at a time through a distance of 30μm. This gave a point-by-point analysis of the filler material over a distance of 30μm. The graphical representation of the results of the analyses is given in Figure 23.

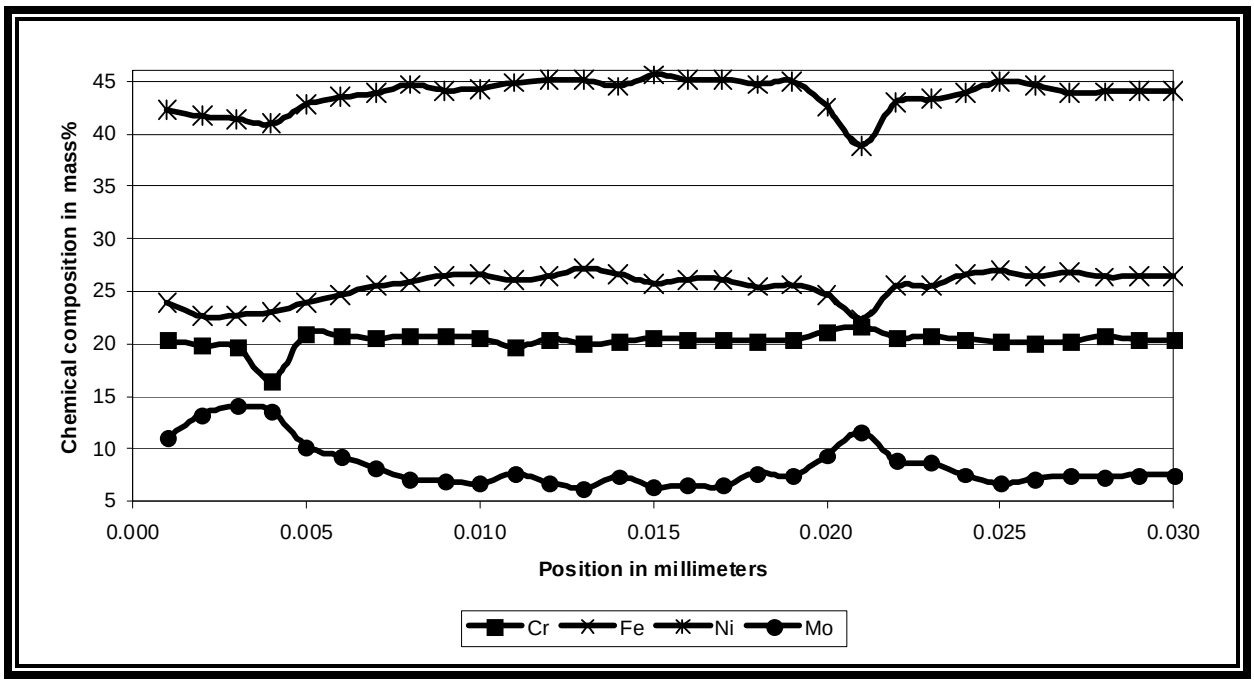

Figure 23: Graphical representation of the point by point microanalyses across the 625 filler material.

From the results of the point-by-point analyses of the cross section of the weld, it can be seen that only small fluctuations in chemical compositions were detected, not necessarily corresponding with phases visually identified.

Cross sections of various filler material samples were also evaluated in the SEM. Mapping was done by measuring the characteristic X-ray counts of different pre-selected elements at different positions. A 2000x magnification was selected with a resolution of 256x256 pixels. This gave the physical size of a pixel close to the minimum of 1µm. A dwell time of 10 seconds per pixel was chosen to allow acceptable results in an achievable timeframe. Although different phases were detectable using backscattered electron imaging mode of the SEM, only limited chemical composition variations were found when using element mapping function. The findings of the mapping done are summarised below; note that the mapping gave only qualitative results:

Type 316L filler.

Definition between delta ferrite and austenite visible on backscattered electron images.

Limited segregation visible, some segregation noticed in Cr, Ni, and Mo during mapping.

Type 317L filler.

Definition between delta ferrite and austenite visible on backscattered electron images.

Limited segregation visible, some segregation noticed in Cr, Ni, and Mo.

Type 309L filler.

Clear differentiation between the delta ferrite and austenite phases in backscatter mode.

Cr – some segregation visible.

Ni – Clear indication of Ni depletion in the ferrite phase.

No other clear indications visible.

Type 309MoL filler material.

Indication of the different phases not as clear as the previous filler materials.

Cr – Some indication of segregation visible.

Ni – Some indication of segregation visible.

Mo - Some indication of segregation visible, but less than for Cr and Ni.

Type 904L filler

Limited contrast with backscattered electron imaging.

Cr – Some indication of segregation visible.

Ni – Some indication of segregation visible.

Mo - Some indication of segregation visible, more than that for Cr and Ni.

Type 2205 filler

No clear indication of the different phases with backscattered electron imaging.

No clear indication of element segregation of elements visible.

Type 2507 filler

Cr – Some indication of segregation visible.

Ni – Some indication of segregation visible – more than with Cr.

Mo - No other clear indications visible.

Type 625 filler

This filler showed the most segregation of all the fillers evaluated, with clear indications of compositional differences with backscattered electron imaging.

Cr – Some indication of segregation visible.

Ni – Some indication of segregation visible.

Mo – Clear indications of segregation visible.

Fe – Clear indications of segregation visible.

Type 825 filler

This filler showed more chemical segregation than most fillers evaluated, but not as much as 625.

Cr – Some indication of segregation visible.

Ni – Some indication of segregation visible.

Mo – Clear indications of segregation visible.

Fe – Clear indications of segregation visible.

3.1.3.2. Colour etching.

As mentioned previously, four modes of solidification can be expected, depending on the Cr_{eq}/Ni_{eq} ratio

- **The Austenite mode: [A-mode]**

The sequence $L \rightarrow [\ L+ \gamma\ ] \rightarrow \gamma$

is limited to steels with $Cr_{eq}/Ni_{eq} < 1.25$.[17]

In this mode, there is an absence of any other transformation reactions during cooling and the solidification structure is retained. Due to the segregation during solidification, the cell/dendrite cores will be relatively low in Cr, Mo, Si, Ti and Al, while being high in Ni, Mn, Cu, N and C.[18, 19].

Considering the Cr_{eq}/Ni_{eq} ratio, as indicated in Table 6, 625, 825 and the 904L fillers should follow the austenite mode of solidification. Figure 24 to Figure 26 show photomicrographs of the 625, 825 and 904L filler materials. In these photomicrographs, a three-step colour etching technique was employed to distinguish between the different phases present in the weld matrix. The specimens were initially etched using a Glyceregia solution consisting of 30 parts HCl, 20 parts glycerin, and 10 parts HNO_3. In some cases, where effective etching was not achieved, glycerin was replaced with water. The initial etch preferentially attacked

the ferrite phase. This was followed by an electrolytic etch using 10% oxalic acid, exposing the grain boundaries, followed by tinting with Murakami's reagent.

This technique was used by Nelson et al.[18] to distinguish between austenite and ferrite in duplex stainless steel weldments. In this paper, he indicated that the ferrite phase ("high" Cr_{eq}, "low" Ni_{eq}) was coloured blue, while the austenite phase ("low" Cr_{eq}, "high" Ni_{eq}) remained white. He was also able to distinguish between "high" Cr_{eq} and "low" Cr_{eq} phases, colouring blue and yellow respectively.

Figure 24 to Figure 26 show photomicrographs of the 625, 825 and 904L filler materials after this etching technique, indicating that the dendrite cores of the type 625 filler material discoloured blue while the matrix displayed a brownish tint. This effect is not as clearly visible in the 825 and 904 filler materials as in the 625 filler material.

The discoloration of the 625 filler dendrite cores is opposite to the expected results, since it was indicated in the work done by Nelson [18] that the Cr rich phase is expected to colour blue. In this case the dendrite cores, which (based on the solidification path) are expected to be Ni-rich, coloured blue. This could be due to the fact that the tinting is based on local anodic and cathodic sites. The original work was performed on duplex grades which were relatively low in Ni compared to type 625 fillers, and hence the tinting effect may not be the same in the all-austenitic material.

- **The austenite-ferrite mode: [AF mode]**

The sequence $L \rightarrow [\ L+\gamma\ ] \rightarrow [\ L+\gamma+\delta\ ] \rightarrow [\ \gamma+\delta\ ]$

is limited to $1.25 < Cr_{eq}/Ni_{eq} < 1.48$.[17]

In this solidification mode, there will be some ferrite present interdendritically. Again, due to the primary phase being austenite, the dendrite cores will be rich in austenite stabilisers

(Ni, N and Mn), while the interdendritic ferrite will be richer in ferrite stabilisers (Cr and Mo).

This mode of solidification was not found in any of the compositions included in this study.

- **The ferrite-austenite mode: [FA mode]**

The sequence $L \rightarrow [\ L+\delta\ ] \rightarrow [\ L+\delta+\gamma\ ] \rightarrow [\ \delta+\gamma\ ]$

is found for steels with $1.48 < Cr_{eq}/Ni_{eq} < 1.95$ [17]

In this solidification mode, there will be some untransformed ferrite present in dendrite centres. The segregation in this mode will be different from the AF mode in the sense that the first material to solidify [dendrite cores] will be rich in ferrite stabilizers, and the interdendritic regions will be rich in austenite stabilizers.

Considering the Cr_{eq}/Ni_{eq} ratio, as indicated in Table 6, 316L, 317L, 309L and 309Mo fillers should follow this mode of solidification. Figure 27 to Figure 30 show photomicrographs of the 316L, 317L, 309L, and 309Mo filler materials. The same three-step colour etching technique as described earlier was used to prepare these photomicrographs. These figures do indicate that the dendrite cores are richer in ferrite stabilising elements while the matrix is richer in austenite stabilising elements, as expected. No significant difference in the microstructures in regards to segregation was detected.

- **The ferrite mode: [F mode]**

The sequence $L \rightarrow [\ L+\delta\ ] \rightarrow\ \delta\ \rightarrow [\ \delta+\gamma\ ]$

is limited to steels with $Cr_{eq}/Ni_{eq} > 1.95$ [17]

For this solidification mode Widmanstätten type austenite can be seen in the ferrite matrix. Figure 31 and Figure 32 show photomicrographs of SAF 2205 and SAF 2507 duplex stainless steel that represent this type of solidification mode. Again, the same three-step colour etching technique, as described earlier, was used to prepare these photomicrographs.

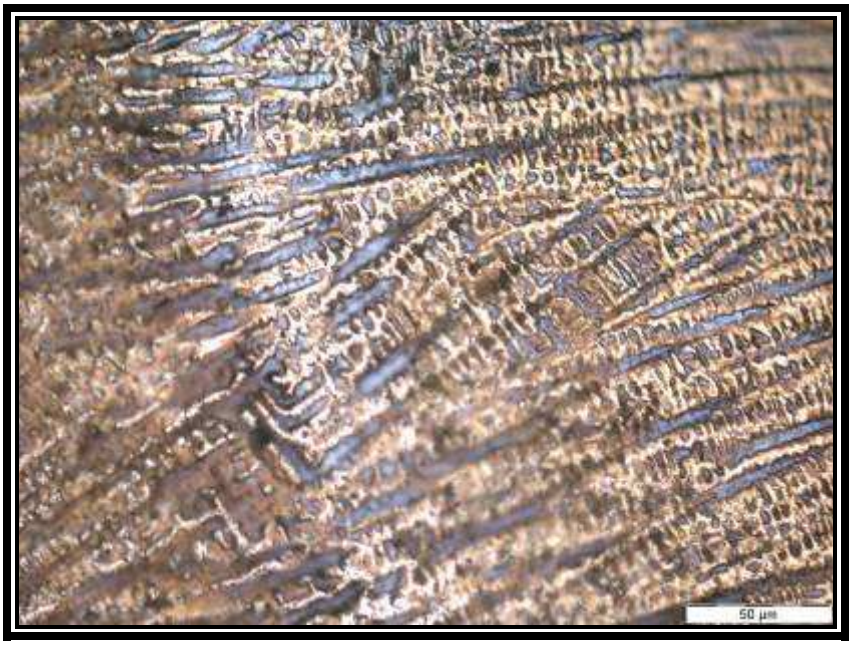

Figure 24: A photomicrograph showing the dendrites of the 625 filler material predicted to follow the austenite mode (A-mode) of solidification; three-step colour-etching technique.

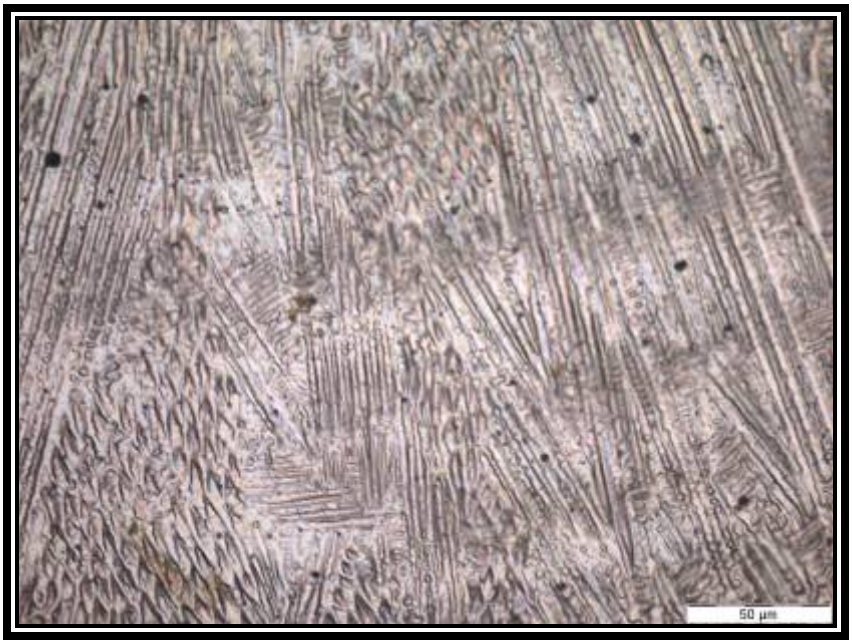

Figure 25: A photomicrograph showing the dendrites of the 825 filler material predicted to follow the austenite mode (A-mode) of solidification; three step colour-etching technique.

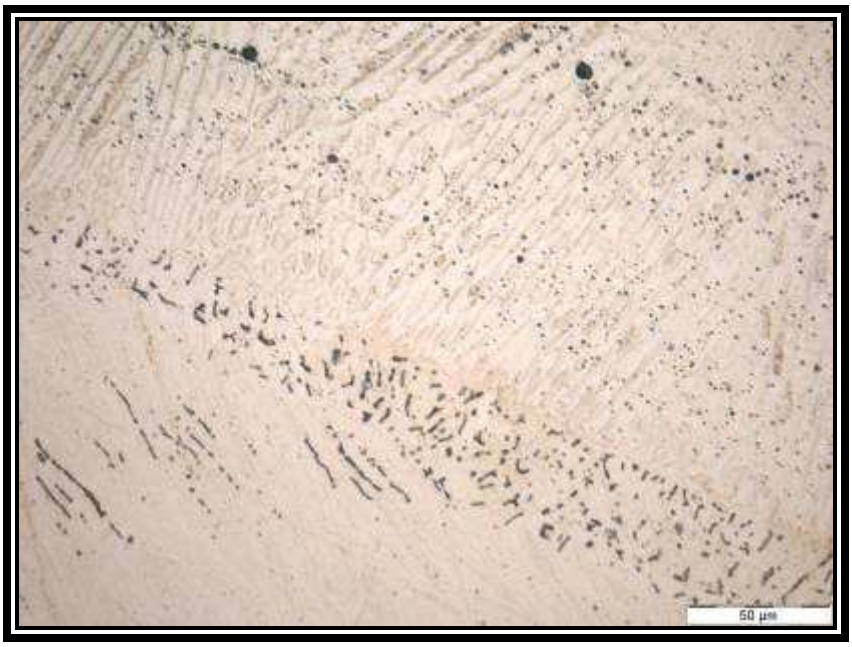

Figure 26: A photomicrograph showing the dendrites of the 904L filler material predicted to follow the austenite mode (A-mode) of solidification, near the fusion line; three-step colour-etching technique.

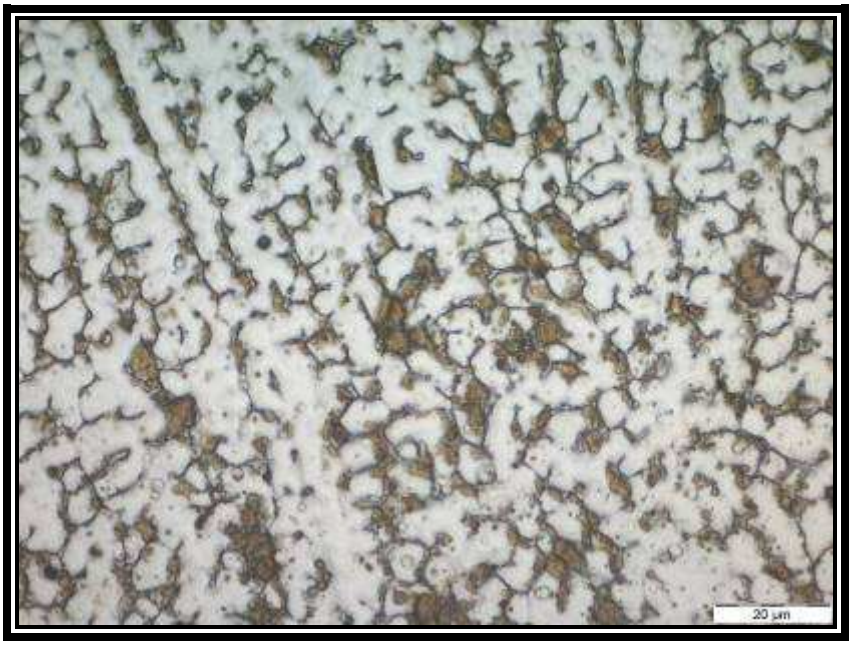

Figure 27: A photomicrograph showing the solidification/transformation dendrites of the 316L filler material, predicted to follow the ferrite-austenite mode (FA-mode) of solidification; three-step colour-etching technique. Note the bluish coloured cores of the dendrites indicating areas with high Cr_{eq}, in comparison to the low Cr_{eq}/Ni_{eq} ratio areas, which remained colourless.

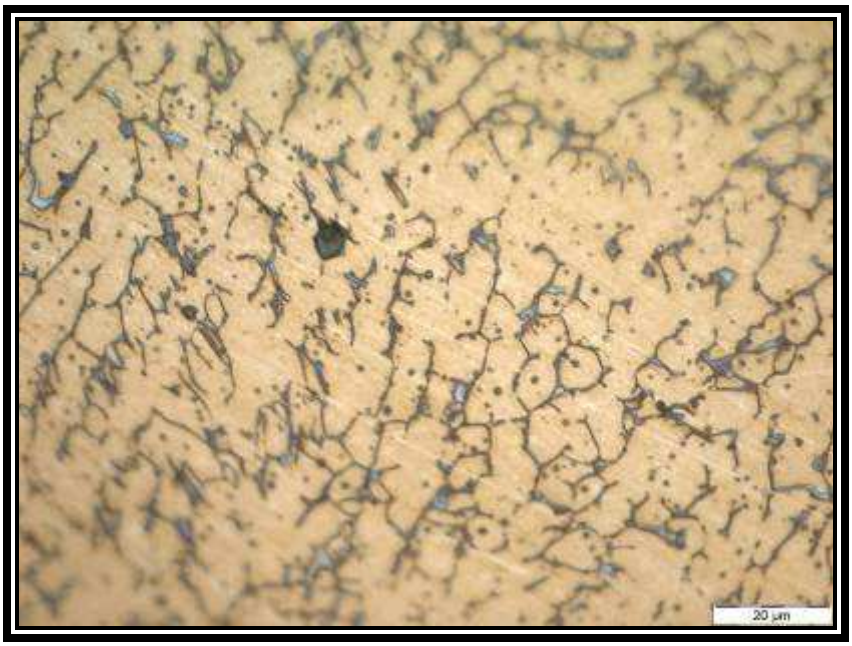

Figure 28: A photomicrograph showing the solidification/transformation dendrites of the 317L filler material, predicted to follow the ferrite-austenite mode (FA-mode) of solidification; three-step colour-etching technique. Note the bluish coloured cores of the dendrites indicating areas with high Cr_{eq} (possibly Mo-rich), in comparison to the low Cr_{eq}/Ni_{eq} ratio areas, which remained "colourless".

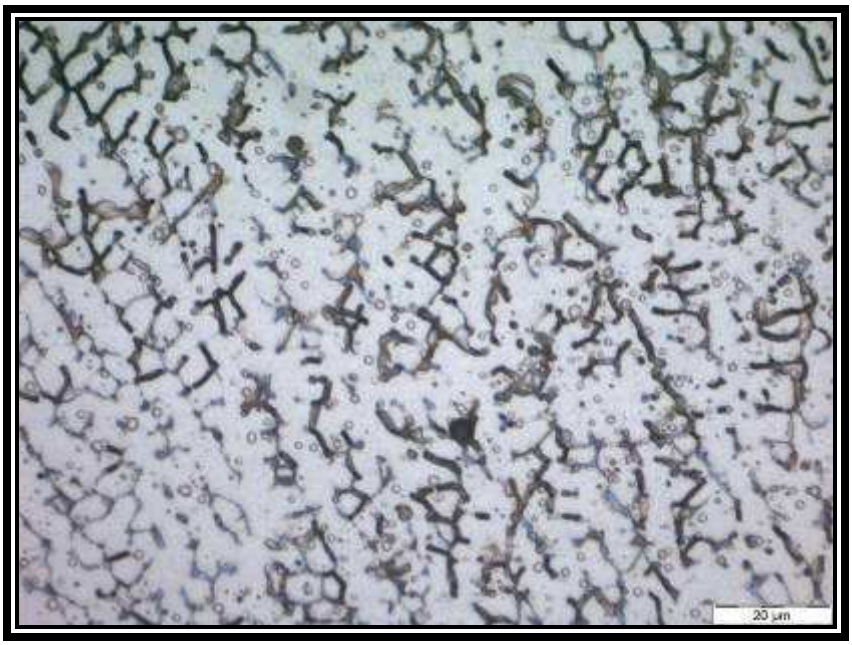

Figure 29: A photomicrograph showing the solidification/transformation dendrites of the 309L filler material, predicted to follow the ferrite-austenite mode (FA-mode) of solidification; three-step colour-etching technique. Note the bluish coloured cores of the dendrites indicating areas with high Cr_{eq}, in comparison to the low Cr_{eq}/Ni_{eq} ratio areas, which remained colourless.

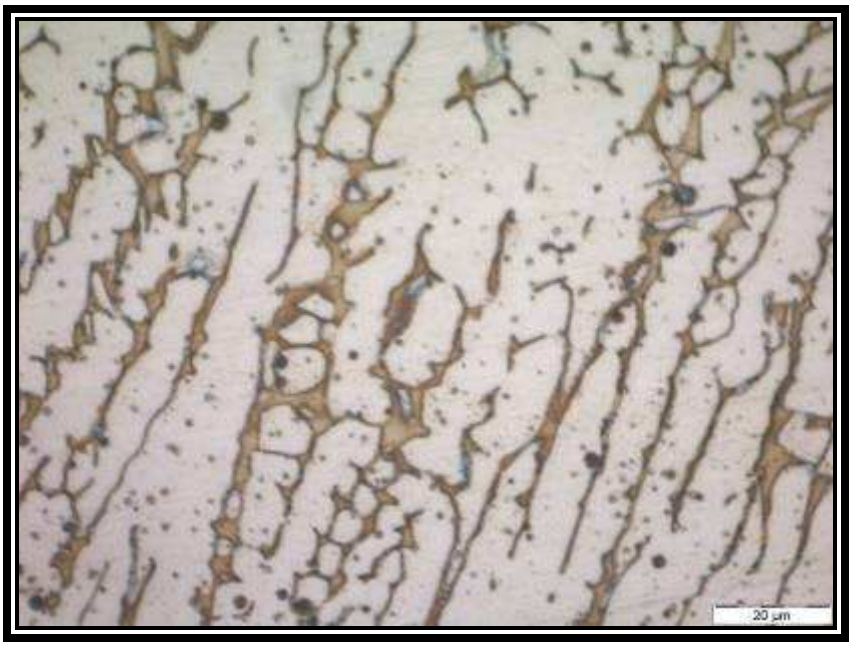

Figure 30: A photomicrograph showing the solidification/transformation dendrites of the 309MoL filler material, predicted to follow the ferrite-austenite mode (FA-mode) of solidification; three-step colour-etching technique. Note the brown/bluish coloured dendrites indicating areas with high Cr_{eq}, in comparison to the low Cr_{eq}/Ni_{eq} ratio areas, which remained colourless.

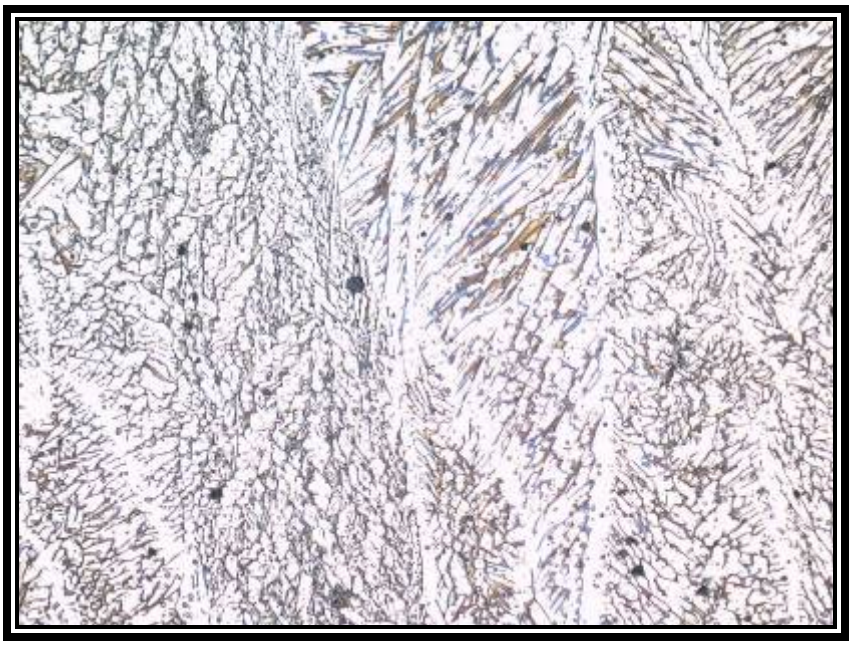

Figure 31: A photomicrograph showing the Widmanstätten type austenite in the ferrite matrix of the SAF 2205 filler material, predicted to follow the ferrite mode (F-mode) of solidification; three-step colour-etching technique. Note the brown/bluish coloured areas with high Cr_{eq}/Ni_{eq} ratio, in comparison to the low Cr_{eq}/Ni_{eq} ratio areas, which remained colourless.

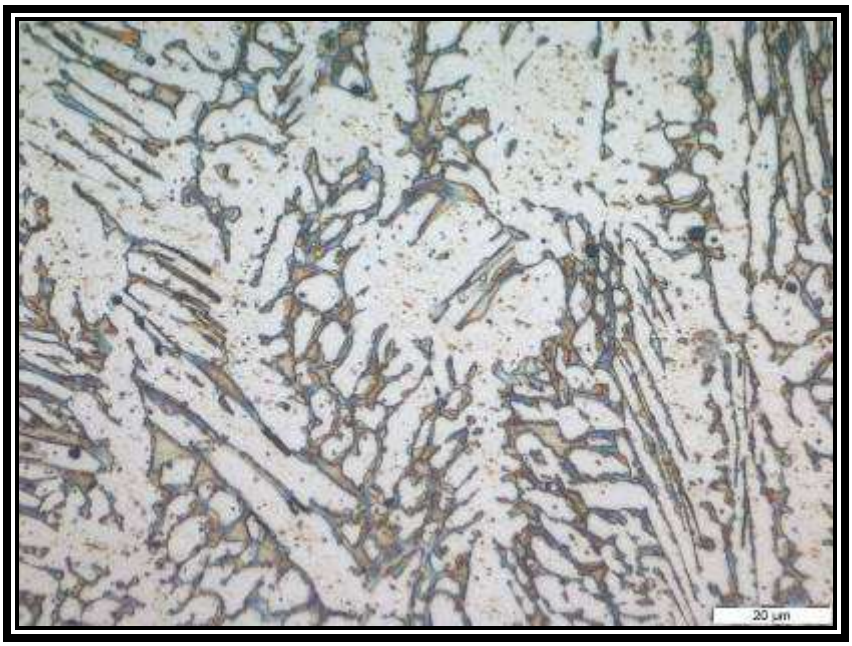

Figure 32: A photomicrograph showing the Widmanstätten type austenite in the ferrite matrix of the SAF 2507 filler material, predicted to follow the ferrite mode (F-mode) of solidification; three-step colour-etching technique. Note the brown/bluish coloured areas with high Cr_{eq}/Ni_{eq} ratio, in comparison to the low $Creq/Ni_{eq}$ ratio areas, which remained colourless.

3.1.3.3. TEM results.

As indicated above, EDS analyses with the SEM did not give conclusive results. Due the fine, intergrown nature of the phases in the welds, it is probable that characteristic X-rays were produced by more than one phase simultaneously during SEM EDS analyses. This resulted in an “average” chemical composition, even when it was attempted to analyse one phase only. To overcome this problem TEM samples were prepared.

Using electron diffraction patterns, it was possible to identify the phase in each analysed area. Figure 15 and Figure 16 show two TEM photos, indicating the [110] crystal plane diffraction patterns of ferrite and austenite, respectively. Note that the plane spacing of FCC (face centred cubic) austenite is different from that of BCC (body centred cubic) ferrite. This was checked for each analysed phase to ensure that the phases were identified correctly.

Figure 33 shows a graphical representation of the results of the chemical analyses performed on the identified phases of selected weld filler material using the EDS function of the TEM, compared with the predicted chemical compositions of the phases as per Thermocalc for a temperature of 1200°C. Figure 34 to Figure 45 show the Thermocalc predictions of the equilibrium chemical composition of the phases present in the filler material during solidification and subsequent cooling. Form these results it can be seen that the equilibrium partitioning of the elements as predicted by Thermocalc is reasonably close to the observed compositions. Therefore the major driving force for the partitioning of the elements lies in the thermodynamical properties as presented by the relevant phase diagrams. The measured phase compositions correspond to the equilibrium compositions for a relatively high temperature of 1200°C, indicating that the relative high cooling rate during the welding process does not allow for much diffusion to take please in the solid state.

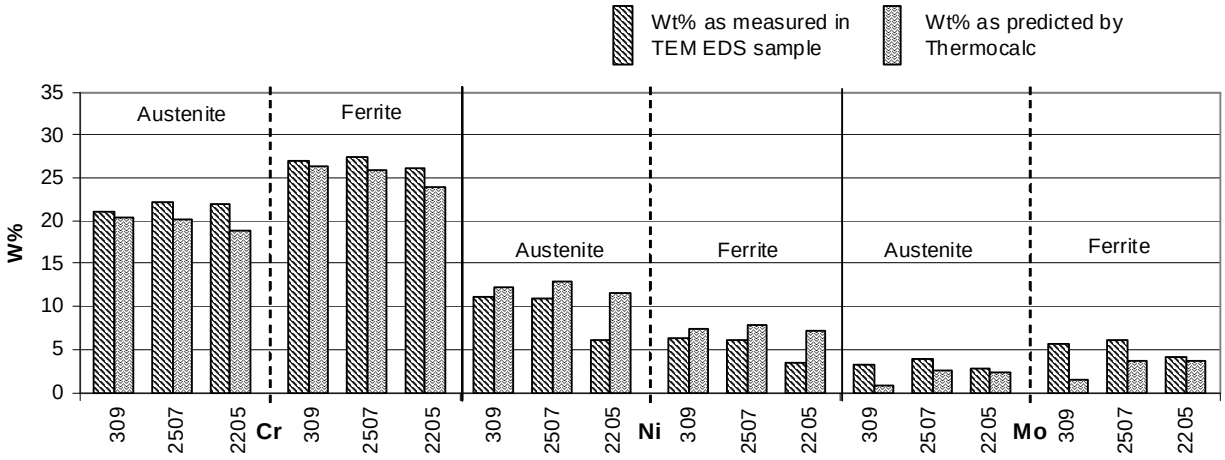

Figure 33: Graphical representation of the results of the chemical EDS analyses performed on TEM samples from various welds compared with the predicted chemical compositions as per Thermocalc results at 1200°C.

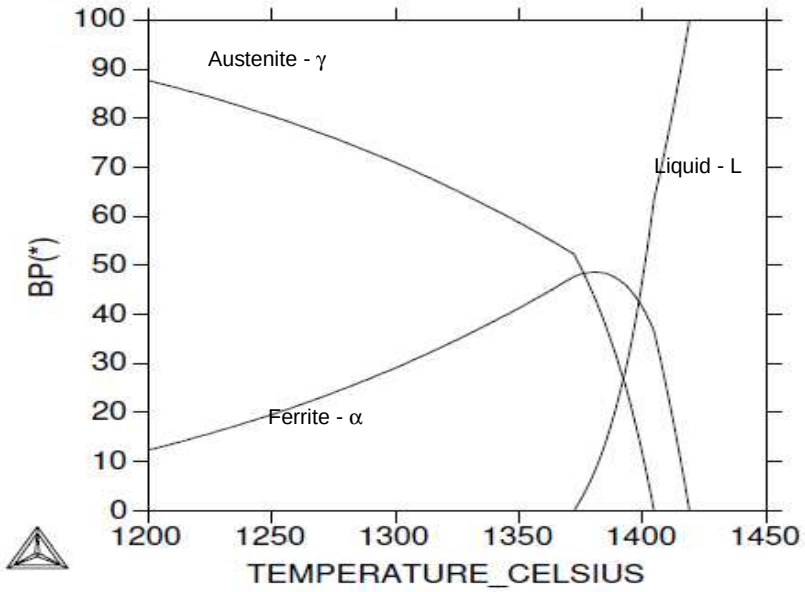

Figure 34: Prediction of phase changes with temperature (according to Thermocalc) for type 309L filler material (FA mode of solidification).

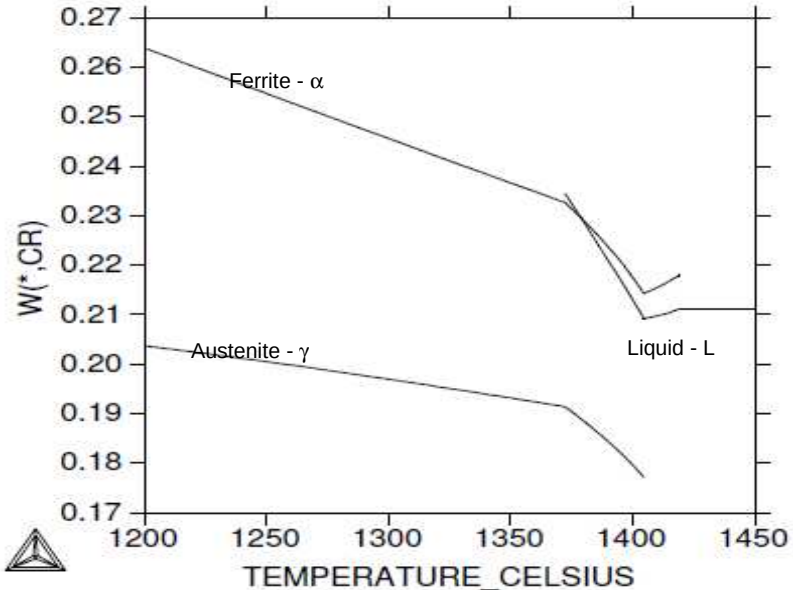

Figure 35: Chromium mass fraction in liquid, BCC and FCC phases as functions of temperature in type 309L filler material, as predicted with Thermocalc. (FA mode of solidification)

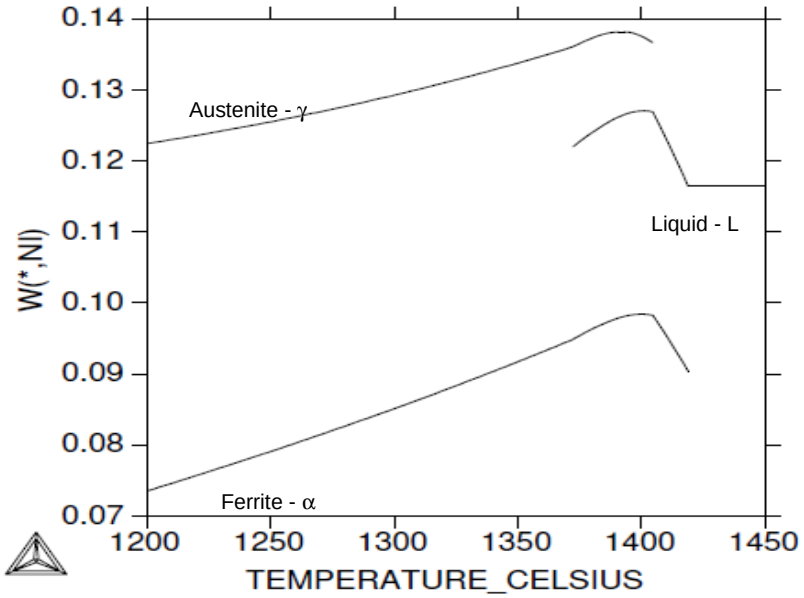

Figure 36: Nickel mass fraction in liquid, BCC and FCC phases as functions of temperature in type 309L filler material, as predicted with Thermocalc. (FA mode of solidification)

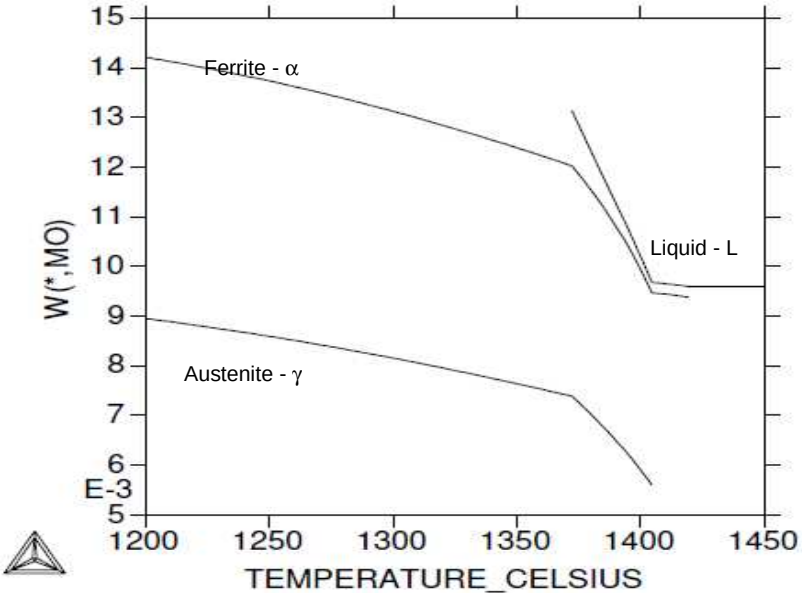

Figure 37: Molybdenum mass fraction in liquid, BCC and FCC as functions of temperature in type 309L filler material, as predicted with Thermocalc. (FA mode of solidification)

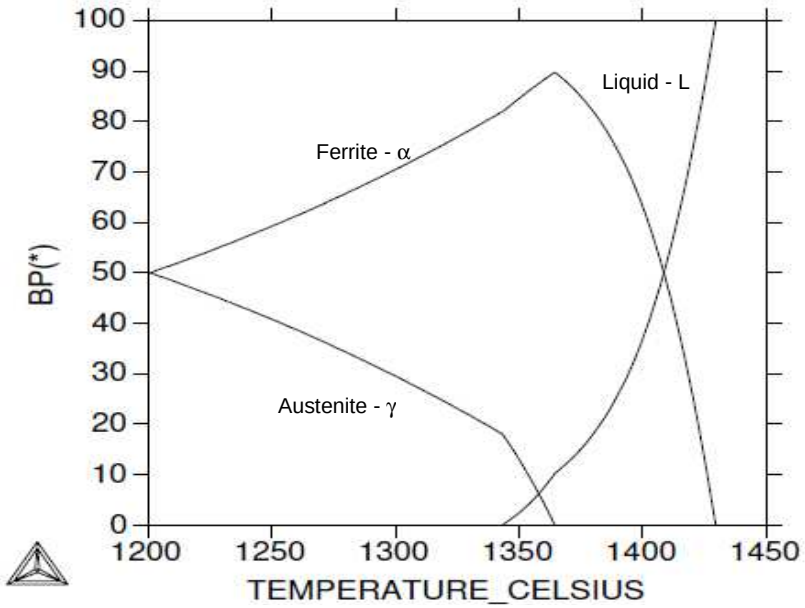

Figure 38: Prediction of phase changes with temperature (according to Thermocalc) for type 2507 filler material. (F mode of solidification)

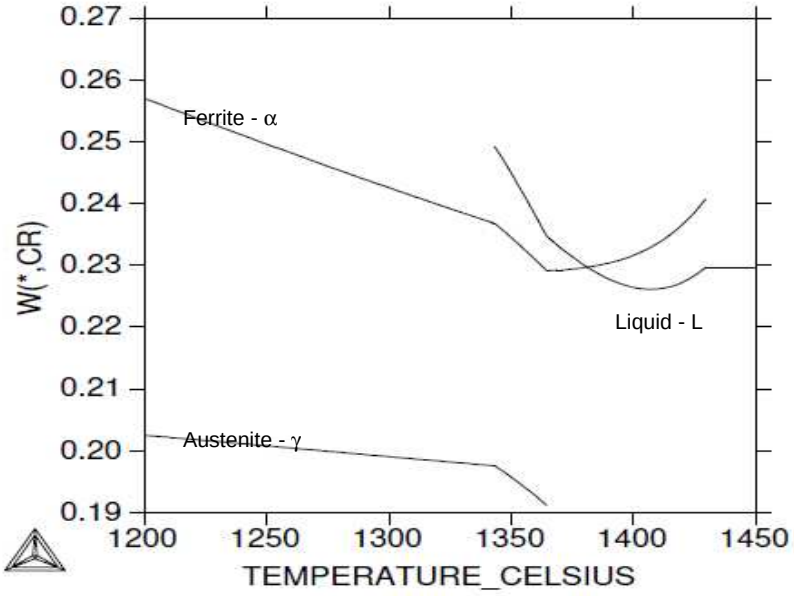

Figure 39: Chromium mass fraction in liquid, BCC and FCC phases as functions of temperature in type 2507 filler material, as predicted with Thermocalc. (F mode of solidification)

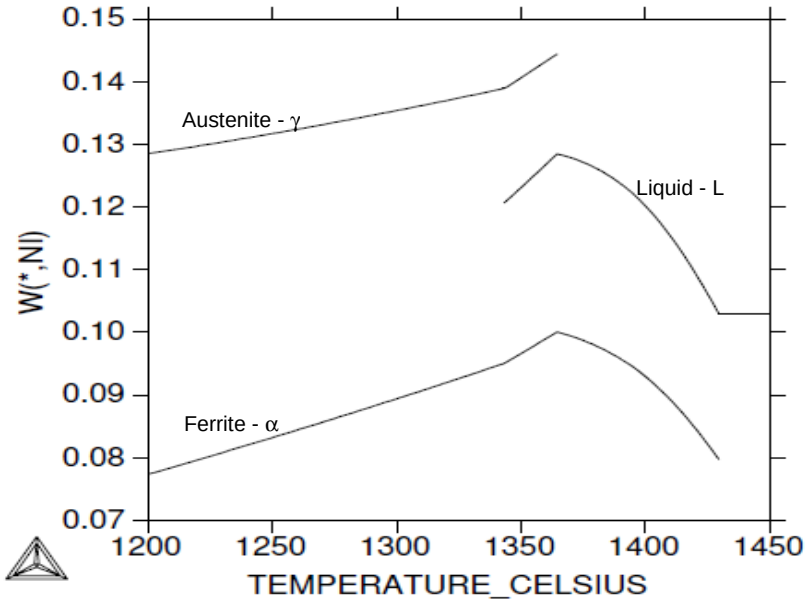

Figure 40: Nickel mass fraction in liquid, BCC and FCC phases as functions of temperature in type 2507 filler material, as predicted with Thermocalc. (F mode of solidification)

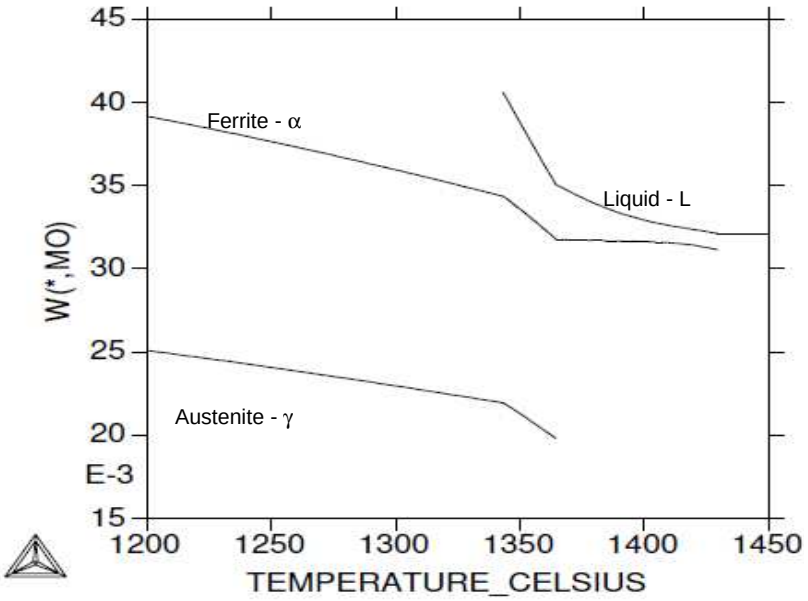

Figure 41: Molybdenum mass fraction in liquid, BCC and FCC as functions of temperature in type 2507 filler material, as predicted with Thermocalc. (F mode of solidification)

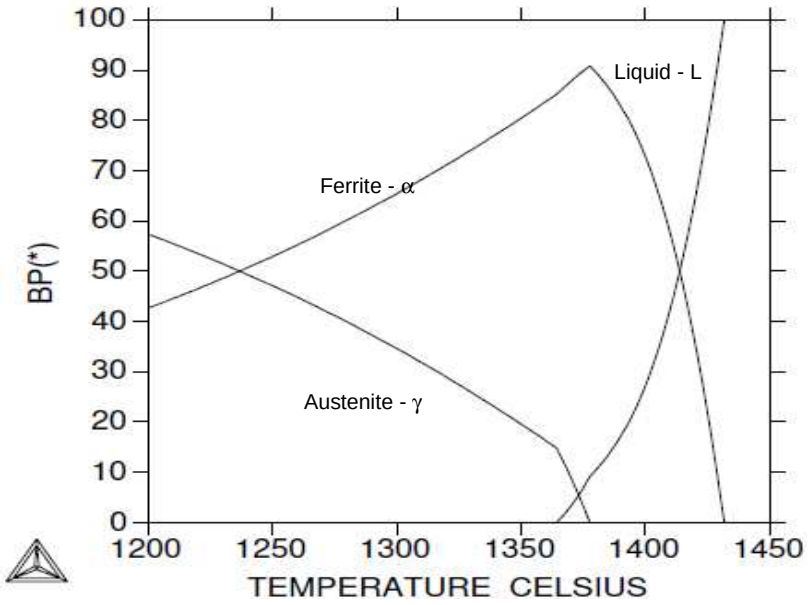

Figure 42: Prediction of phase changes with temperature (according to Thermocalc) for type 2205 filler material. (F mode of solidification)

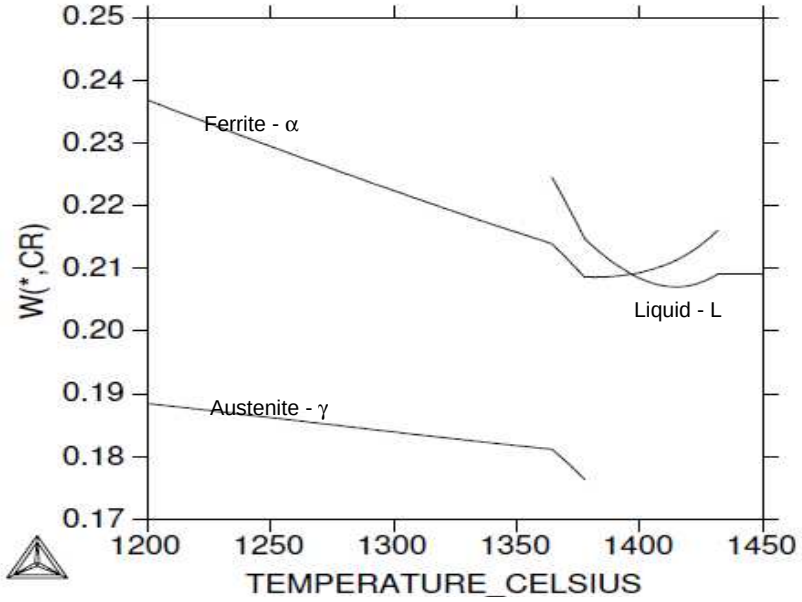

Figure 43: Chromium mass fraction in liquid, BCC and FCC phases as functions of temperature in type 2205 filler material, as predicted with Thermocalc. (F mode of solidification)

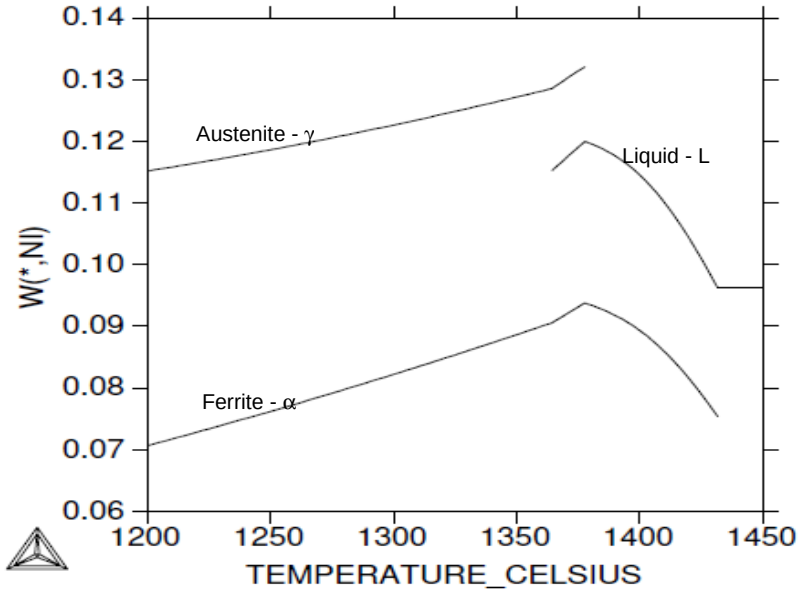

Figure 44: Nickel mass fraction in liquid, BCC and FCC phases as functions of temperature in type 2205 filler material, as predicted with Thermocalc. (F mode of solidification)

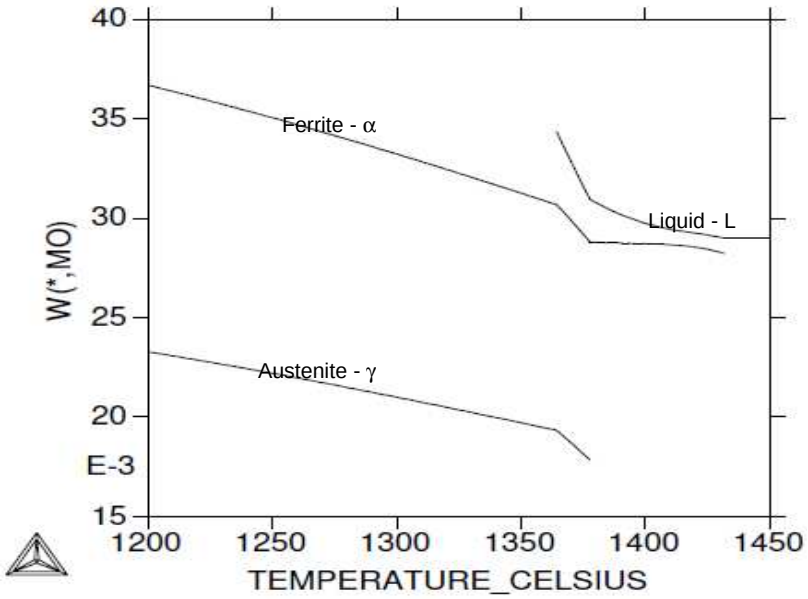

Figure 45: Molybdenum mass fraction in liquid, BCC and FCC phases as functions of temperature in type 2205 filler material, as predicted with Thermocalc. (F mode of solidification)

3.2. Exposure tests.

3.2.1. Visual and Stereo results.

All surfaces of samples exposed to the operating environment were evaluated using the scanning electron microscope. A summary of this evaluation is presented in Table 9, while actual surfaces are presented in Figure 46 through to Figure 145.

Table 9: Summary of surface condition various filler materials evaluated during this study after exposure to operating conditions for 214 days as indicated in Table 4 and Table 5. See the bottom of the table for explanation of the abbreviations.

	316L	317L	309L	309 MoL	904	625	825	2205	2507	316L plate
A	CW EP D(d) PN Figure 46	CW EP D(d) PN Figure 47	CW EP DC PN Figure 48	CW EP Ddel PN Figure 49	CB EP D(d) PP Figure 50	CB E(p) D(d) PN Figure 51	CB E(p) D(d) PP Figure 52	CB EN DI PN Figure 53	CB EN D(d) PN Figure 54	NG IC GD Figure 55
B	CW EP D(d) PN Figure 56	CW EP D(d) PN Figure 57	CW EN DC PN Figure 58	CW EN DC PN Figure 59	CB EP D(d) PP Figure 60	CB E(p) D(d) PN Figure 61	CB EP D(d) PP Figure 62	CW EN DI PN Figure 63	CW E(p) D(d) PN Figure 64	NG IC SE Figure 65
C	CW E(p) Ddel PN Figure 66	CW E(p) Ddel PN Figure 67	CW EP DC PN Figure 68	CW EN Ddel PN Figure 69	CB EP D(d) PP Figure 70	CB E(p) DI PN Figure 71	CB EP D(d) PP Figure 72	CW EN DI PN Figure 73	CB E(p) D(d) PN Figure 74	NG IC SE Figure 75
D	CW EP Ddel PN Figure 76	CW EP Ddel PN Figure 77	CW EP DC PN Figure 78	CW EN Ddel PN Figure 79	CB EN D(d) PP Figure 80	CB E(p) DI PN Figure 81	CB E(p) D(d) PP Figure 82	CB EN DI PN Figure 83	CB E(p) D(d) PN Figure 84	NG IC SE Figure 85
E	CW EP Ddel PN Figure 86	CW E(p) Ddel PN Figure 87	CW E(p) DC PN Figure 88	C(w) EN DC PN Figure 89	CB EN D(d) PP Figure 90	CB E(p) DI PN Figure 91	CB EN D(d) PP Figure 92	CW EN DI PN Figure 93	CB E(p) D(d) PN Figure 94	NG IC SE Figure 95
F	C(w) EP Ddel PN Figure 96	C(w) E(p) Ddel PN Figure 97	CW E(p) D(d) PN Figure 98	C(w) EN Ddel PN Figure 99	CB EN D(d) PP Figure 100	CB EN D(d) PN Figure 101	CB E(p) D(d) PP Figure 102	CB EN DI PN Figure 103	CB EN D(d) PN Figure 104	NG IC SE Figure 105
G	CW EP Ddel PN Figure 106	CW E(p) Ddel PN Figure 107	CW EP Ddel PN Figure 108	CW EN Ddel PN Figure 109	CB EN D(d) PP Figure 110	CB E(p) DI PN Figure 111	CB E(p) D(d) PP Figure 112	CW EN DI PN Figure 113	CW E(p) D(d) PN Figure 114	NG IC SE Figure 115

Table 9: continued…

	316L	317L	309L	309 MoL	904	625	825	2205	2507	316L plate
H	CW EP D(d) PN Figure 116	CW EN Ddel PN Figure 117	CW E(p) DC PN Figure 118	CW EN Ddel PN Figure 119	CB E(p) DC PP Figure 120	CB E(p) D(d) PN Figure 121	CB E(p) DI PP Figure 122	CW EN DI PN Figure 123	CB EN D(d) PN Figure 124	 NG IC SE Figure 125
I	CW EP D(d) PN Figure 126	CW EP D(d) PN Figure 127	CW EP D(d) PN Figure 128	CW EP D(d) PN Figure 129	C(w) EP D(d) PP Figure 130	CB E(p) DI PN Figure 131	CB E(p) D(d) PP Figure 132	CW EN D(d) PN Figure 133	CW E(p) D(d) PN Figure 134	 NG IC SE Figure 135
J	CW EN Ddel PN Figure 136	CW EN Ddel PN Figure 137	CW EN DC PN Figure 138	C(w) EN Ddel PN Figure 139	CB EN D(d) PP Figure 140	CB E(p) DI PN Figure 141	CB EN D(d) PP Figure 142	C(w) EN D(d) PN Figure 143	CB EN D(d) PN Figure 144	 NG IC SE Figure 145

CW – rate of corrosion of weld filler material faster than base material
C(w) – rate of corrosion of weld filler material similar to the base material.
CB – rate of corrosion of weld filler material less than base material.
EP – large amount of etch pits visible on the welds filler material.
E(p) – minimal amount of etch pits visible on the weld filler material.
EN – no etch pits visible on the weld filler material.
DC – dendrite cores corroded preferentially.
DI – interdendritical areas corroded preferentially.
D(d) – both dendrite cores and interdendritical cavities corroded at similar rates.
Ddel – both dendrite cores and interdendritical cavities corroded at similar rates, but delta ferrite visible (little less corroded than base material).
PP – pitting observed of weld filler material.
PN – no pitting of weld filler material observed.
NG – No galvanic corrosion between weld filler material and base material.
IC – Intergranular corrosion of base material observed.
GD – “grain dropping” corrosion observed.
SE – Slip plane etching of matrix

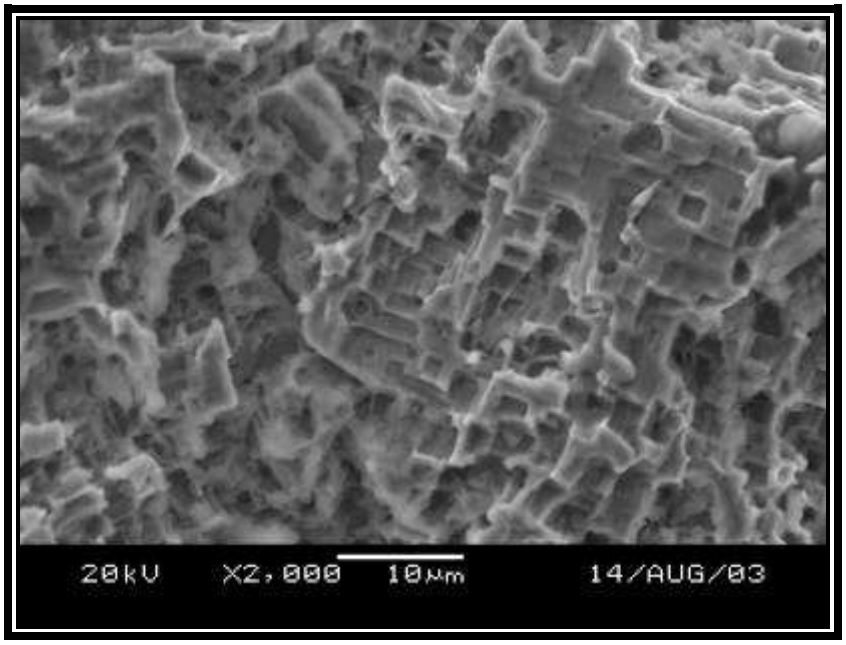

Figure 46: SEM photograph of type 316L filler material surface after 214 days exposure to a mixture of formic, acetic, propionic and heavier acids at an operating temperature of approximately 145 °C during the distillation of these organic acids as indicated in column A of Table 4 and Table 5.

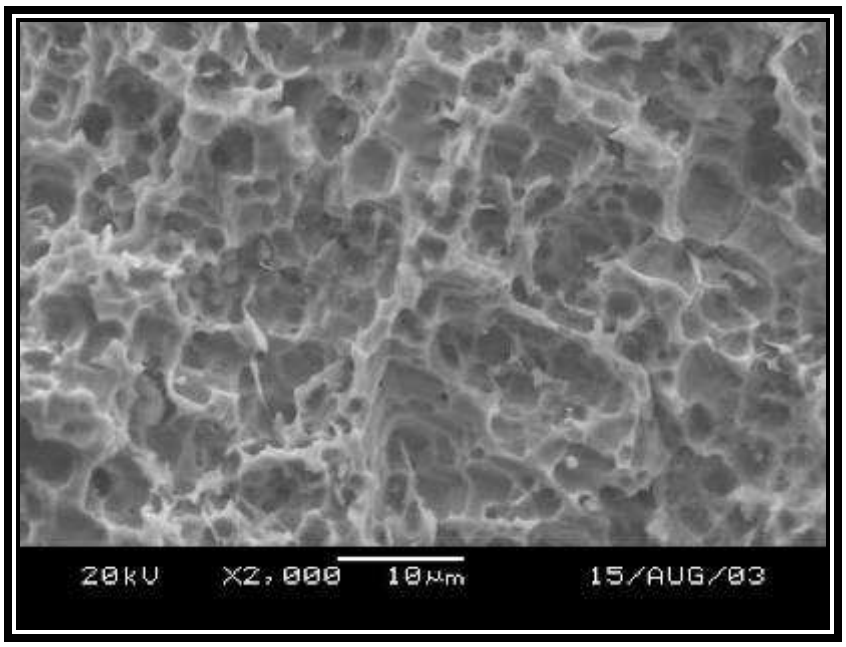

Figure 47: SEM photograph of type 317L filler material surface after 214 days exposure to a mixture of formic, acetic, propionic and heavier acids at an operating temperature of approximately 145 °C during the distillation of these organic acids as indicated in column A of Table 4 and Table 5.

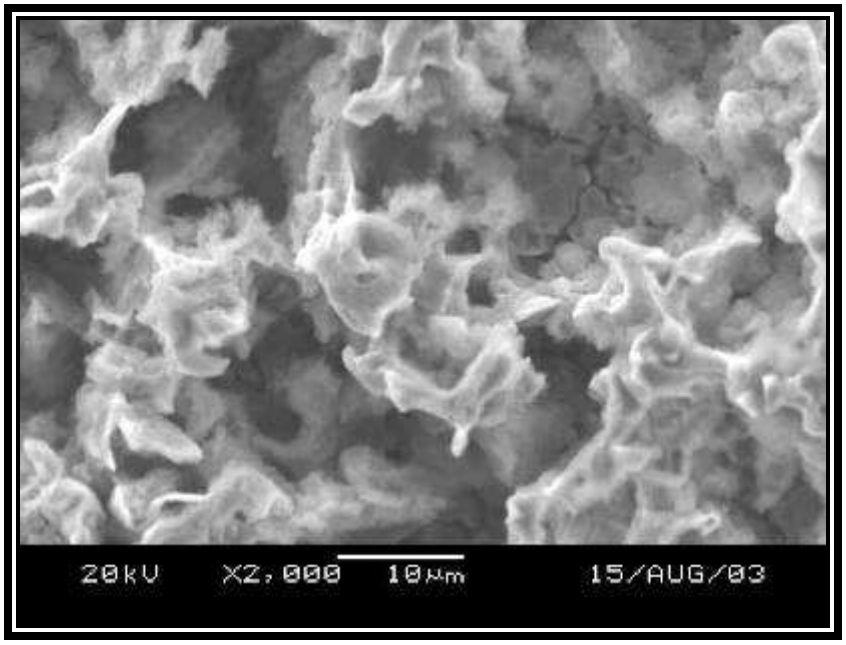

Figure 48: SEM photograph of type 309L filler material surface after 214 days exposure to a mixture of formic, acetic, propionic and heavier acids at an operating temperature of approximately 145 °C during the distillation of these organic acids as indicated in column A of Table 4 and Table 5.

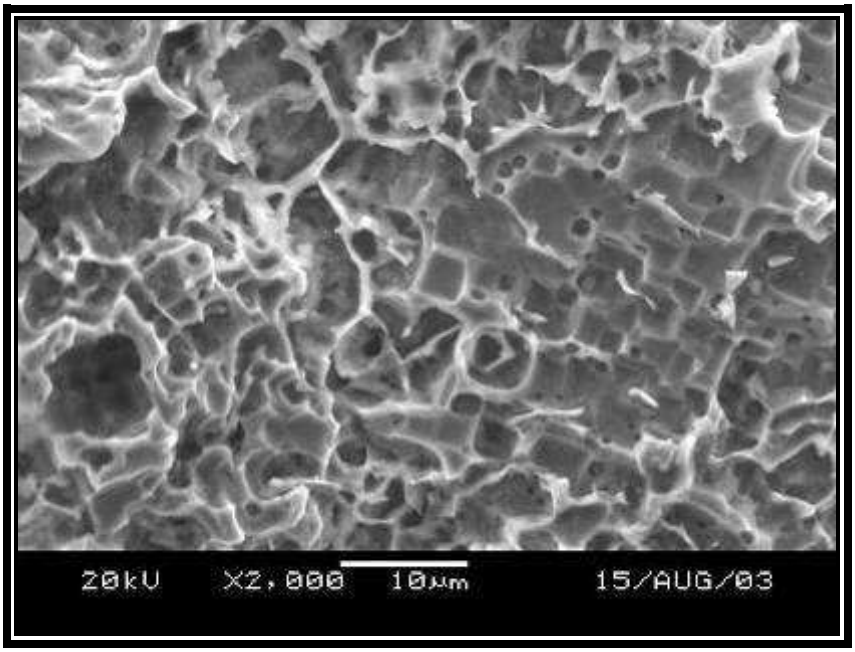

Figure 49: SEM photograph of type 309MoL filler material surface after 214 days exposure to a mixture of formic, acetic, propionic and heavier acids at an operating temperature of approximately 145 °C during the distillation of these organic acids as indicated in column A of Table 4 and Table 5.

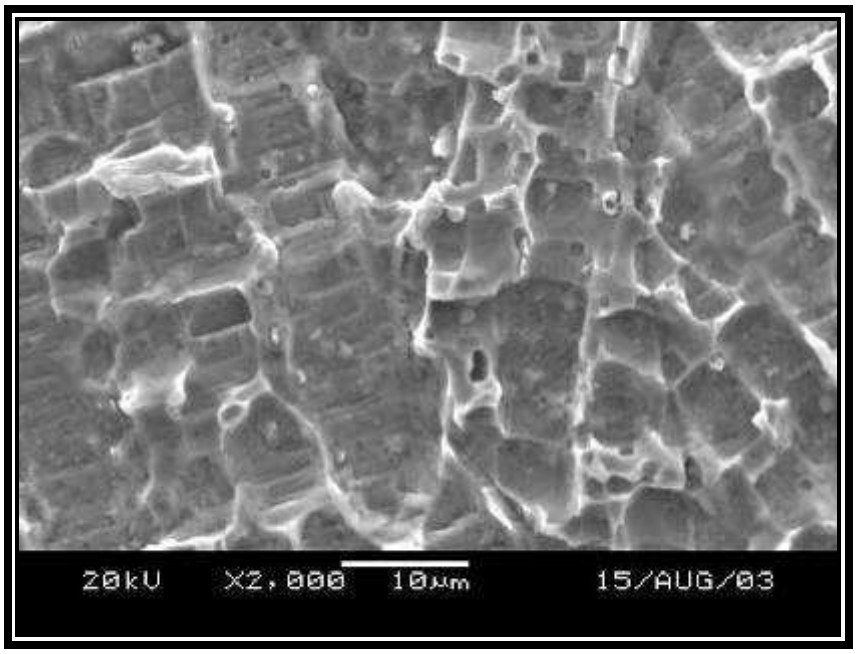

Figure 50: SEM photograph of type 904L filler material surface after 214 days exposure to a mixture of formic, acetic, propionic and heavier acids at an operating temperature of approximately 145 °C during the distillation of these organic acids as indicated in column A of Table 4 and Table 5.

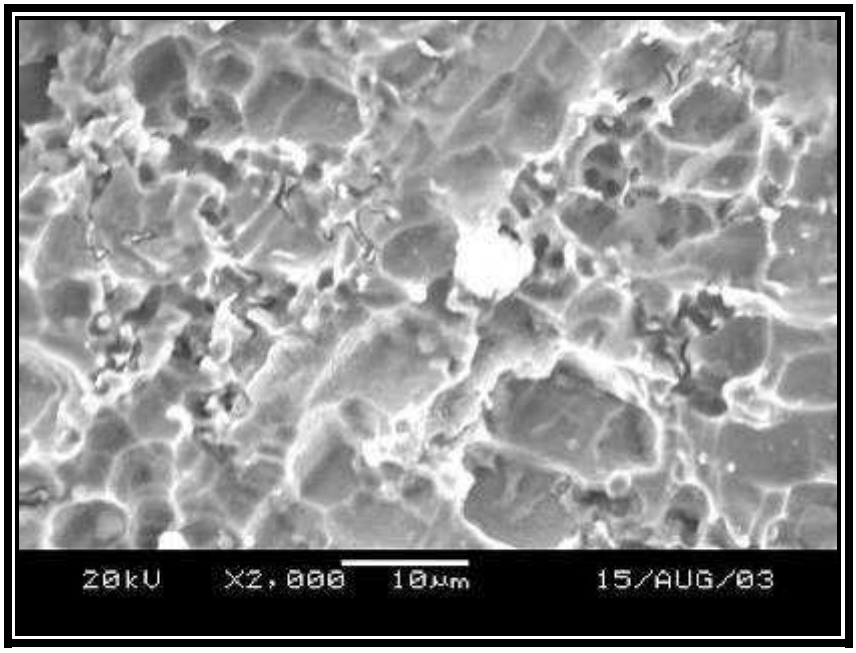

Figure 51: SEM photograph of type 625 filler material surface after 214 days exposure to a mixture of formic, acetic, propionic and heavier acids at an operating temperature of approximately 145 °C during the distillation of these organic acids as indicated in column A of Table 4 and Table 5.

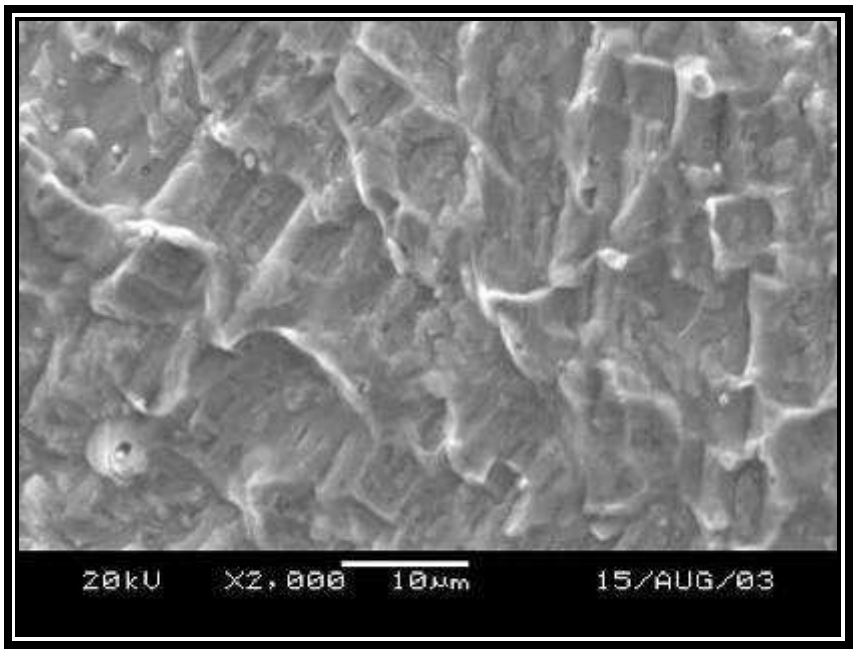

Figure 52: SEM photograph of type 825 filler material surface after 214 days exposure to a mixture of formic, acetic, propionic and heavier acids at an operating temperature of approximately 145 °C during the distillation of these organic acids as indicated in column A of Table 4 and Table 5.

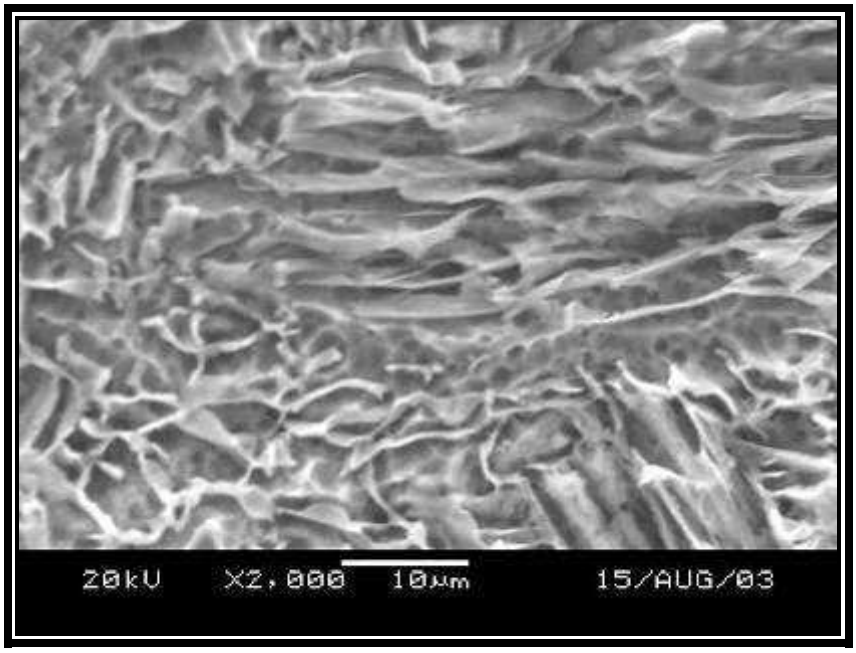

Figure 53: SEM photograph of type 2205 filler material surface after 214 days exposure to a mixture of formic, acetic, propionic and heavier acids at an operating temperature of approximately 145 °C during the distillation of these organic acids as indicated in column A of Table 4 and Table 5.

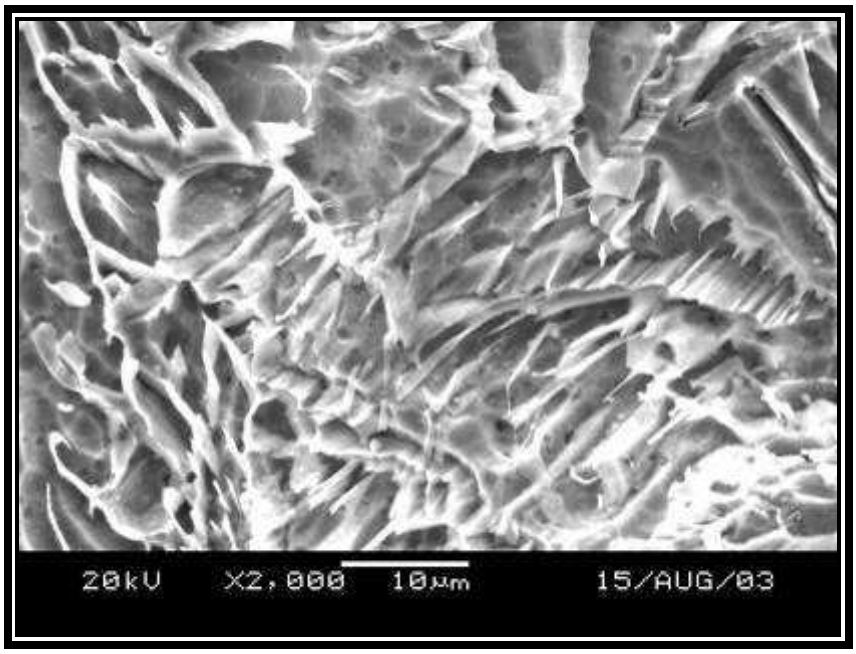

Figure 54: SEM photograph of type 2507 filler material surface after 214 days exposure to a mixture of formic, acetic, propionic and heavier acids at an operating temperature of approximately 145 °C during the distillation of these organic acids as indicated in column A of Table 4 and Table 5.

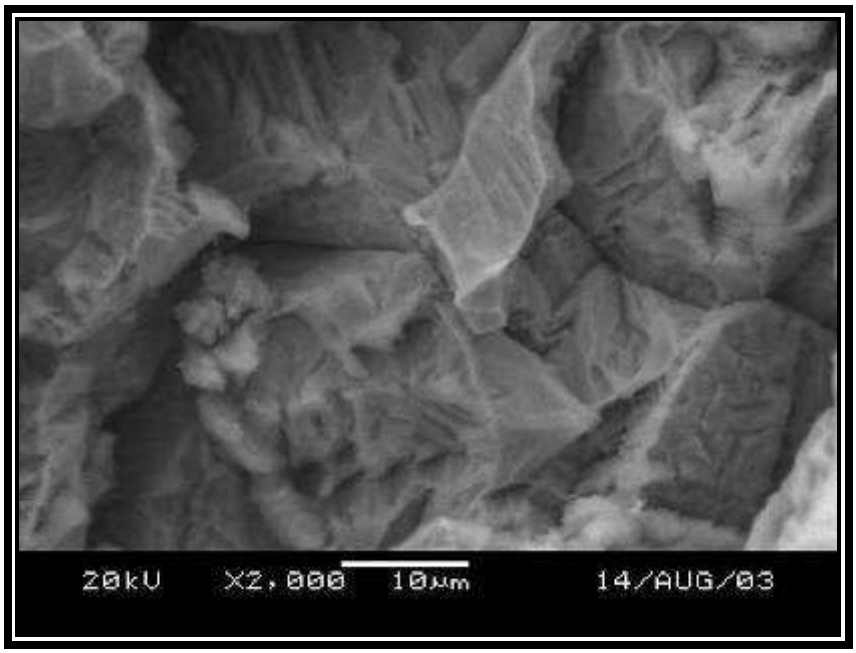

Figure 55: SEM photograph of type 316L plate material surface after 214 days exposure to a mixture of formic, acetic, propionic and heavier acids at an operating temperature of approximately 145 °C during the distillation of these organic acids as indicated in column A of Table 4 and Table 5.

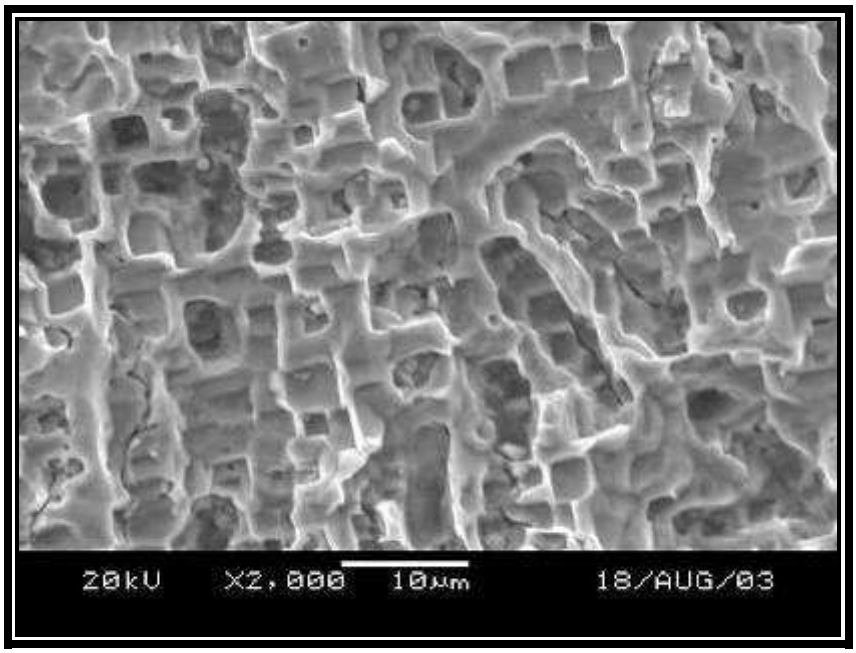

Figure 56: SEM photograph of type 316L weld filler material surface, after 214 days of exposure to a mixture of propionic and heavier acids at an operating temperature of approximately 179 °C during the distillation of organic acids as indicated in column B of Table 4 and Table 5.

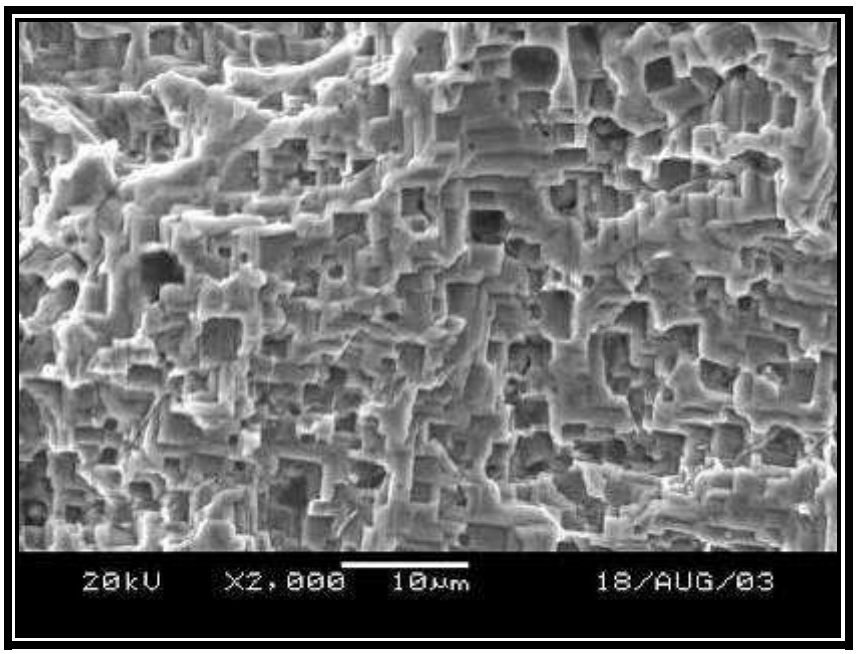

Figure 57: SEM photograph of type 317L weld filler material surface, after 214 days of exposure to a mixture of propionic and heavier acids at an operating temperature of approximately 179 °C during the distillation of organic acids as indicated in column B of Table 4 and Table 5.

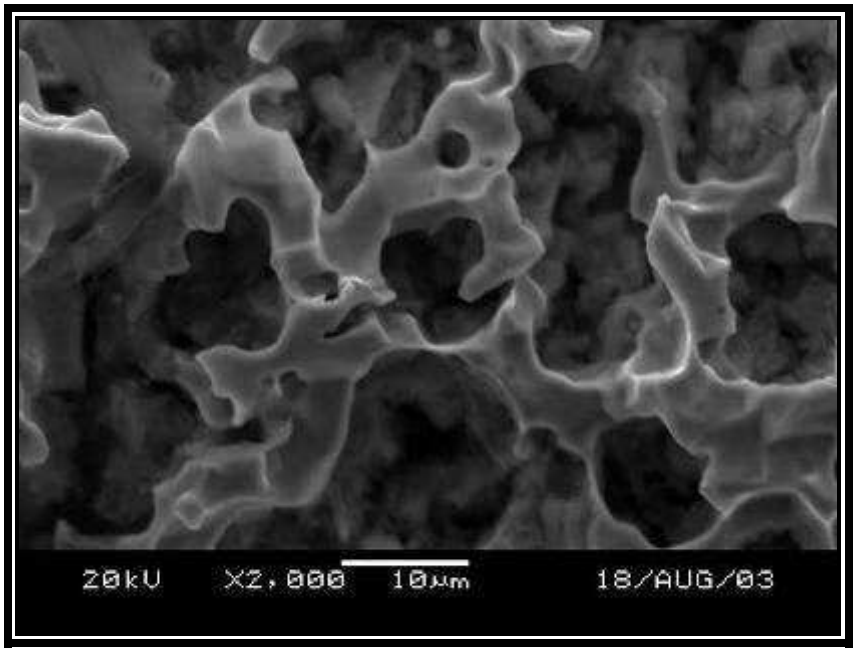

Figure 58: SEM photograph of type 309L weld filler material surface, after 214 days of exposure to a mixture of propionic and heavier acids at an operating temperature of approximately 179 °C during the distillation of organic acids as indicated in column B of Table 4 and Table 5.

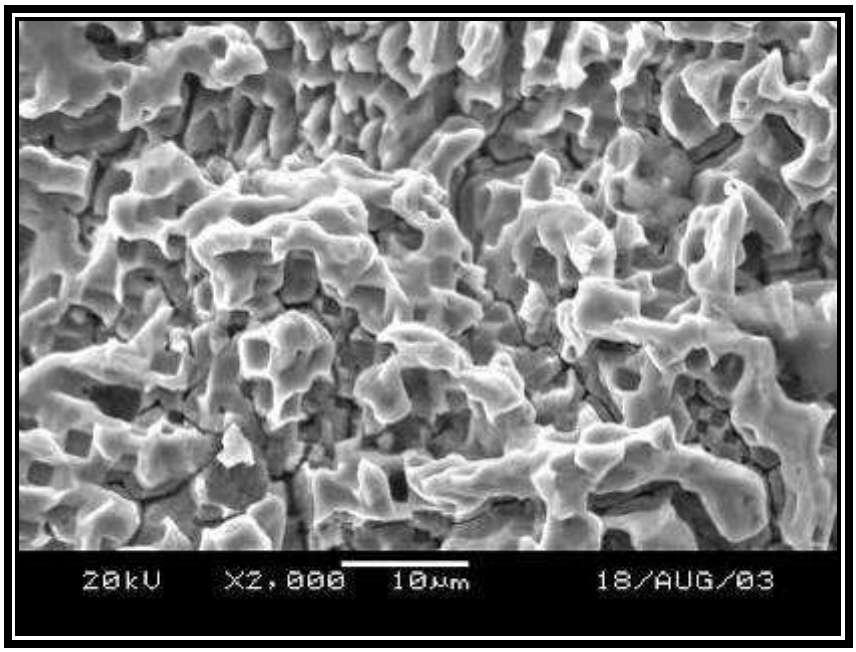

Figure 59: SEM photograph of type 309MoL weld filler material surface, after 214 days of to a mixture of propionic and heavier acids at an operating temperature of approximately 179 °C during the distillation of organic acids as indicated in column B of Table 4 and Table 5.

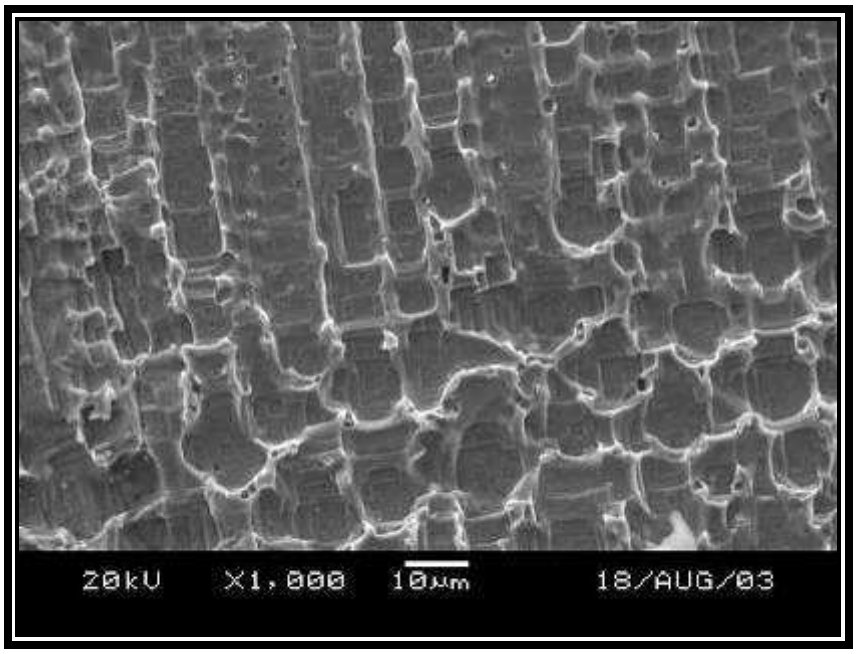

Figure 60: SEM photograph of type 904 weld filler material surface, after 214 days of to a mixture of propionic and heavier acids at an operating temperature of approximately 179 °C during the distillation of organic acids as indicated in column B of Table 4 and Table 5.

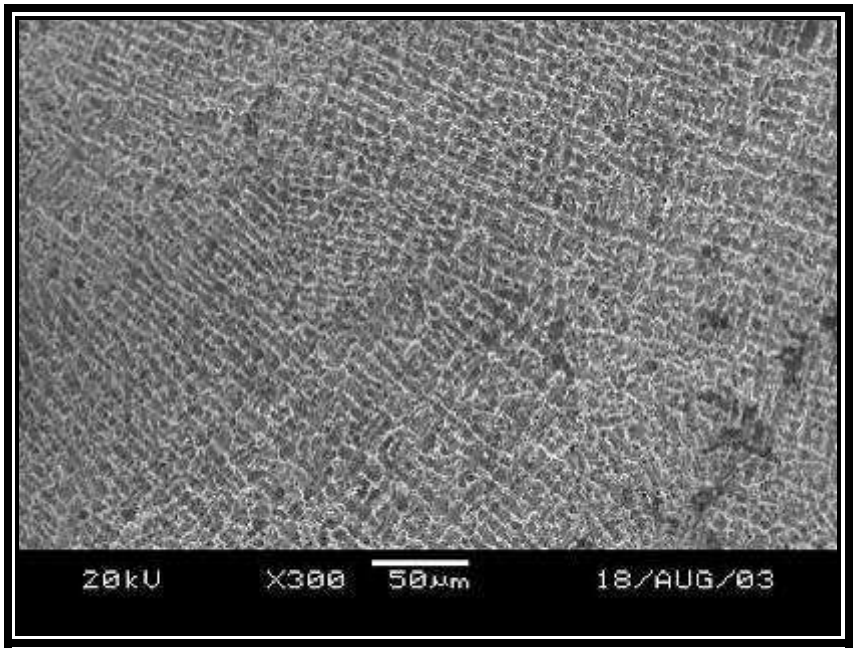

Figure 61: SEM photograph of type 625 weld filler material surface, after 214 days of to a mixture of propionic and heavier acids at an operating temperature of approximately 179 °C during the distillation of organic acids as indicated in column B of Table 4 and Table 5.

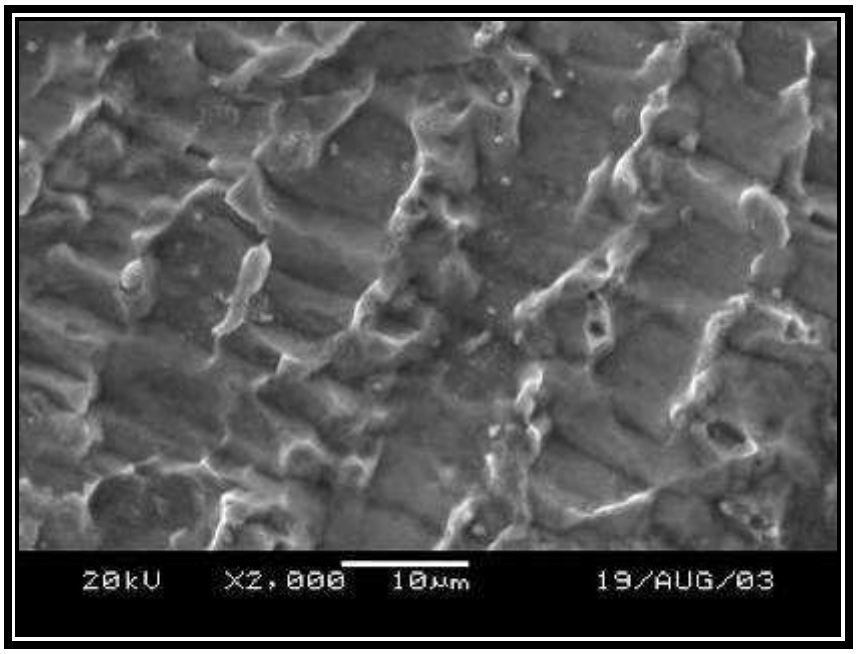

Figure 62: SEM photograph of type 825 weld filler material surface, after 214 days of to a mixture of propionic and heavier acids at an operating temperature of approximately 179 °C during the distillation of organic acids as indicated in column B of Table 4 and Table 5.

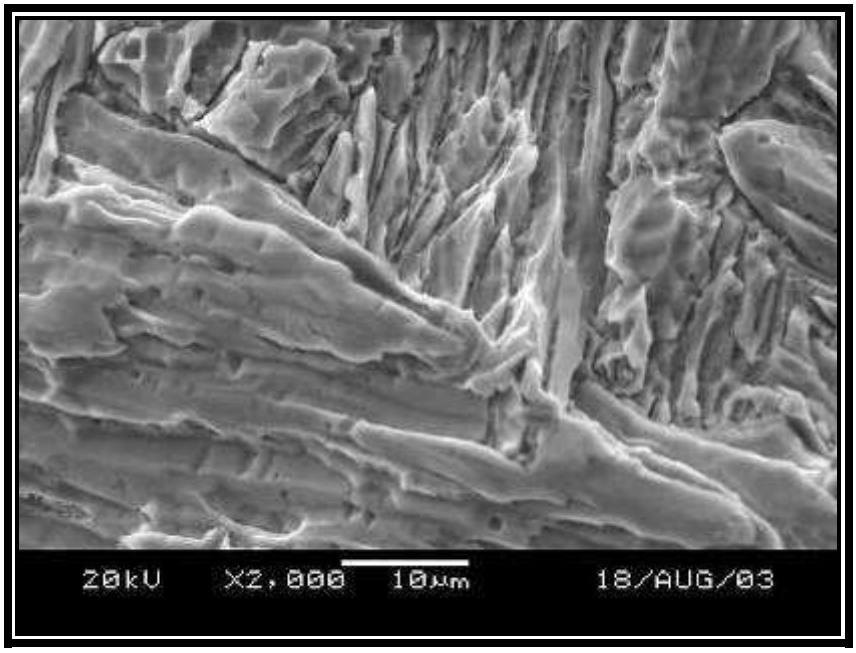

Figure 63: SEM photograph of type 2205 weld filler material surface, after 214 days of exposure to a mixture of propionic and heavier acids at an operating temperature of approximately 179 °C during the distillation of organic acids as indicated in column B of Table 4 and Table 5.

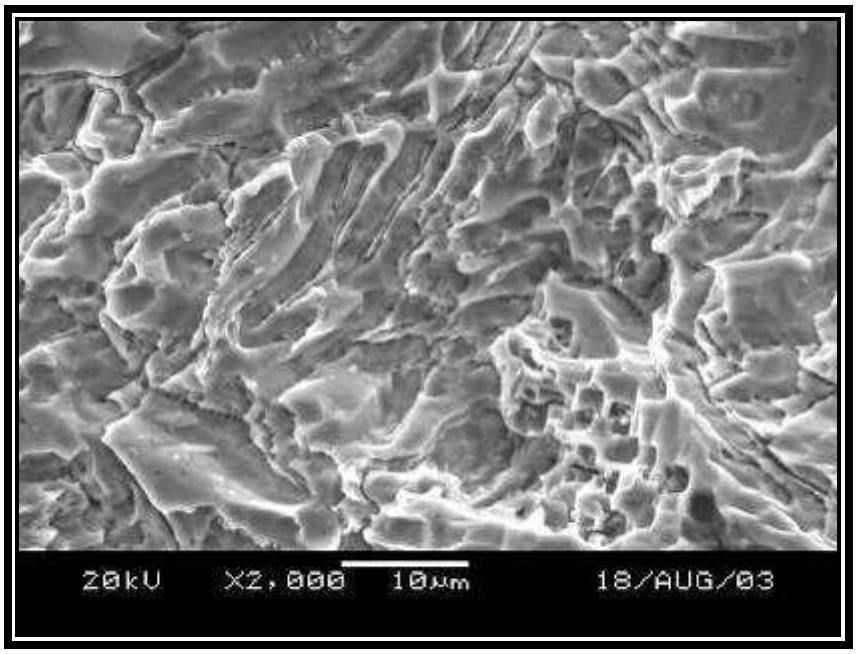

Figure 64: SEM photograph of type 2507 weld filler material surface, after 214 days of to a mixture of propionic and heavier acids at an operating temperature of approximately 179 °C during the distillation of organic acids as indicated in column B of Table 4 and Table 5.

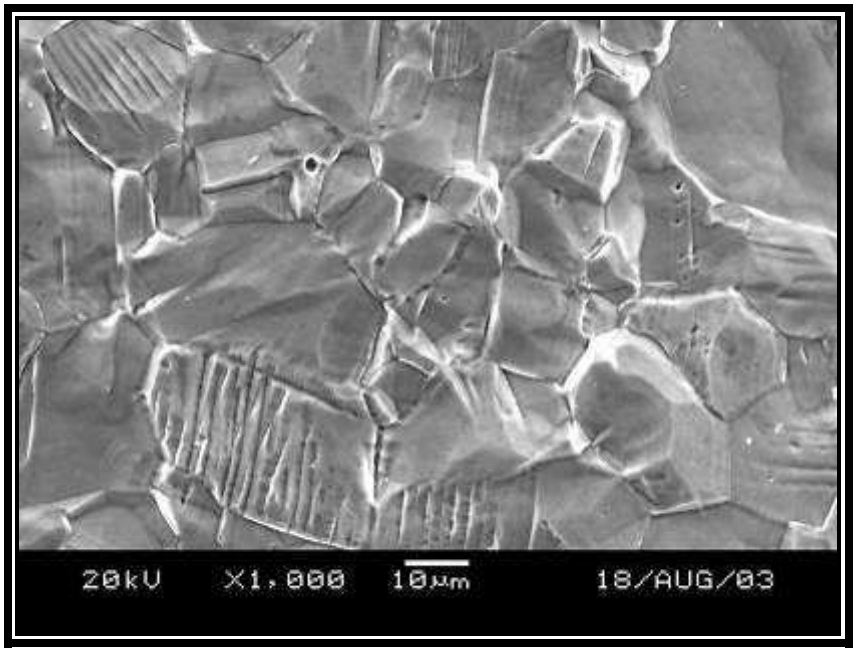

Figure 65: SEM photograph of type 316L plate material surface, after 214 days of to a mixture of propionic and heavier acids at an operating temperature of approximately 179 °C during the distillation of organic acids as indicated in column B of Table 4 and Table 5.

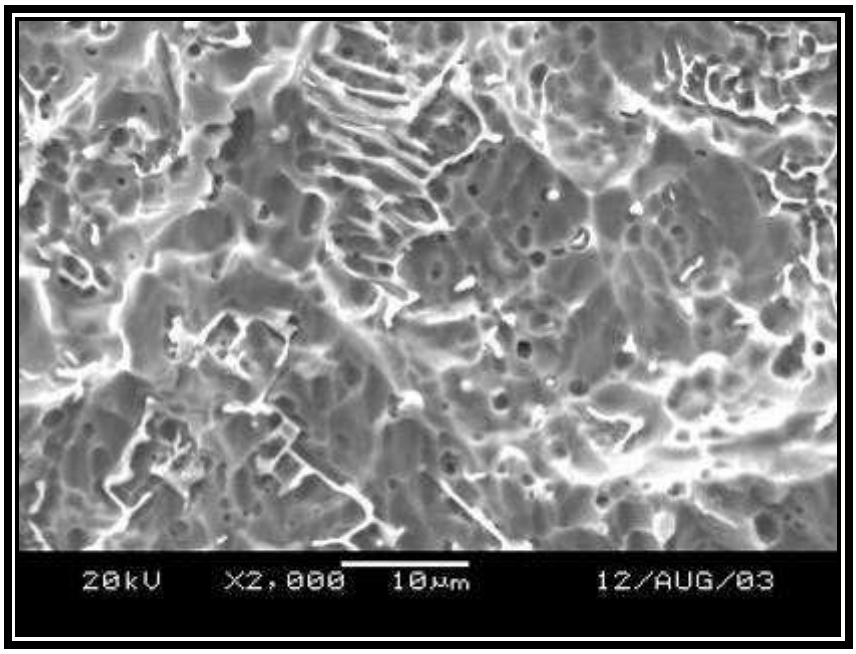

Figure 66: SEM photograph of type 316L weld filler material surface, after 214 days of exposure to a mixture of formic, acetic, propionic and heavier acids at an operating temperature of approximately 125 °C during the distillation of organic acids as indicated in column C of Table 4 and Table 5.

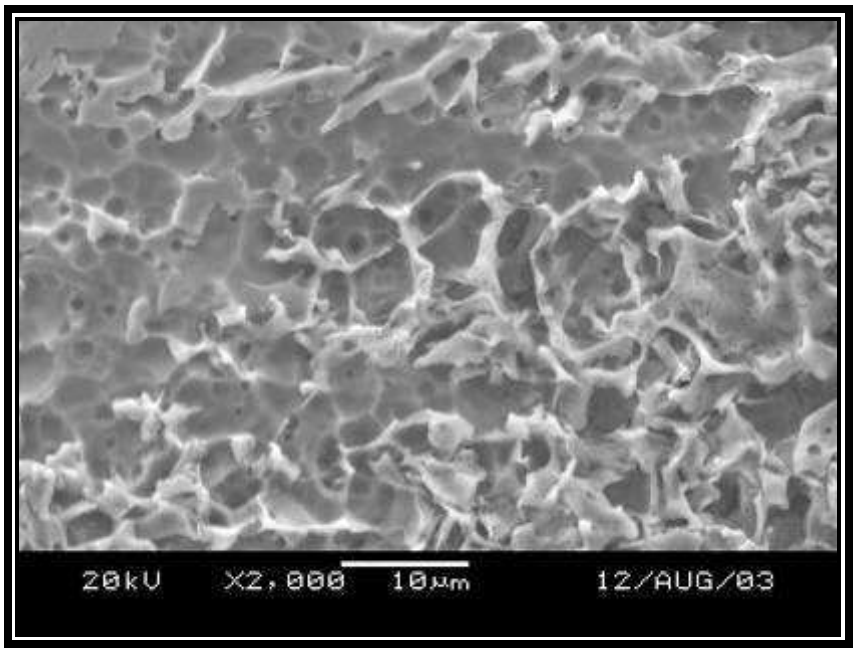

Figure 67: SEM photograph of type 317L weld filler material surface, after 214 days of exposure to a mixture of formic, acetic, propionic and heavier acids at an operating temperature of approximately 125 °C during the distillation of organic acids as indicated in column C of Table 4 and Table 5.

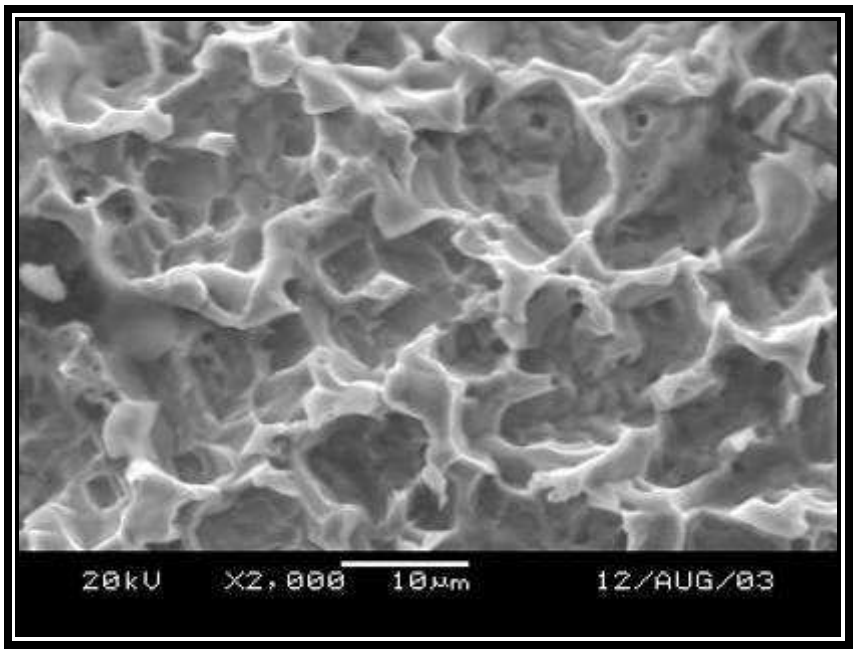

Figure 68: SEM photograph of type 309L weld filler material surface, after 214 days of exposure to a mixture of formic, acetic, propionic and heavier acids at an operating temperature of approximately 125 °C during the distillation of organic acids as indicated in column C of Table 4 and Table 5.

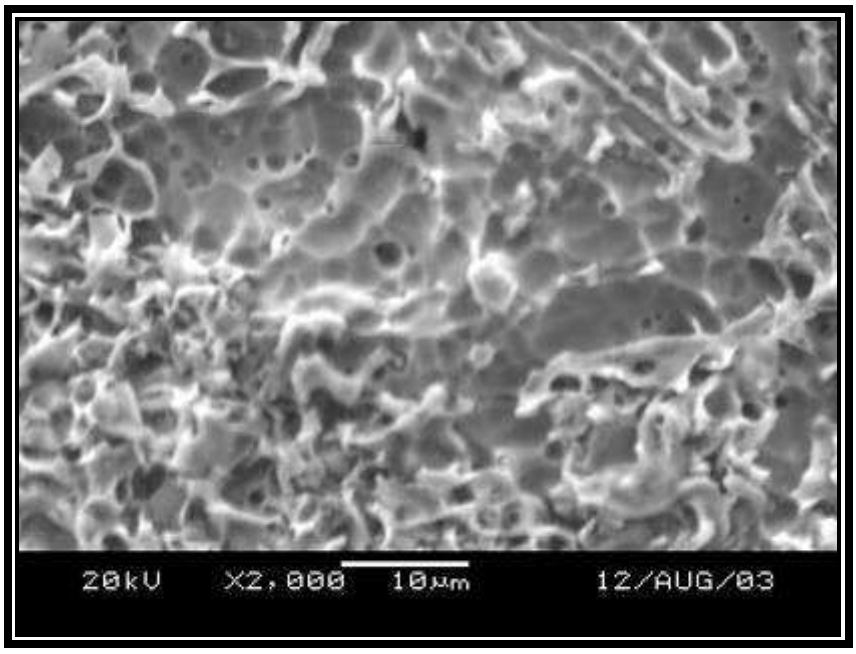

Figure 69: SEM photograph of type 309MoL weld filler material surface, after 214 days of exposure to a mixture of formic, acetic, propionic and heavier acids at an operating temperature of approximately 125 °C during the distillation of organic acids as indicated in column C of Table 4 and Table 5.

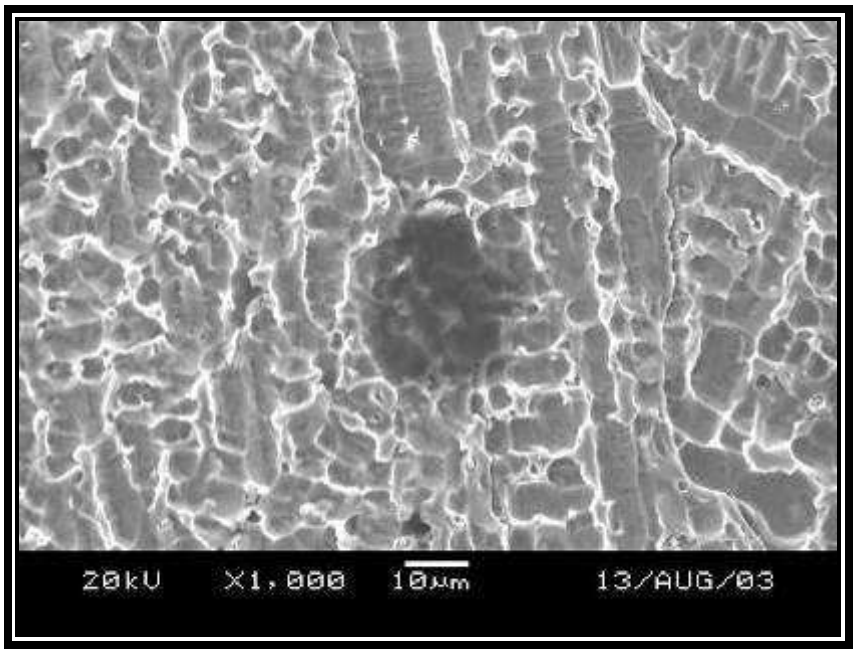

Figure 70: SEM photograph of type 904 weld filler material surface, after 214 days of exposure to a mixture of formic, acetic, propionic and heavier acids at an operating temperature of approximately 125 °C during the distillation of organic acids as indicated in column C of Table 4 and Table 5.

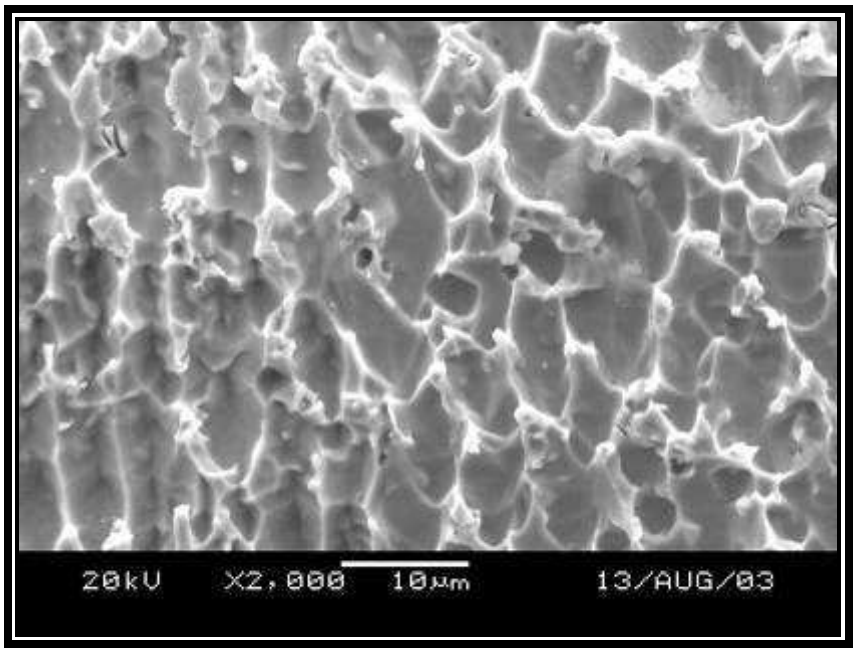

Figure 71: SEM photograph of type 625 weld filler material surface, after 214 days of exposure to a mixture of formic, acetic, propionic and heavier acids at an operating temperature of approximately 125 °C during the distillation of organic acids as indicated in column C of Table 4 and Table 5.

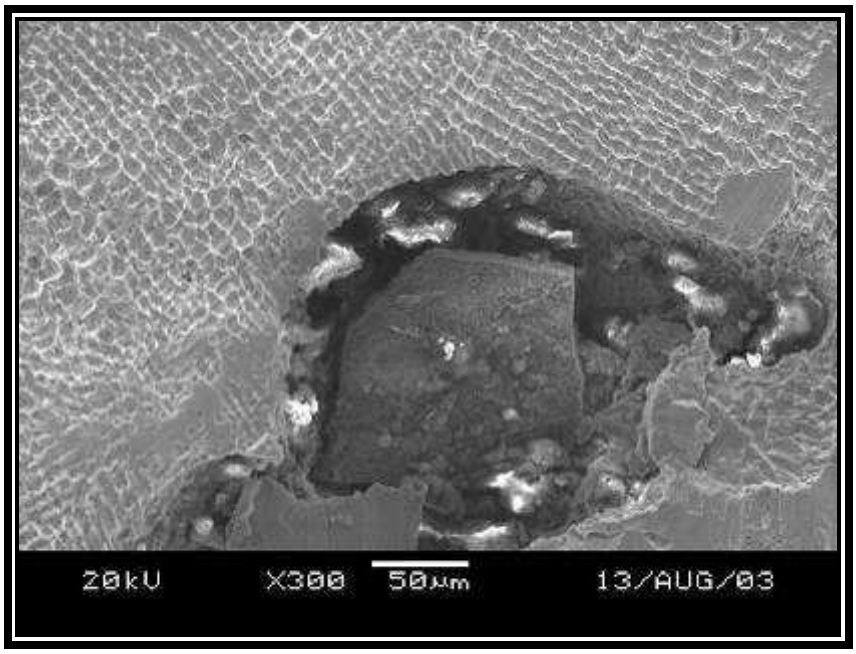

Figure 72: SEM photograph of type 825 weld filler material surface, after 214 days of exposure to a mixture of formic, acetic, propionic and heavier acids at an operating temperature of approximately 125 °C during the distillation of organic acids as indicated in column C of Table 4 and Table 5.

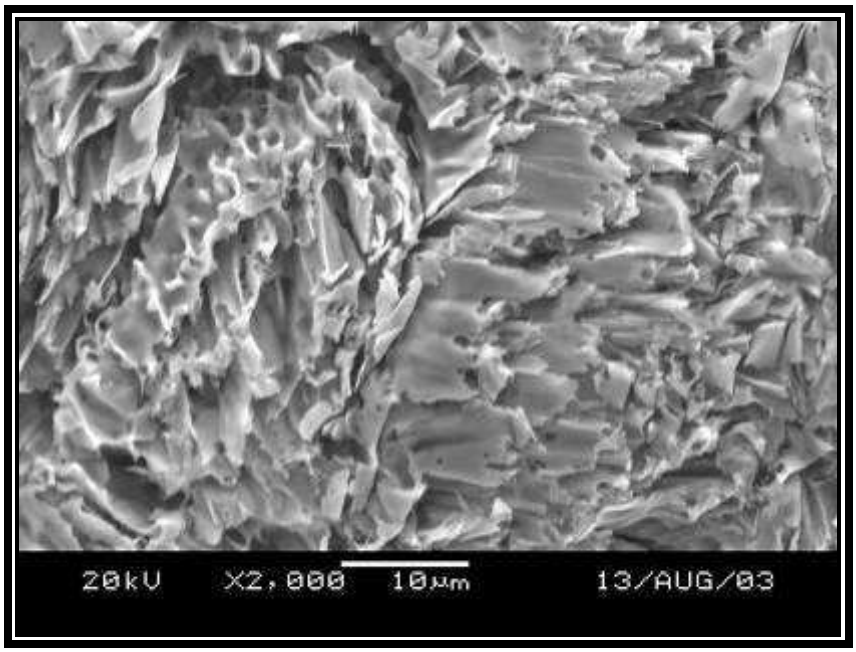

Figure 73: SEM photograph of type 2205 weld filler material surface, after 214 days of exposure to a mixture of formic, acetic, propionic and heavier acids at an operating temperature of approximately 125 °C during the distillation of organic acids as indicated in column C of Table 4 and Table 5.

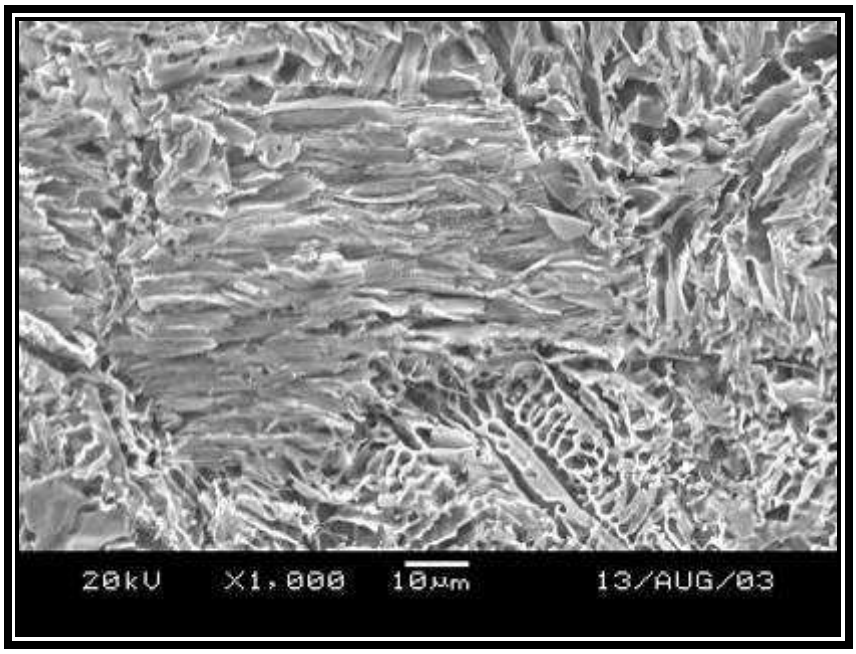

Figure 74: SEM photograph of type 2507 weld filler material surface, after 214 days of exposure to a mixture of formic, acetic, propionic and heavier acids at an operating temperature of approximately 125 °C during the distillation of organic acids as indicated in column C of Table 4 and Table 5.

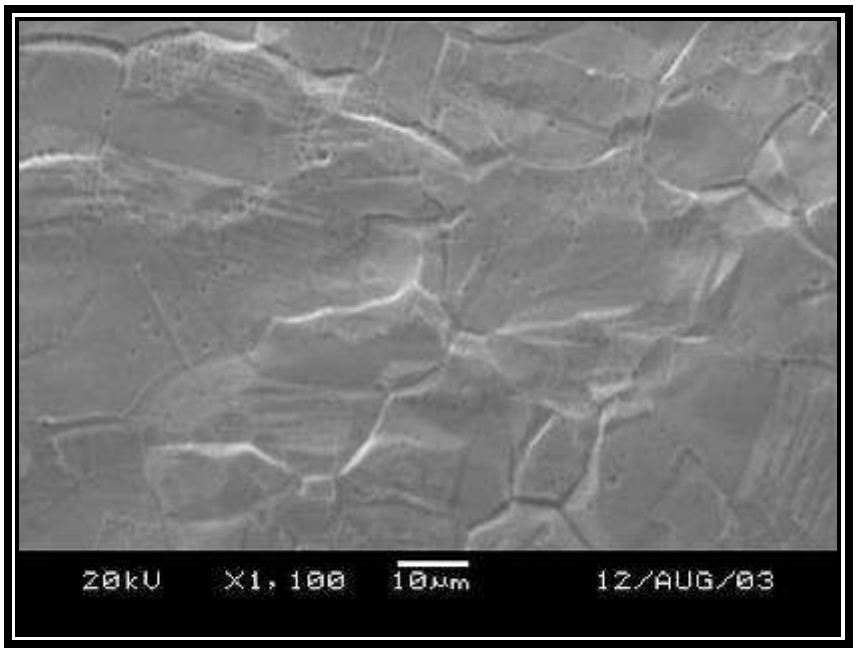

Figure 75: SEM photograph of type 316L plate material surface, after 214 days of exposure to a mixture of formic, acetic, propionic and heavier acids at an operating temperature of approximately 125 °C during the distillation of organic acids as indicated in column C of Table 4 and Table 5.

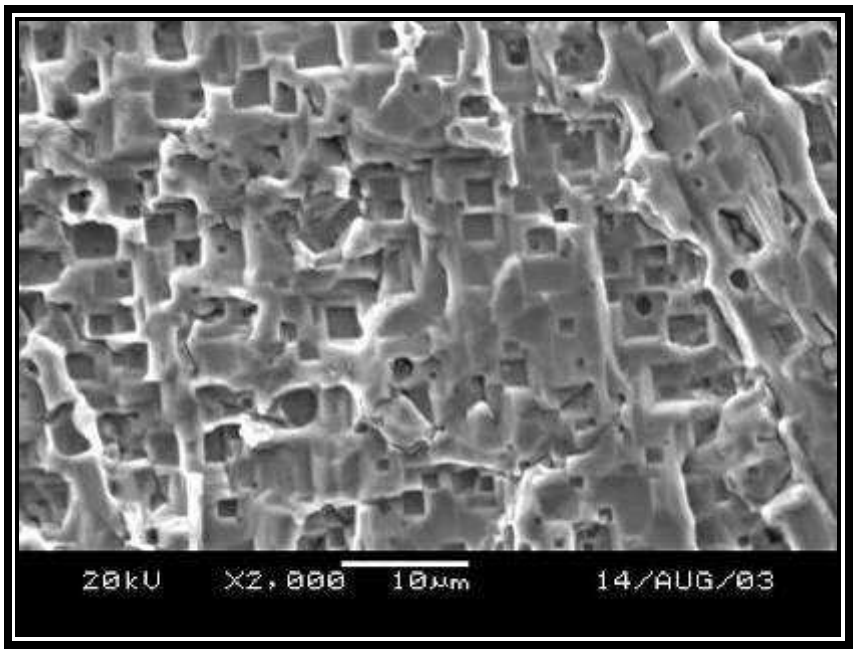

Figure 76: SEM photograph of type 316L weld filler material surface, after 214 days of exposure to a mixture of formic, acetic and propionic acids at an operating temperature of approximately 119 °C during the distillation of organic acids as indicated in column D of Table 4 and Table 5.

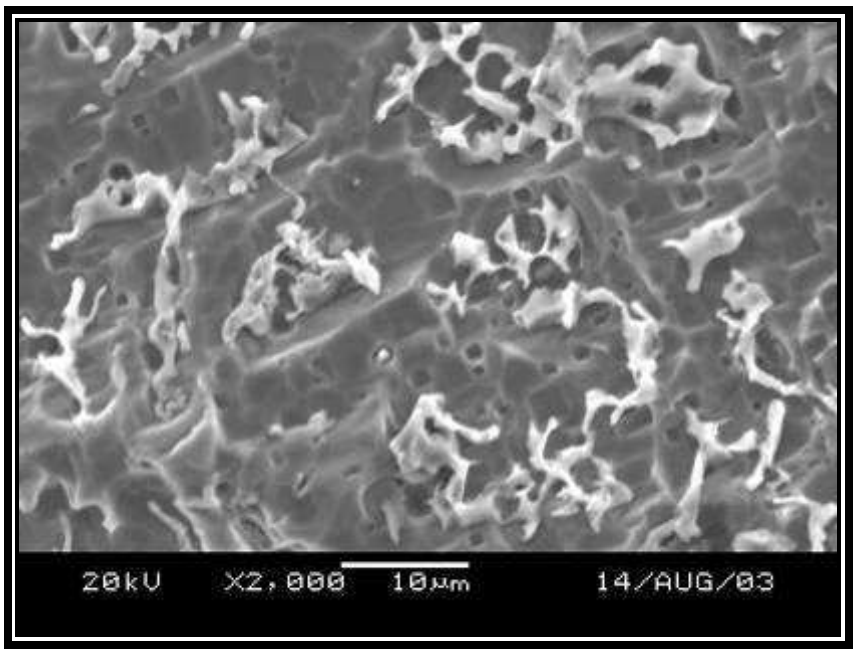

Figure 77: SEM photograph of type 317L weld filler material surface, after 214 days of exposure to a mixture of formic, acetic and propionic acids at an operating temperature of approximately 119 °C during the distillation of organic acids as indicated in column D of Table 4 and Table 5.

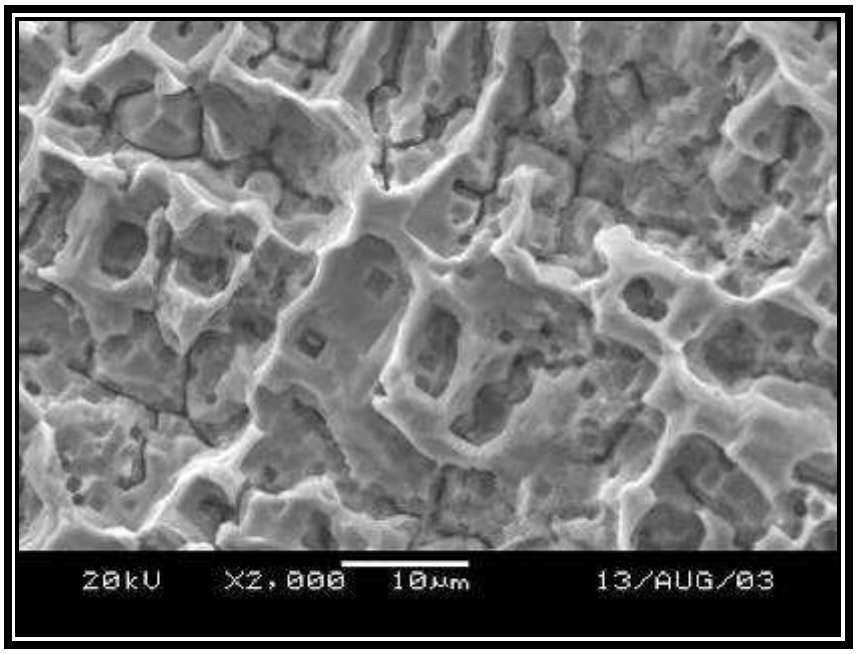

Figure 78: SEM photograph of type 309L weld filler material surface, after 214 days of exposure to a mixture of formic, acetic and propionic acids at an operating temperature of approximately 119 °C during the distillation of organic acids as indicated in column D of Table 4 and Table 5.

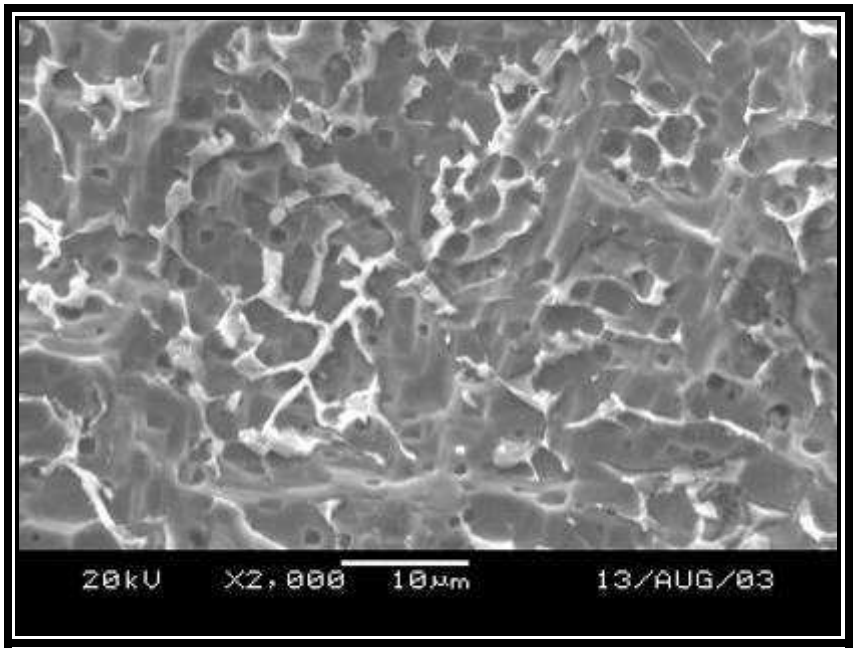

Figure 79: SEM photograph of type 309MoL weld filler material surface, after 214 days of exposure to a mixture of formic, acetic and propionic acids at an operating temperature of approximately 119 °C during the distillation of organic acids as indicated in column D of Table 4 and Table 5.

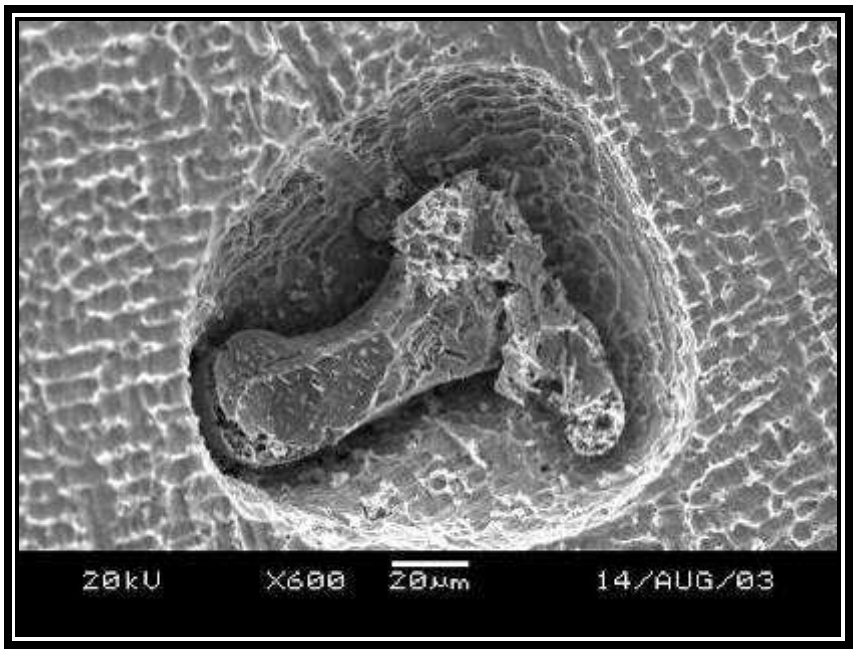

Figure 80: SEM photograph of type 904L weld filler material surface, after 214 days of exposure to a mixture of formic, acetic and propionic acids at an operating temperature of approximately 119 °C during the distillation of organic acids as indicated in column D of Table 4 and Table 5.

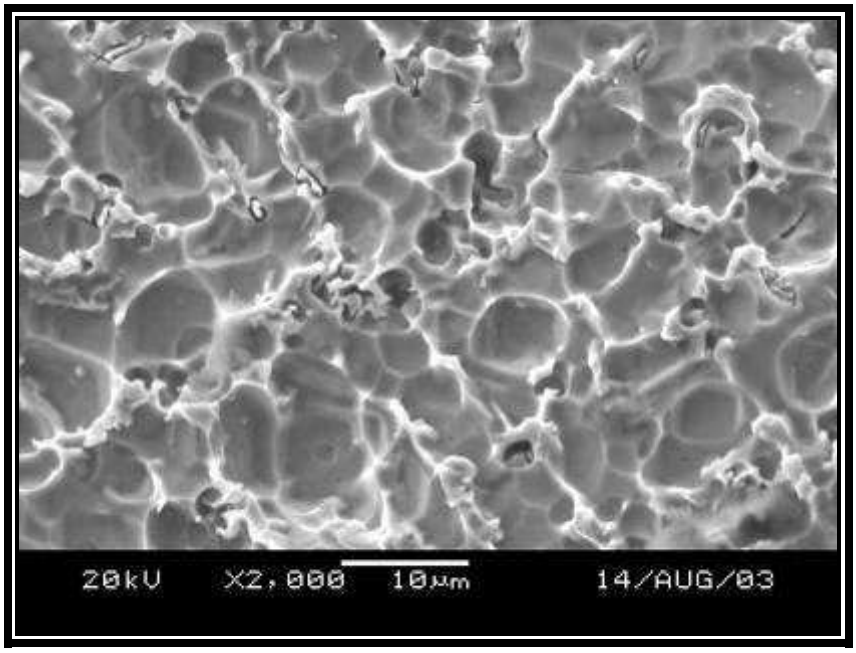

Figure 81: SEM photograph of type 625 weld filler material surface, after 214 days of exposure to a mixture of formic, acetic and propionic acids at an operating temperature of approximately 119 °C during the distillation of organic acids as indicated in column D of Table 4 and Table 5.

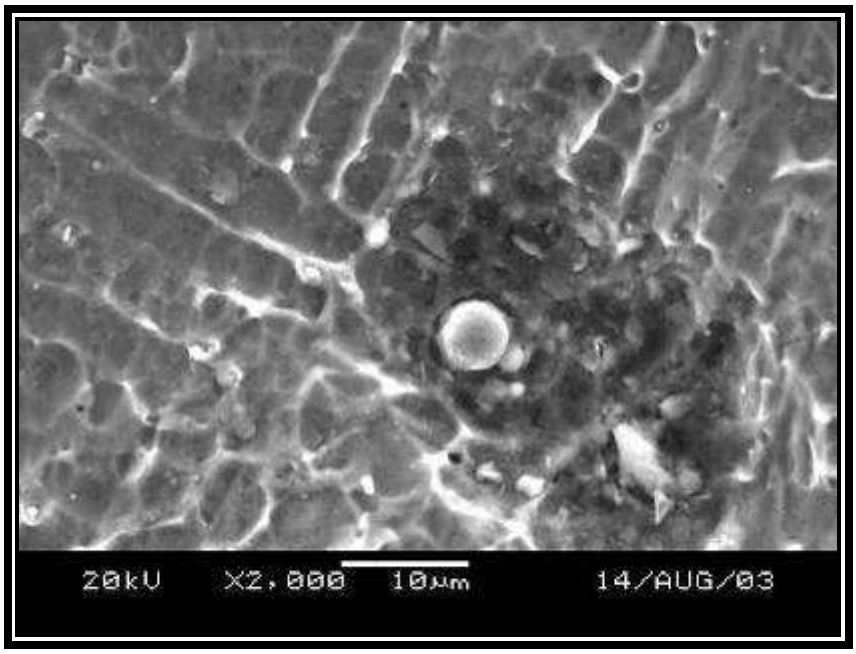

Figure 82: SEM photograph of type 825 weld filler material surface, after 214 days of exposure to a mixture of formic, acetic and propionic acids at an operating temperature of approximately 119 °C during the distillation of organic acids as indicated in column D of Table 4 and Table 5.

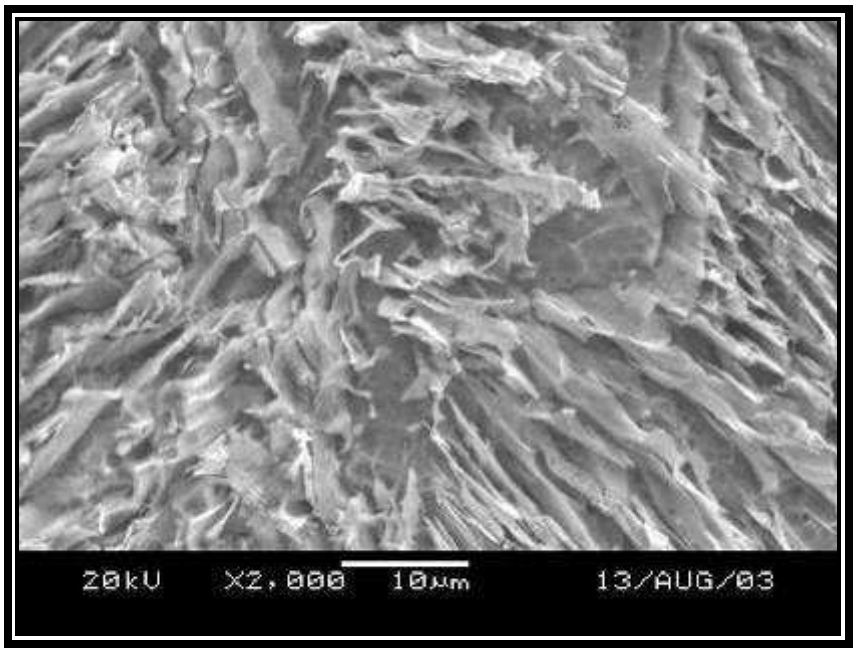

Figure 83: SEM photograph of type 2205 weld filler material surface, after 214 days of exposure to a mixture of formic, acetic and propionic acids at an operating temperature of approximately 119 °C during the distillation of organic acids as indicated in column D of Table 4 and Table 5.

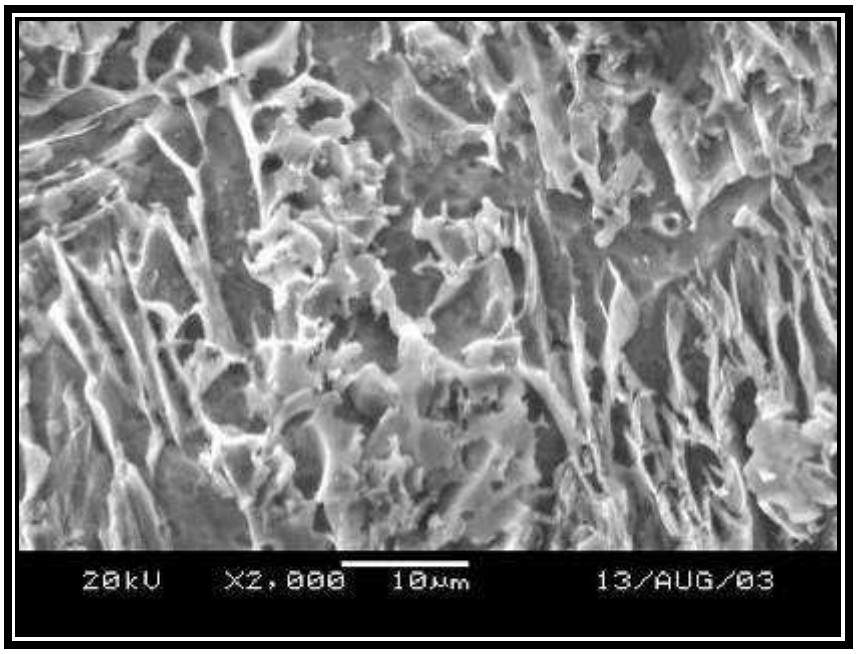

Figure 84: SEM photograph of type 2507 weld filler material surface, after 214 days of exposure to a mixture of formic, acetic and propionic acids at an operating temperature of approximately 119 °C during the distillation of organic acids as indicated in column D of Table 4 and Table 5.

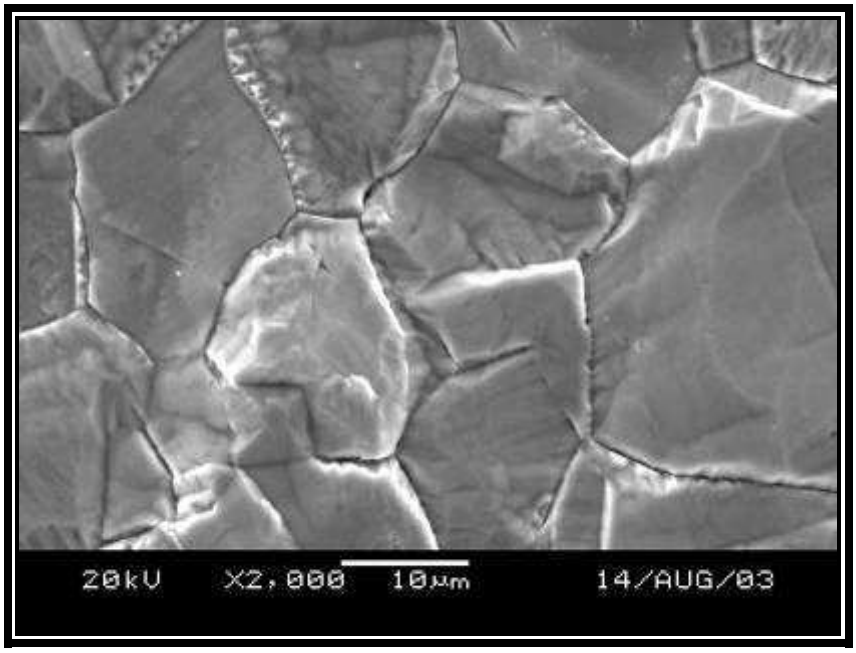

Figure 85: SEM photograph of type 316L plate material surface, after 214 days of exposure to a mixture of formic, acetic and propionic acids at an operating temperature of approximately 119 °C during the distillation of organic acids as indicated in column D of Table 4 and Table 5.

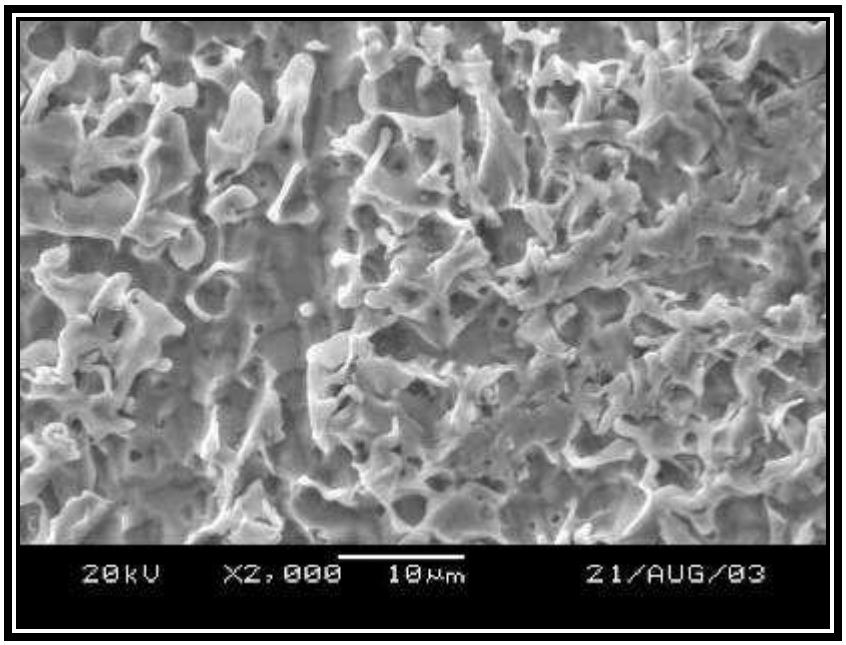

Figure 86: SEM photograph of type 316L weld filler material surface, after 214 days of exposure to propionic acid at an operating temperature of approximately 156 °C during the distillation of organic acids as indicated in column E of Table 4 and Table 5.

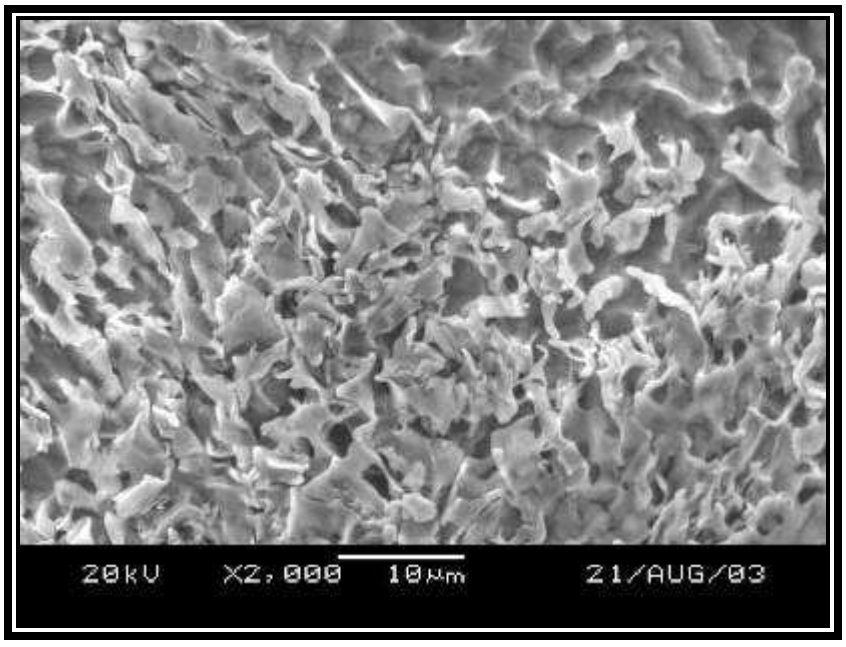

Figure 87: SEM photograph of type 317L weld filler material surface, after 214 days of exposure to propionic acid at an operating temperature of approximately 156 °C during the distillation of organic acids as indicated in column E of Table 4 and Table 5.

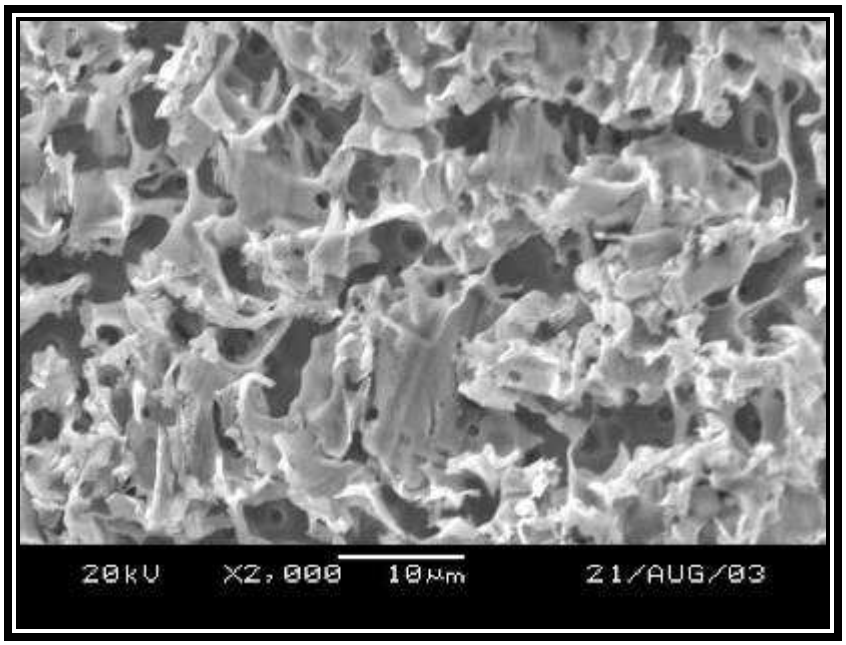

Figure 88: SEM photograph of type 309L weld filler material surface, after 214 days of exposure to propionic acid at an operating temperature of approximately 156 °C during the distillation of organic acids as indicated in column E of Table 4 and Table 5.

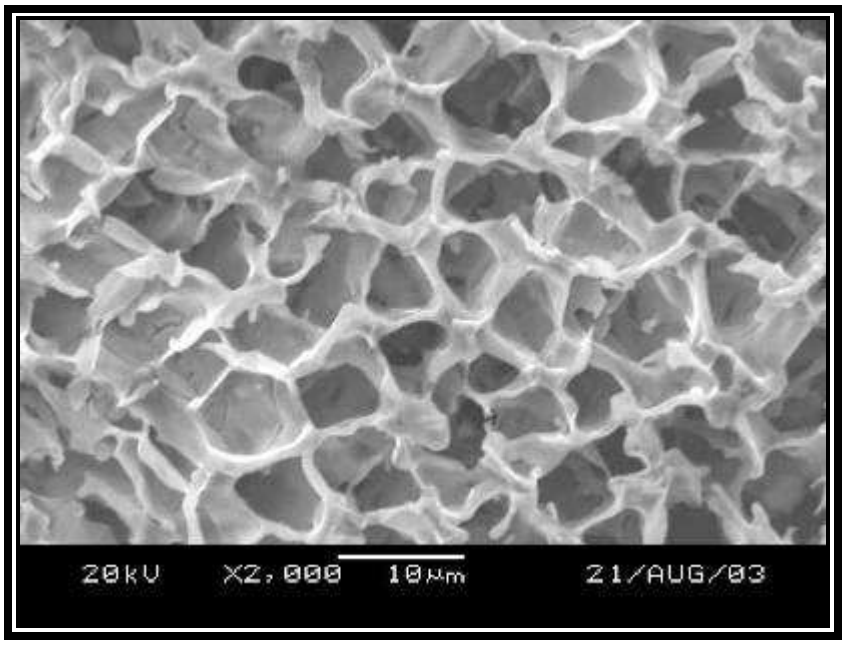

Figure 89: SEM photograph of type 309MoL weld filler material surface, after 214 days of exposure to propionic acid at an operating temperature of approximately 156 °C during the distillation of organic acids as indicated in column E of Table 4 and Table 5.

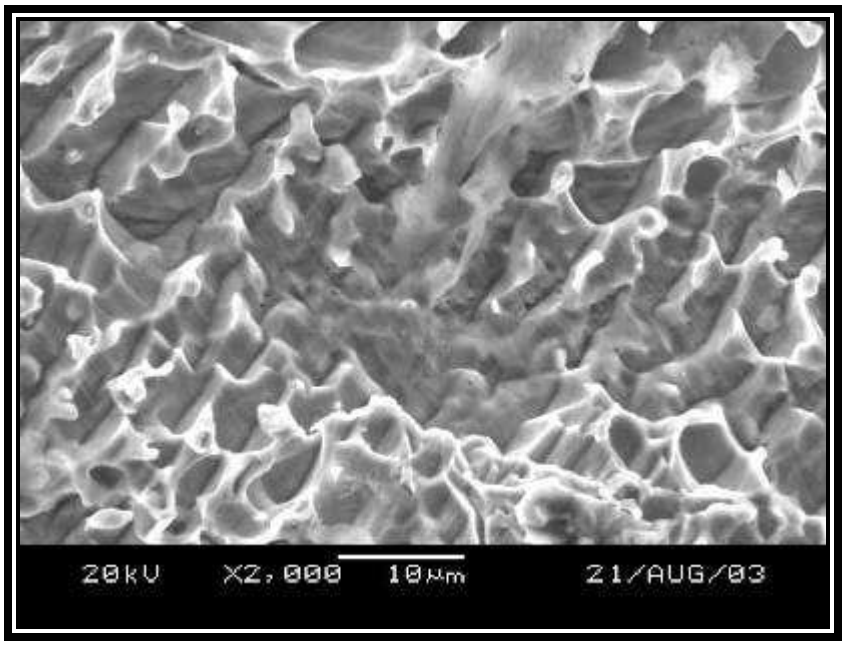

Figure 90: SEM photograph of type 904L weld filler material surface, after 214 days of exposure to propionic acid at an operating temperature of approximately 156 °C during the distillation of organic acids as indicated in column E of Table 4 and Table 5.

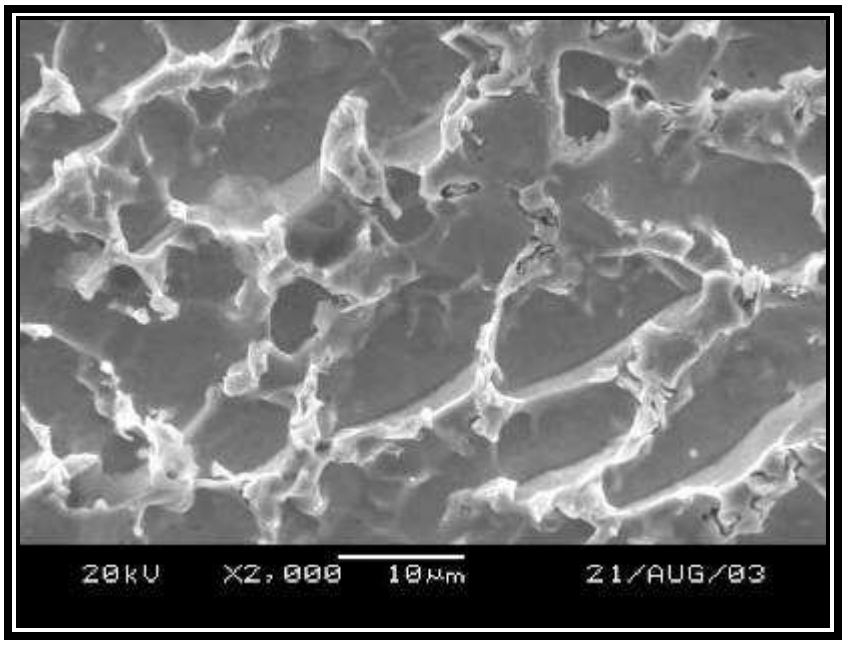

Figure 91: SEM photograph of type 625 weld filler material surface, after 214 days of exposure to propionic acid at an operating temperature of approximately 156 °C during the distillation of organic acids as indicated in column E of Table 4 and Table 5.

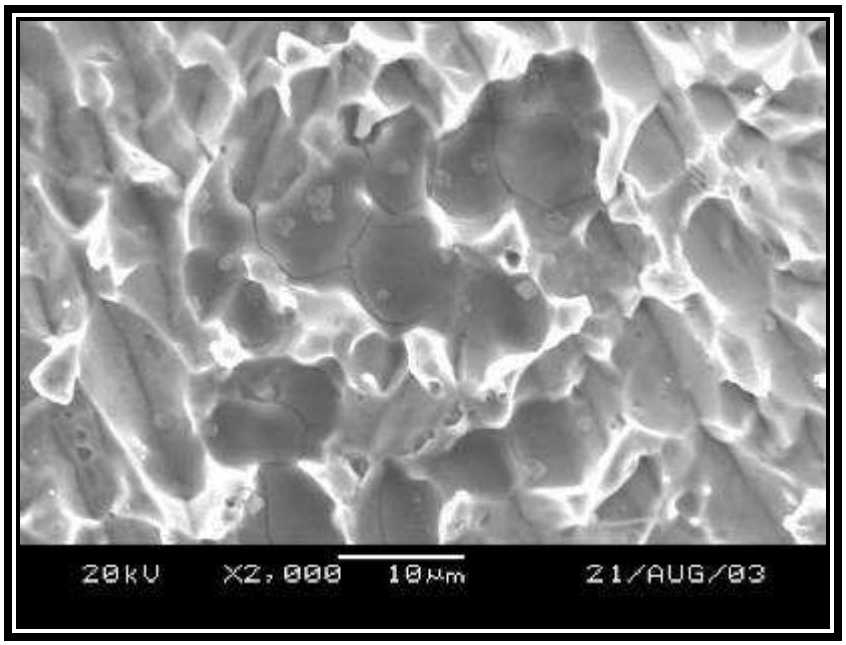

Figure 92: SEM photograph of type 825 weld filler material surface, after 214 days of exposure to propionic acid at an operating temperature of approximately 156 °C during the distillation of organic acids as indicated in column E of Table 4 and Table 5.

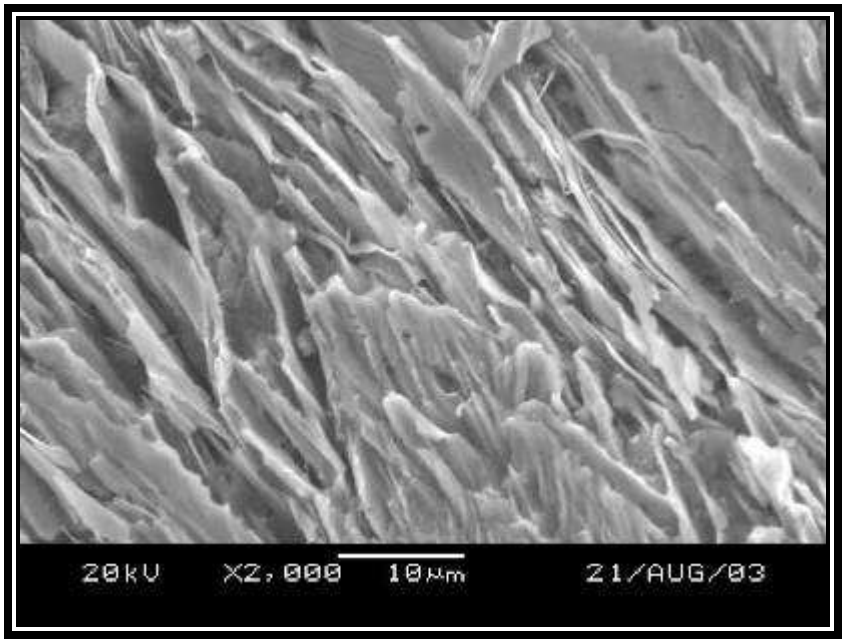

Figure 93: SEM photograph of type 2205 weld filler material surface, after 214 days of exposure to propionic acid at an operating temperature of approximately 156 °C during the distillation of organic acids as indicated in column E of Table 4 and Table 5.

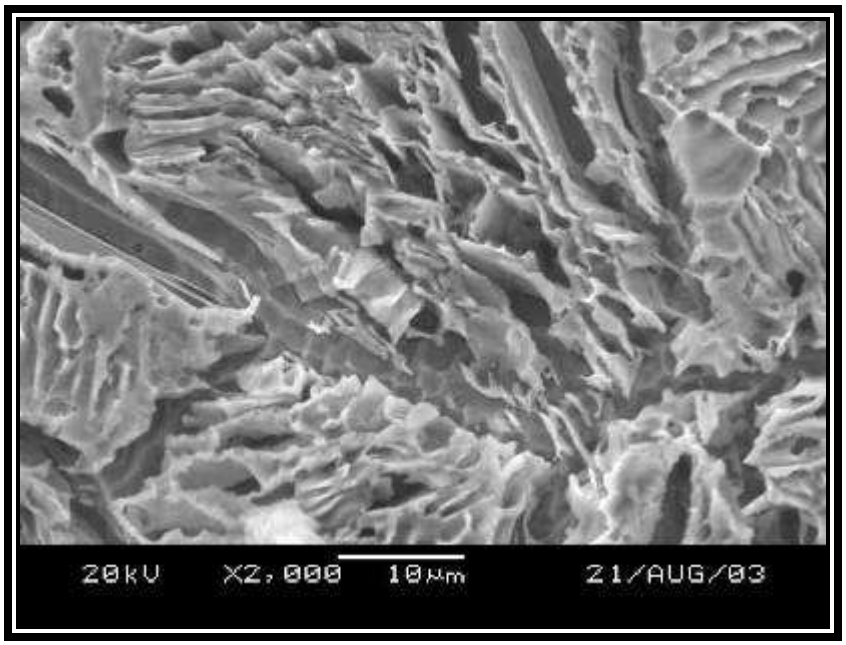

Figure 94: SEM photograph of type 2507 weld filler material surface, after 214 days of exposure to propionic acid at an operating temperature of approximately 156 °C during the distillation of organic acids as indicated in column E of Table 4 and Table 5.

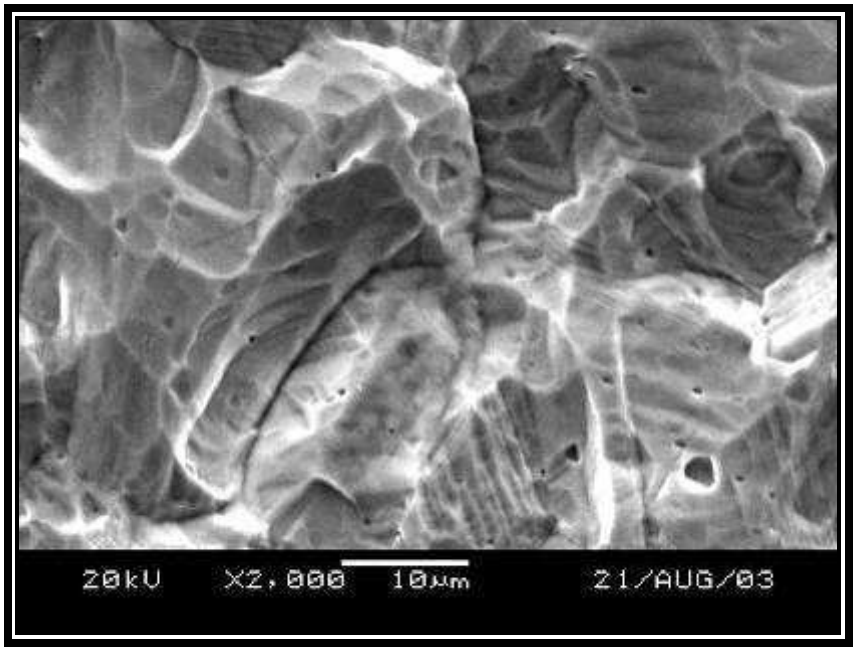

Figure 95: SEM photograph of type 316L plate material surface, after 214 days of exposure to propionic acid at an operating temperature of approximately 156 °C during the distillation of organic acids as indicated in column E of Table 4 and Table 5.

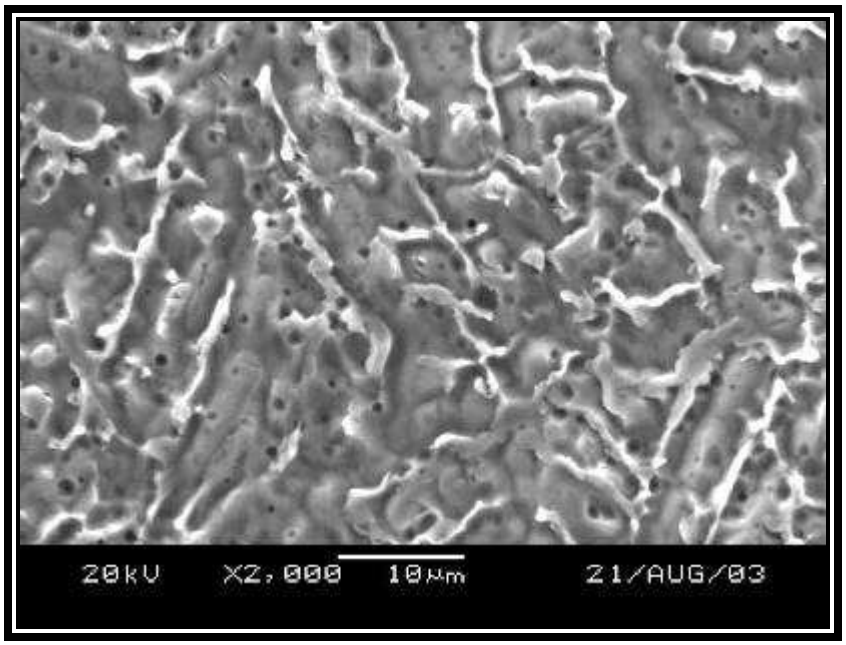

Figure 96: SEM photograph of type 316L weld filler material surface, after 214 days of exposure to formic, acetic and propionic acids at an operating temperature of approximately 154 °C during the distillation of organic acids as indicated in column F of Table 4 and Table 5.

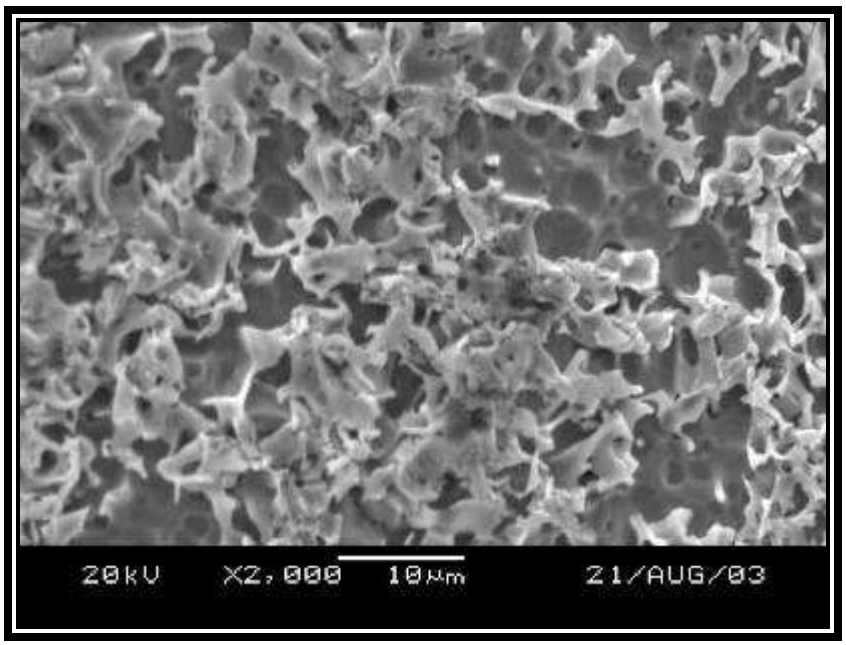

Figure 97: SEM photograph of type 317L weld filler material surface, after 214 days of exposure to formic, acetic and propionic acids at an operating temperature of approximately 154 °C during the distillation of organic acids as indicated in column F of Table 4 and Table 5.

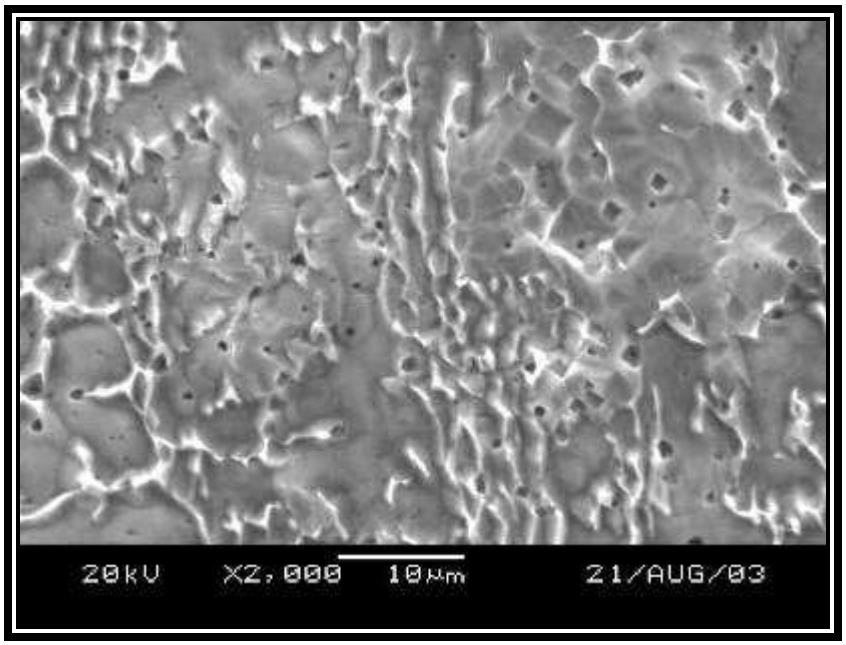

Figure 98: SEM photograph of type 309L weld filler material surface, after 214 days of exposure to formic, acetic and propionic acids at an operating temperature of approximately 154 °C during the distillation of organic acids as indicated in column F of Table 4 and Table 5.

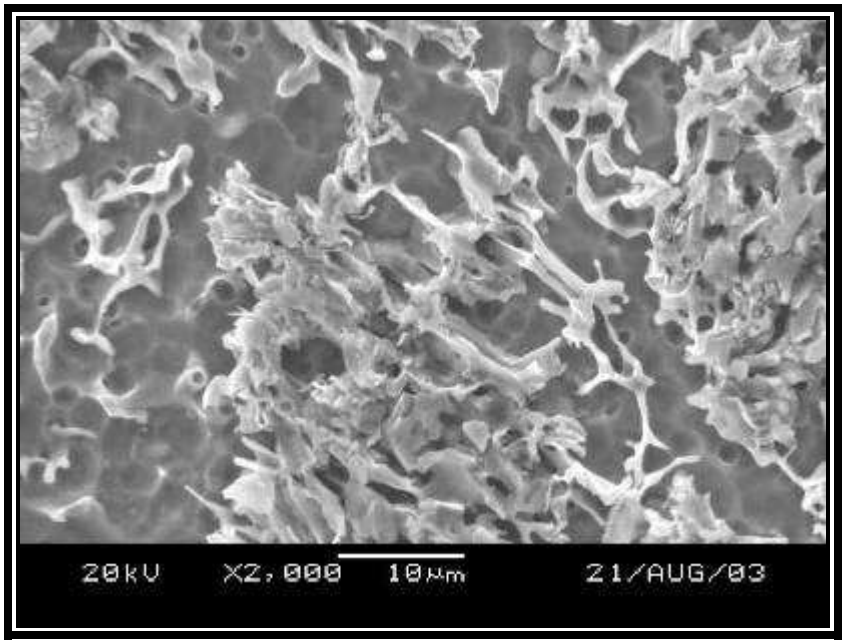

Figure 99: SEM photograph of type 309MoL weld filler material surface, after 214 days of exposure to formic, acetic and propionic acids at an operating temperature of approximately 154 °C during the distillation of organic acids as indicated in column F of Table 4 and Table 5.

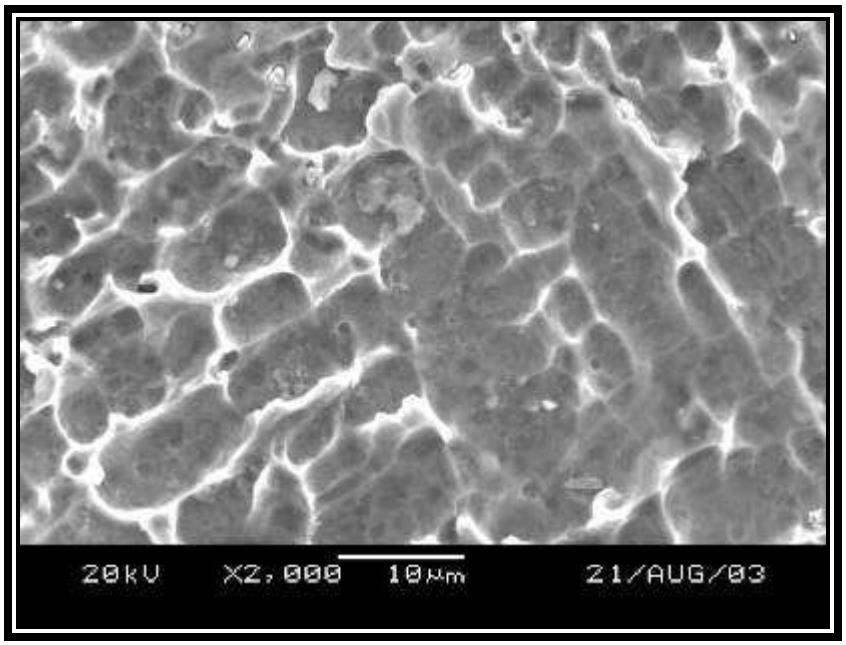

Figure 100: SEM photograph of type 904 weld filler material surface, after 214 days of exposure to formic, acetic and propionic acids at an operating temperature of approximately 154 °C during the distillation of organic acids as indicated in column F of Table 4 and Table 5.

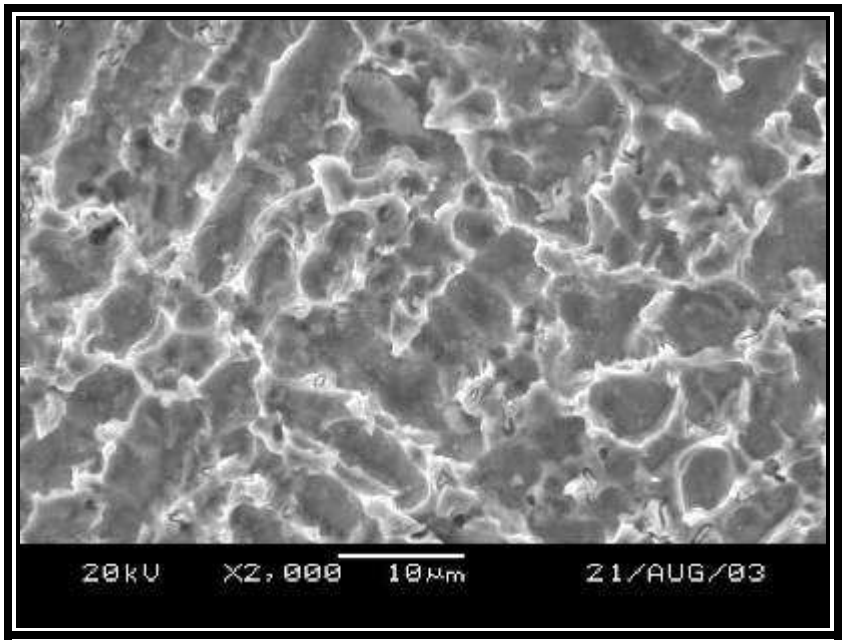

Figure 101: SEM photograph of type 625 weld filler material surface, after 214 days of exposure to formic, acetic and propionic acids at an operating temperature of approximately 154 °C during the distillation of organic acids as indicated in column F of Table 4 and Table 5.

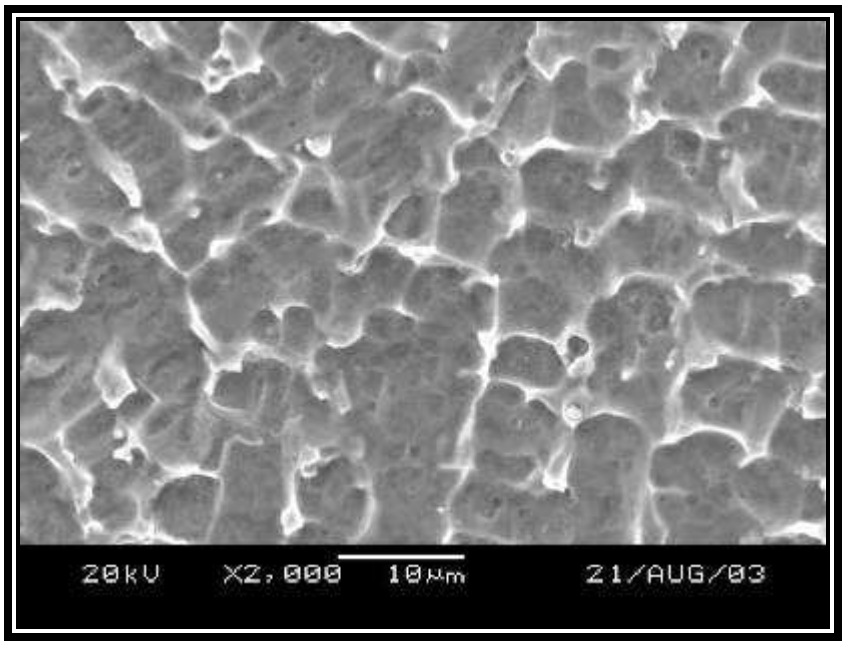

Figure 102: SEM photograph of type 825 weld filler material surface, after 214 days of exposure to formic, acetic and propionic acids at an operating temperature of approximately 154 °C during the distillation of organic acids as indicated in column F of Table 4 and Table 5.

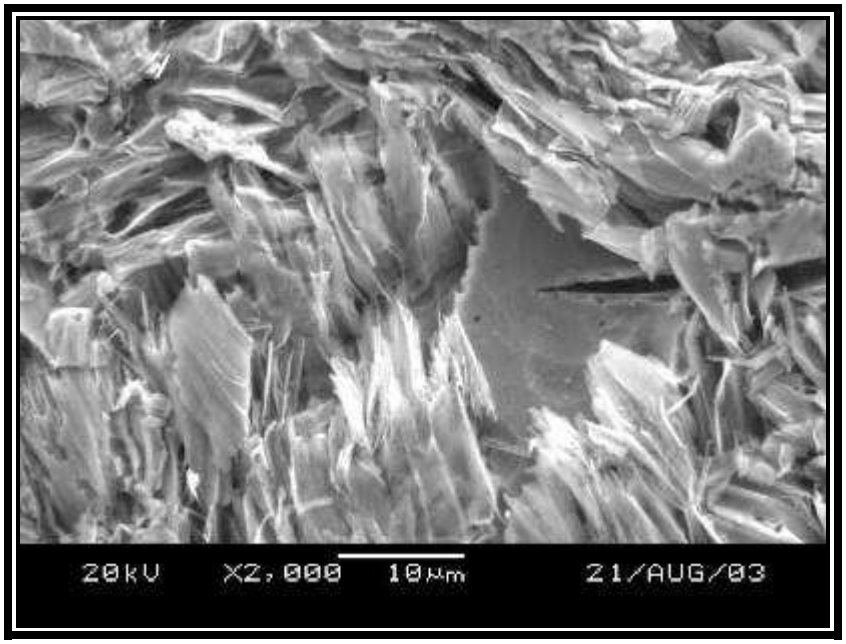

Figure 103: SEM photograph of type 2205 weld filler material surface, after 214 days of exposure to formic, acetic and propionic acids at an operating temperature of approximately 154 °C during the distillation of organic acids as indicated in column F of Table 4 and Table 5.

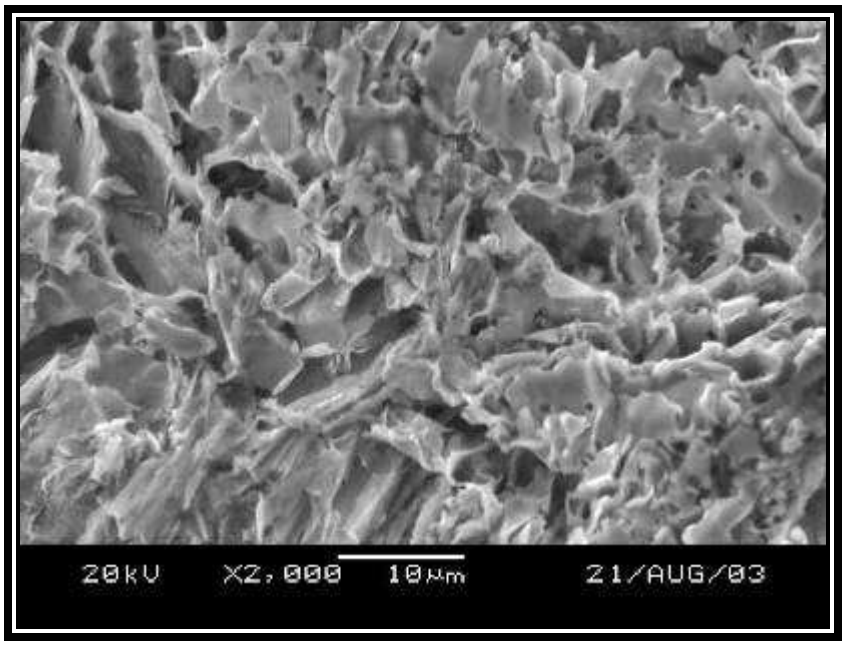

Figure 104: SEM photograph of type 2507 weld filler material surface, after 214 days of exposure to formic, acetic and propionic acids at an operating temperature of approximately 154 °C during the distillation of organic acids as indicated in column F of Table 4 and Table 5.

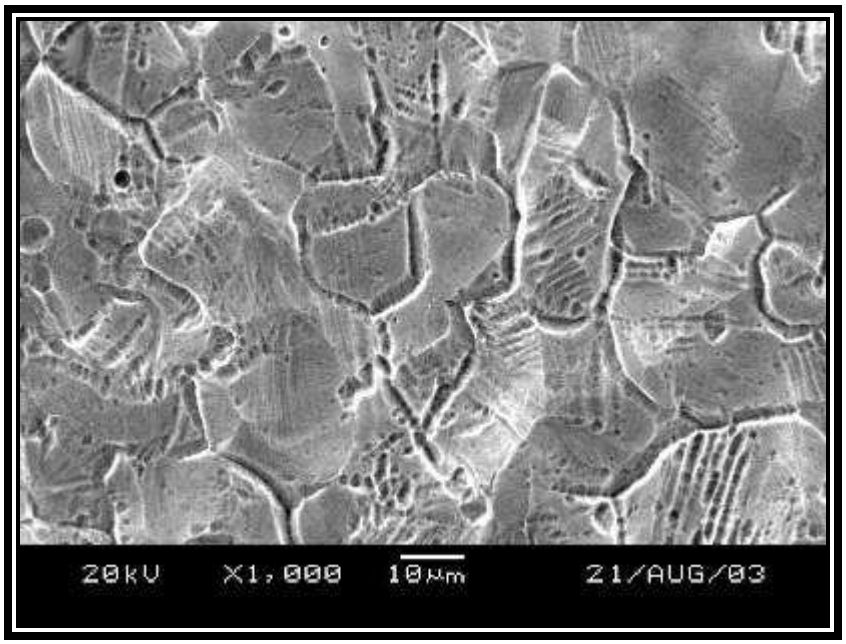

Figure 105: SEM photograph of type 316L plate material surface, after 214 days of to formic, acetic and propionic acids at an operating temperature of approximately 154 °C during the distillation of organic acids as indicated in column F of Table 4 and Table 5.

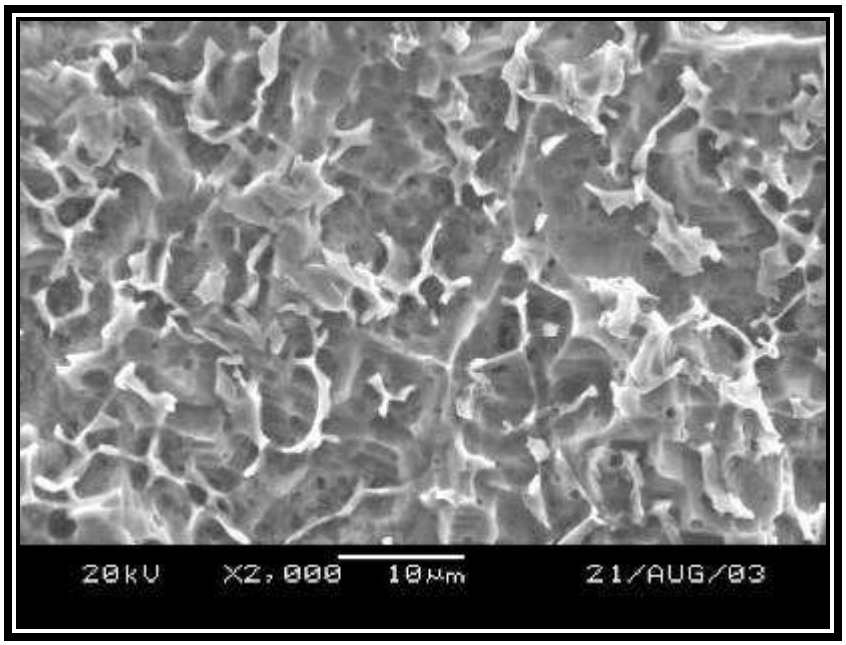

Figure 106: SEM photograph of type 316L weld filler material surface, after 214 days of exposure to formic and acetic acids at an operating temperature of approximately 111 °C during the distillation of organic acids as indicated in column G of Table 4 and Table 5.

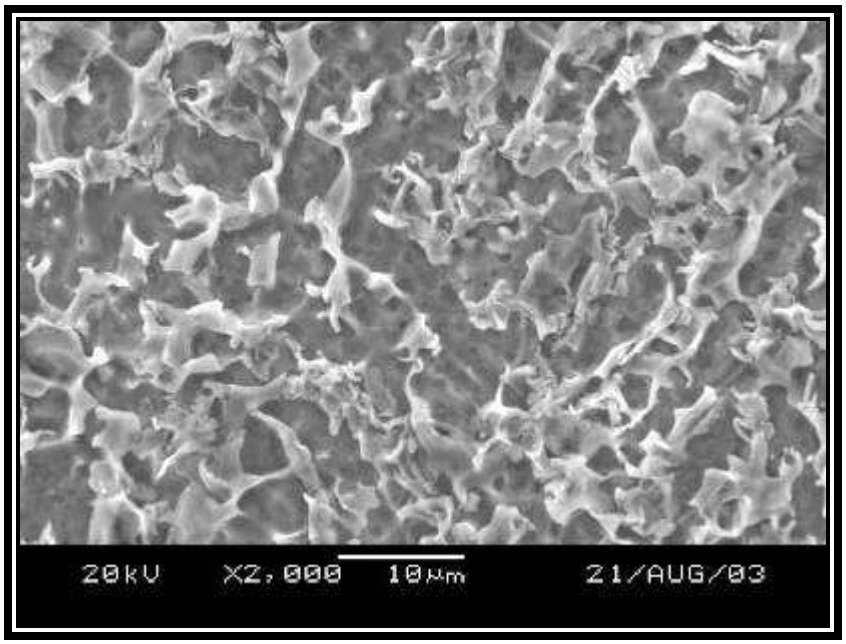

Figure 107: SEM photograph of type 317L weld filler material surface, after 214 days of exposure to formic and acetic acids at an operating temperature of approximately 111 °C during the distillation of organic acids as indicated in column G of Table 4 and Table 5.

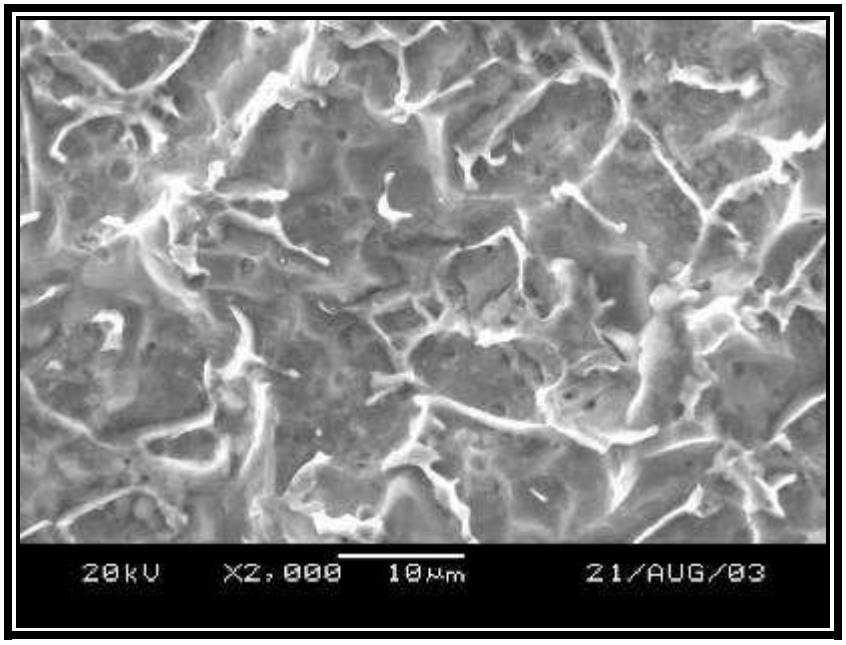

Figure 108: SEM photograph of type 309L weld filler material surface, after 214 days of exposure to formic and acetic acids at an operating temperature of approximately 111 °C during the distillation of organic acids as indicated in column G of Table 4 and Table 5.

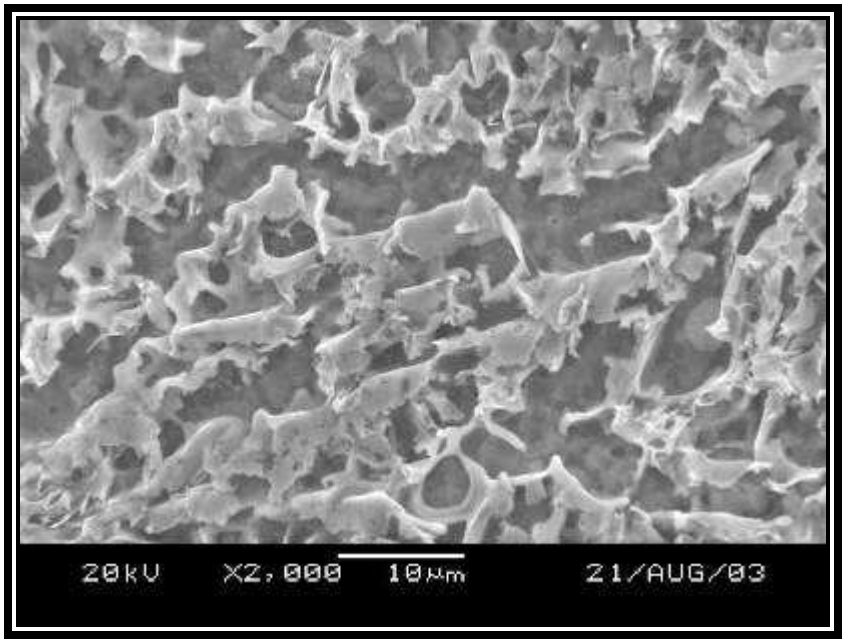

Figure 109: SEM photograph of type 309MoL weld filler material surface, after 214 days of exposure to formic and acetic acids at an operating temperature of approximately 111 °C during the distillation of organic acids as indicated in column G of Table 4 and Table 5.

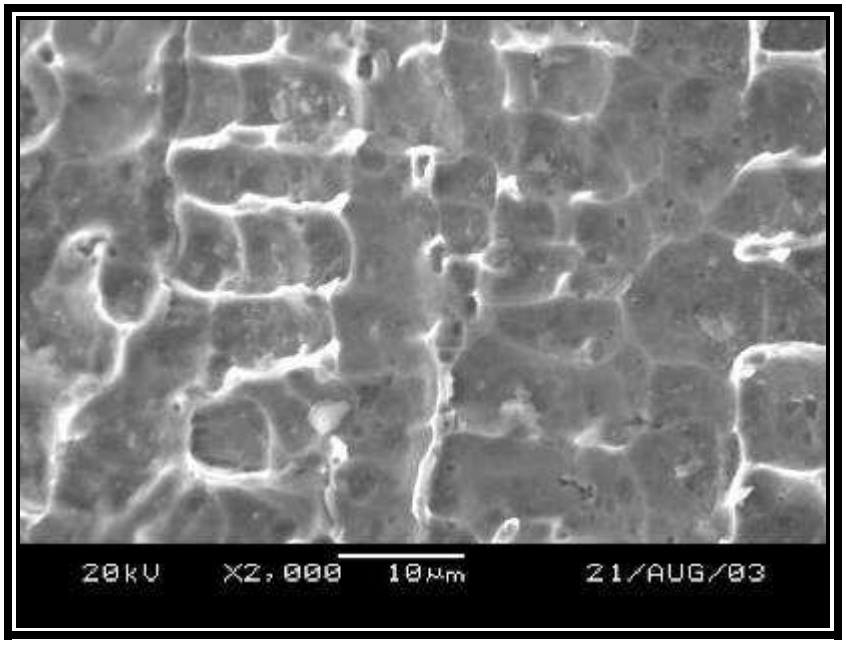

Figure 110: SEM photograph of type 904 weld filler material surface, after 214 days of exposure to formic and acetic acids at an operating temperature of approximately 111 °C during the distillation of organic acids as indicated in column G of Table 4 and Table 5.

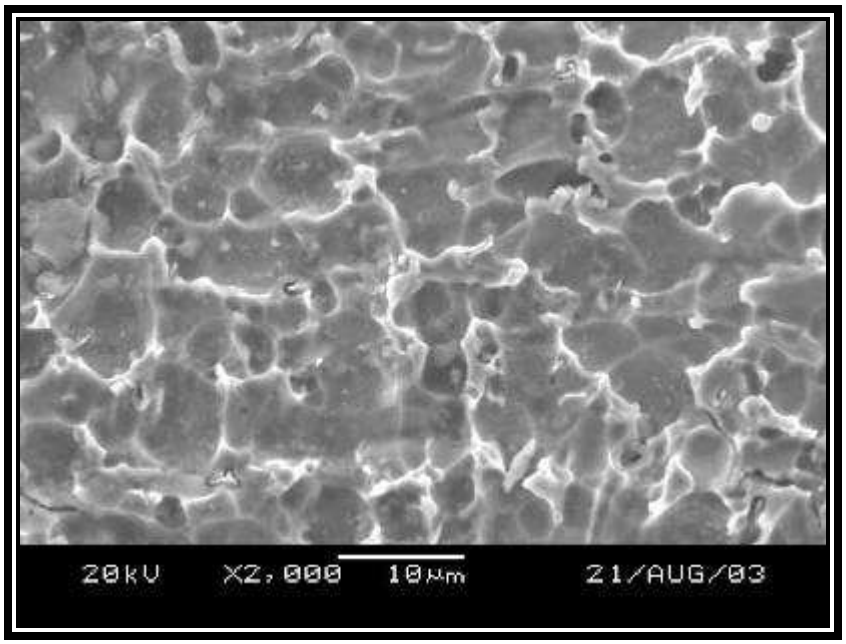

Figure 111: SEM photograph of type 625 weld filler material surface, after 214 days of exposure to formic and acetic acids at an operating temperature of approximately 111 °C during the distillation of organic acids as indicated in column G of Table 4 and Table 5.

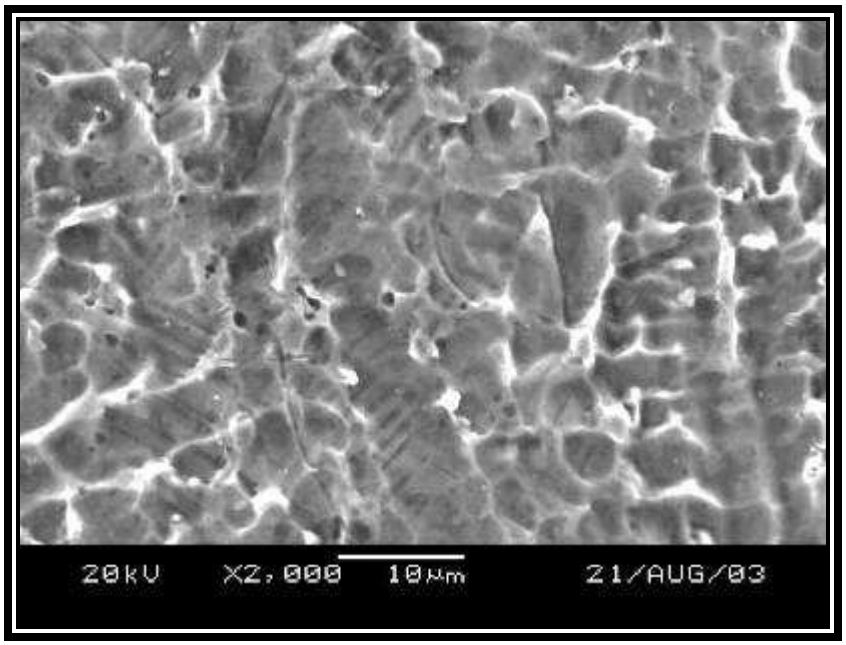

Figure 112: SEM photograph of type 825 weld filler material surface, after 214 days of exposure to formic and acetic acids at an operating temperature of approximately 111 °C during the distillation of organic acids as indicated in column G of Table 4 and Table 5.

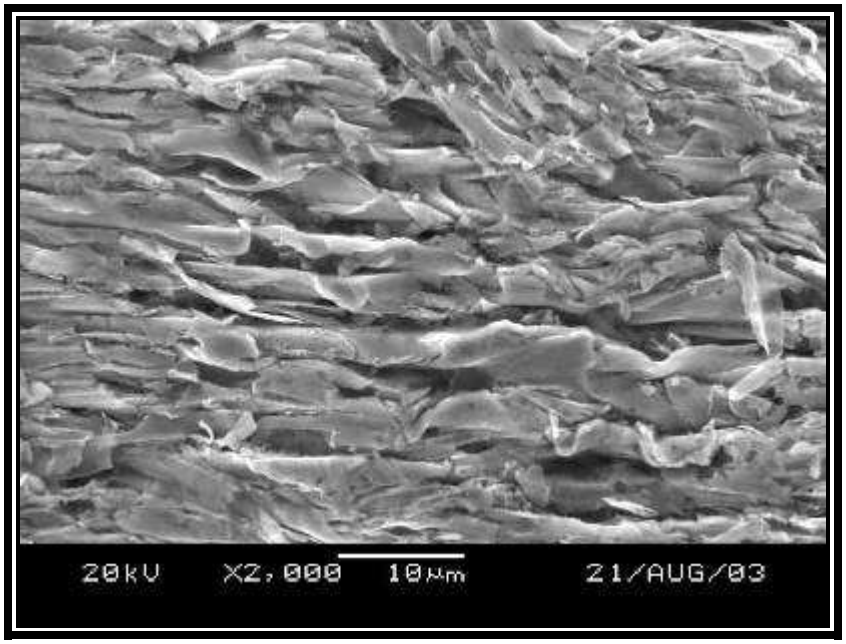

Figure 113: SEM photograph of type 2205 weld filler material surface, after 214 days of exposure to formic and acetic acids at an operating temperature of approximately 111 °C during the distillation of organic acids as indicated in column G of Table 4 and Table 5.

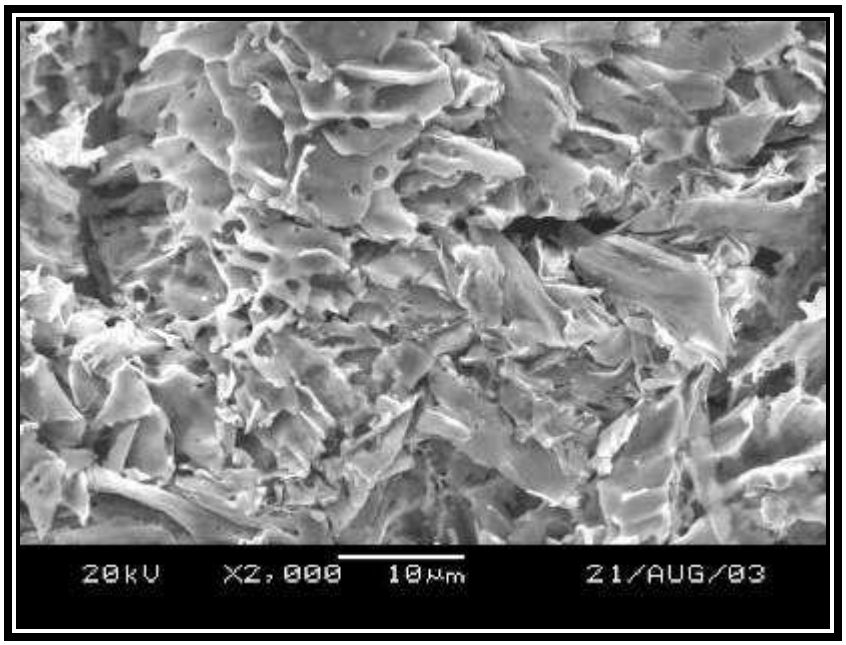

Figure 114: SEM photograph of type 2507 weld filler material surface, after 214 days of exposure to formic and acetic acids at an operating temperature of approximately 111 °C during the distillation of organic acids as indicated in column G of Table 4 and Table 5.

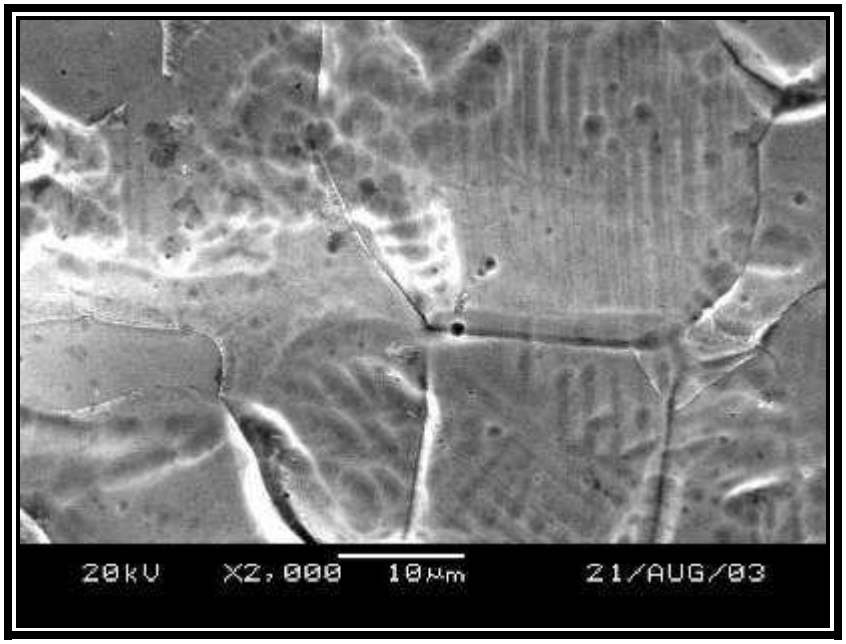

Figure 115: SEM photograph of type 316L plate material surface, after 214 days of exposure to formic and acetic acids at an operating temperature of approximately 111 °C during the distillation of organic acids as indicated in column G of Table 4 and Table 5.

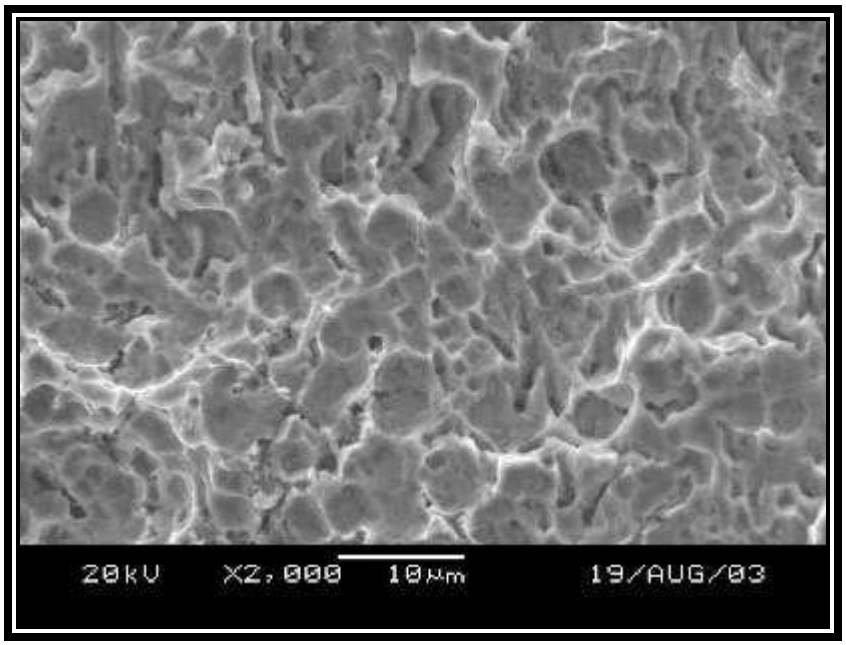

Figure 116: SEM photograph of type 316L weld filler material surface, after 214 days of exposure to formic and acetic acids at an operating temperature of approximately 130 °C during the distillation of organic acids as indicated in column H of Table 4 and Table 5.

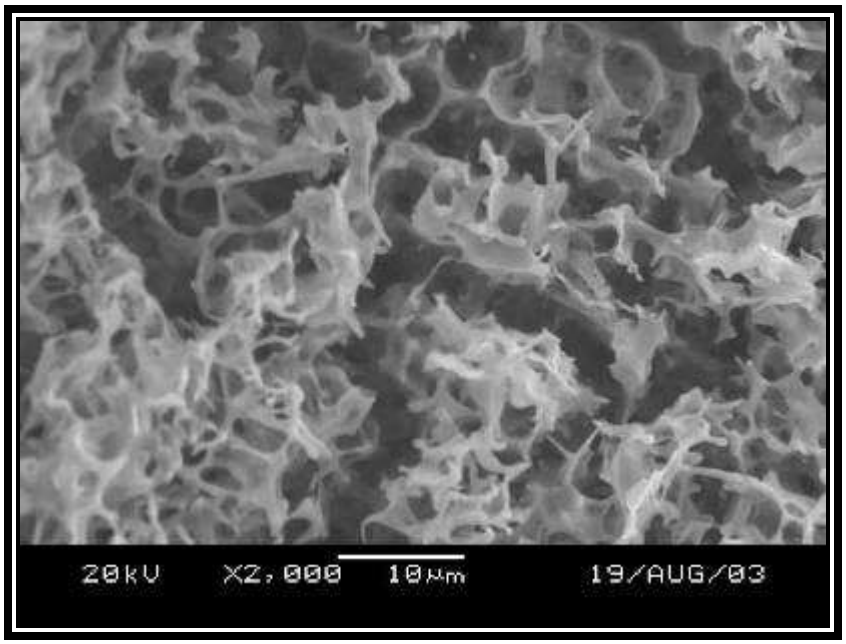

Figure 117: SEM photograph of type 317L weld filler material surface, after 214 days of exposure to formic and acetic acids at an operating temperature of approximately 130 °C during the distillation of organic acids as indicated in column H of Table 4 and Table 5.

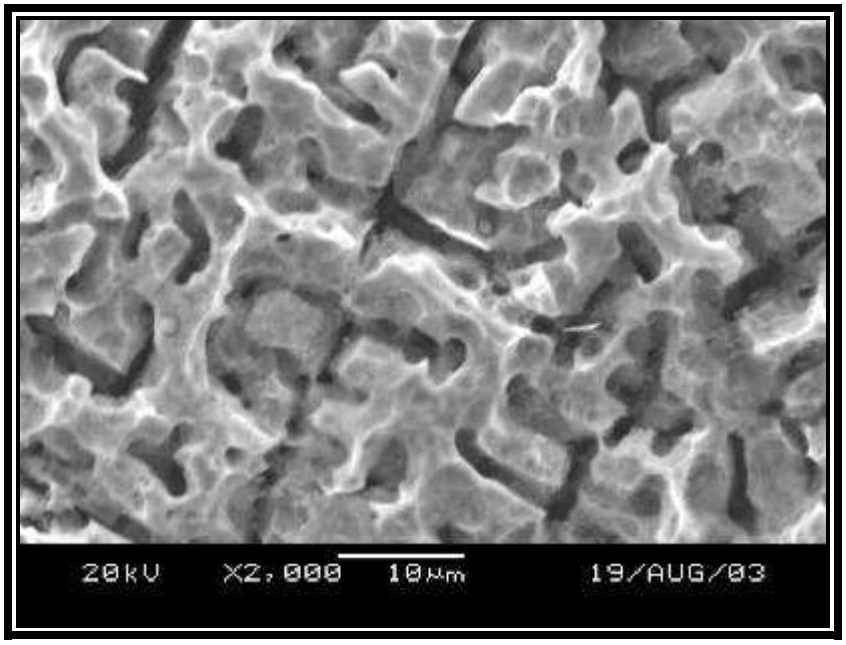

Figure 118: SEM photograph of type 309L weld filler material surface, after 214 days of exposure to formic and acetic acids at an operating temperature of approximately 130 °C during the distillation of organic acids as indicated in column H of Table 4 and Table 5.

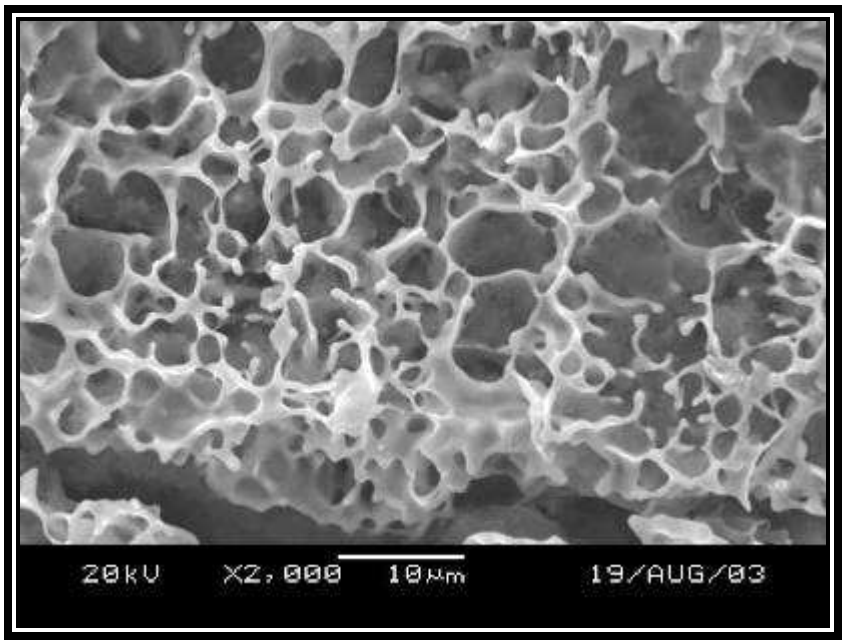

Figure 119: SEM photograph of type 309MoL weld filler material surface, after 214 days of exposure to formic and acetic acids at an operating temperature of approximately 130 °C during the distillation of organic acids as indicated in column H of Table 4 and Table 5.

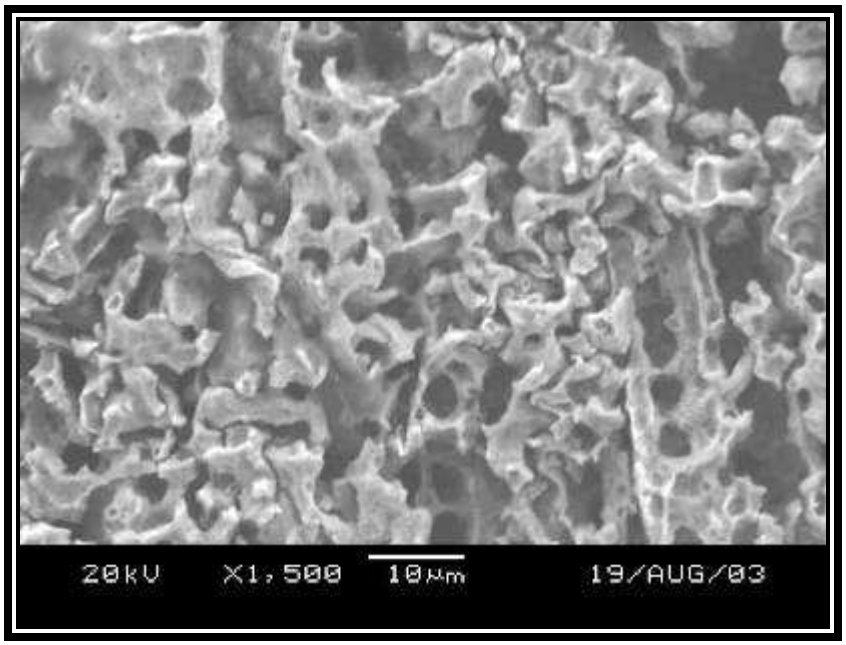

Figure 120: SEM photograph of type 904 weld filler material surface, after 214 days of exposure to formic and acetic acids at an operating temperature of approximately 130 °C during the distillation of organic acids as indicated in column H of Table 4 and Table 5.

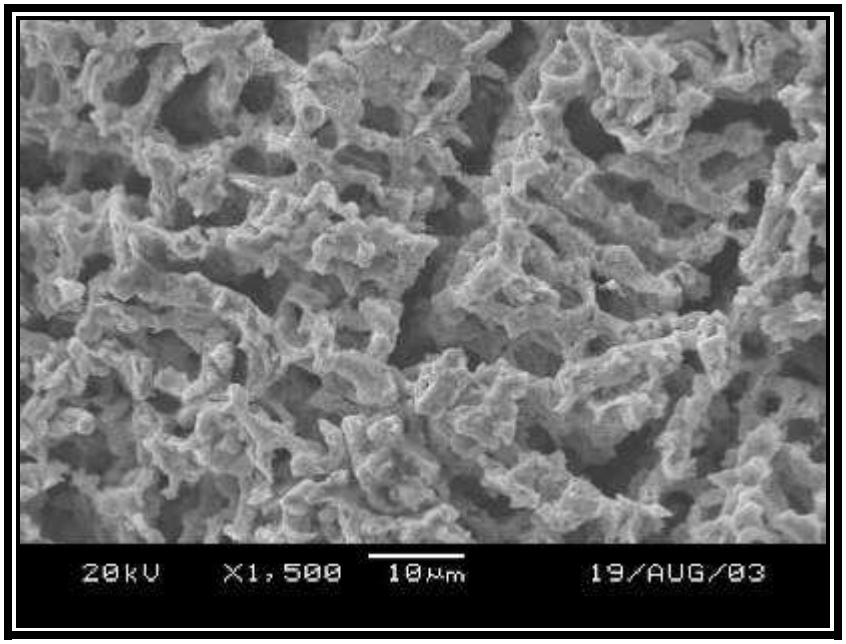

Figure 121: SEM photograph of type 625 weld filler material surface, after 214 days of exposure to formic and acetic acids at an operating temperature of approximately 130 °C during the distillation of organic acids as indicated in column H of Table 4 and Table 5.

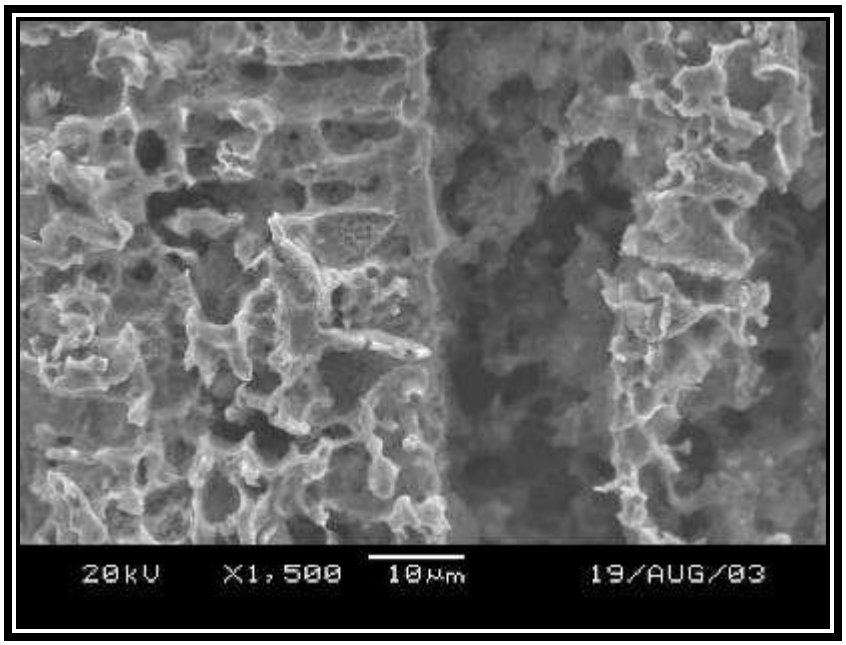

Figure 122: SEM photograph of type 825 weld filler material surface, after 214 days of exposure to formic and acetic acids at an operating temperature of approximately 130 °C during the distillation of organic acids as indicated in column H of Table 4 and Table 5.

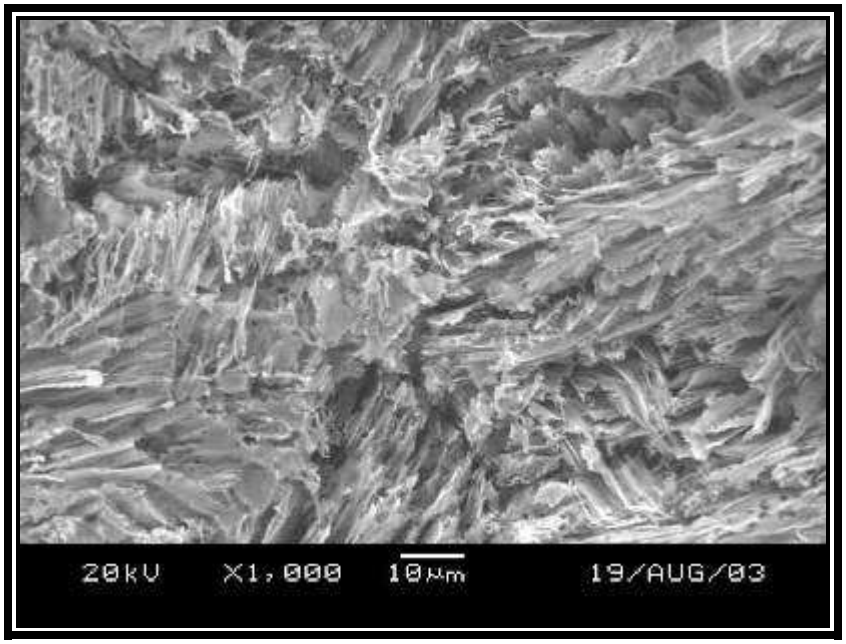

Figure 123: SEM photograph of type 2205 weld filler material surface, after 214 days of exposure to formic and acetic acids at an operating temperature of approximately 130 °C during the distillation of organic acids as indicated in column H of Table 4 and Table 5.

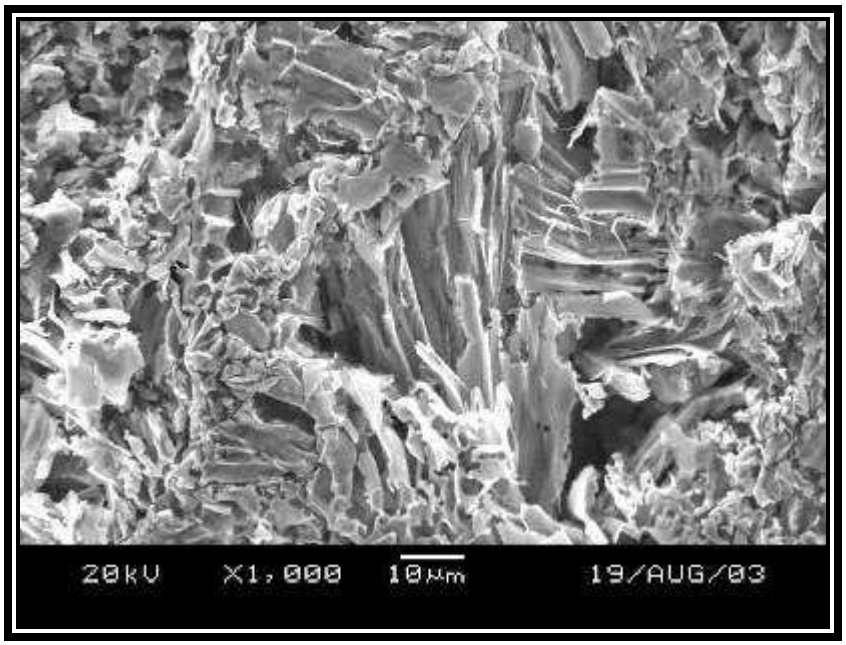

Figure 124: SEM photograph of type 2507 weld filler material surface, after 214 days of exposure to formic and acetic acids at an operating temperature of approximately 130 °C during the distillation of organic acids as indicated in column H of Table 4 and Table 5.

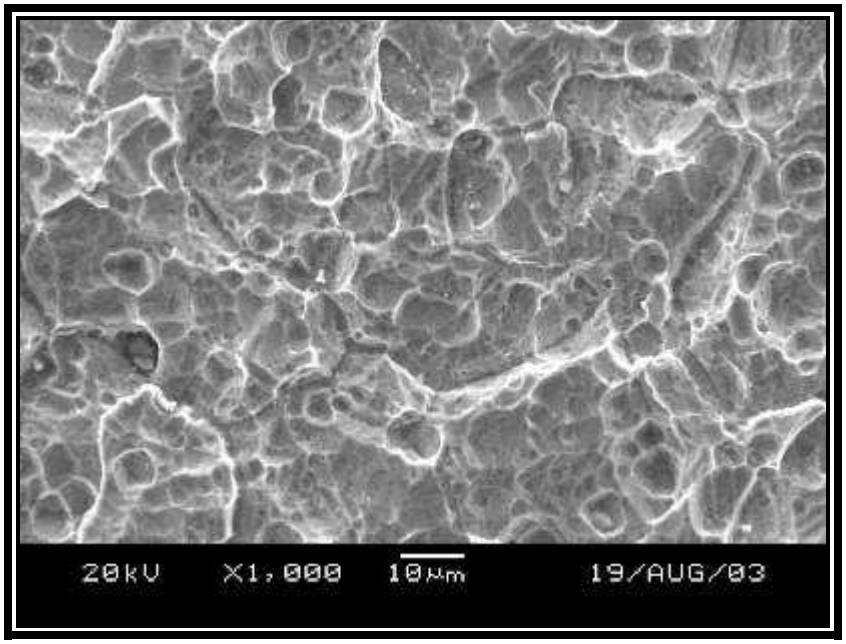

Figure 125: SEM photograph of type 316L plate material surface, after 214 days of exposure to formic and acetic acids at an operating temperature of approximately 130 °C during the distillation of organic acids as indicated in column H of Table 4 and Table 5.

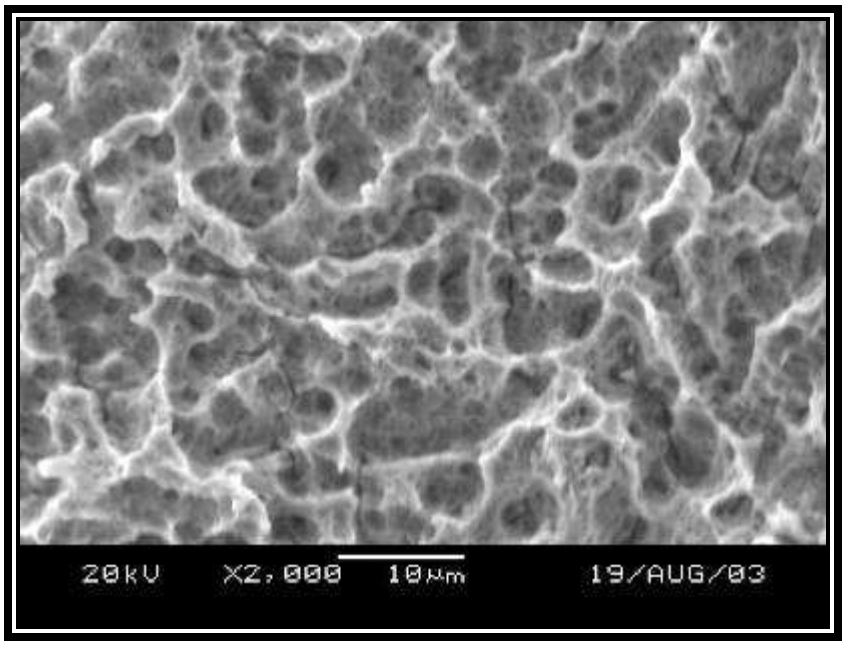

Figure 126: SEM photograph of type 316L weld filler material surface, after 214 days of exposure to formic and acetic acids at an operating temperature of approximately 126°C during the distillation of organic acids as indicated in column I of Table 4 and Table 5.

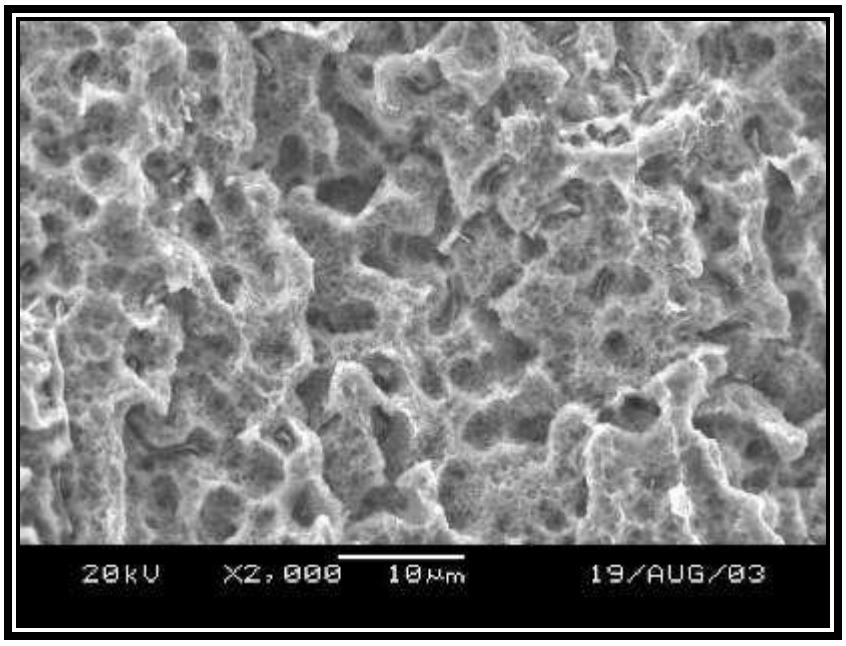

Figure 127: SEM photograph of type 317L weld filler material surface, after 214 days of exposure to formic and acetic acids at an operating temperature of approximately 126°C during the distillation of organic acids as indicated in column I of Table 4 and Table 5.

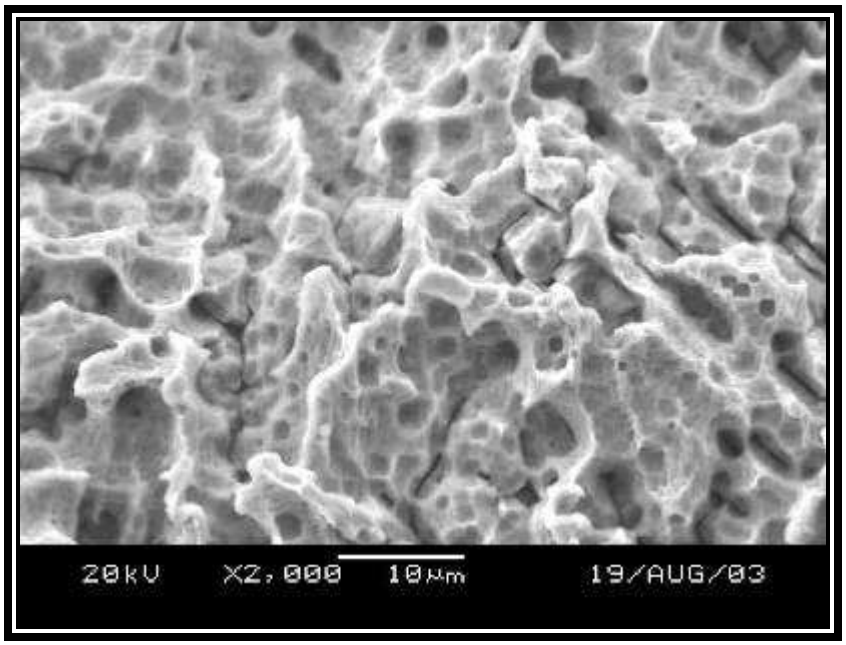

Figure 128: SEM photograph of type 309L weld filler material surface, after 214 days of exposure to formic and acetic acids at an operating temperature of approximately 126°C during the distillation of organic acids as indicated in column I of Table 4 and Table 5.

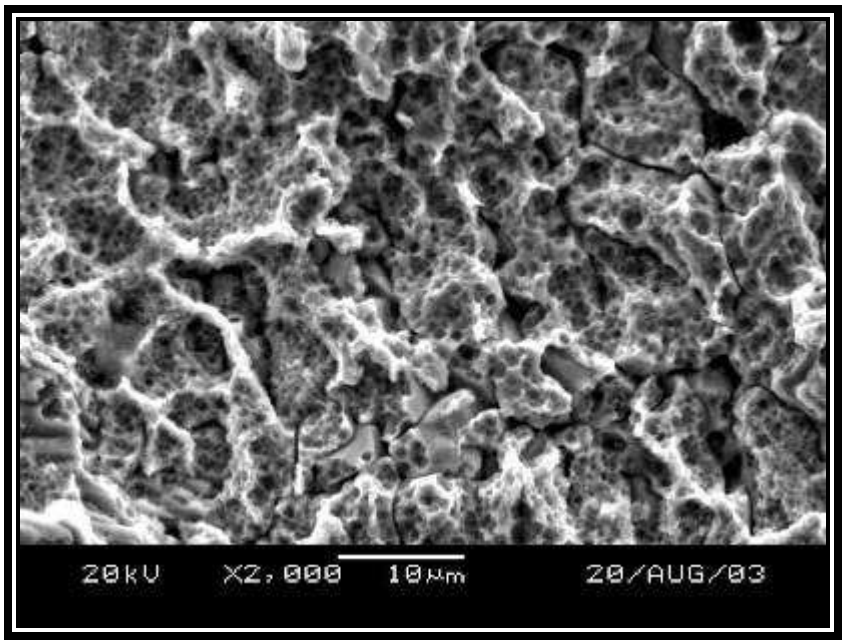

Figure 129: SEM photograph of type 309MoL weld filler material surface, after 214 days of exposure to formic and acetic acids at an operating temperature of approximately 126°C during the distillation of organic acids as indicated in column I of Table 4 and Table 5.

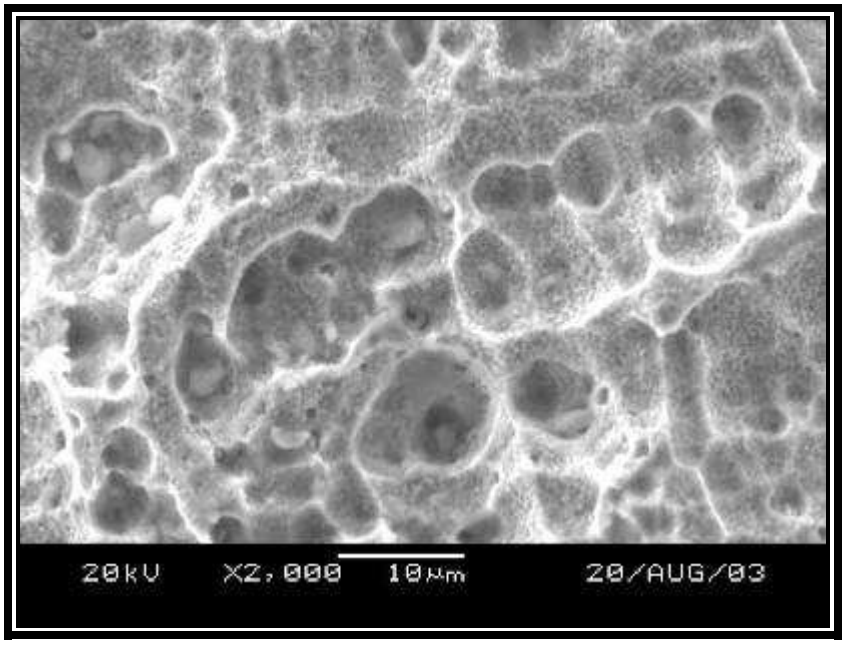

Figure 130: SEM photograph of type 904 weld filler material surface, after 214 days of exposure to formic and acetic acids at an operating temperature of approximately 126°C during the distillation of organic acids as indicated in column I of Table 4 and Table 5.

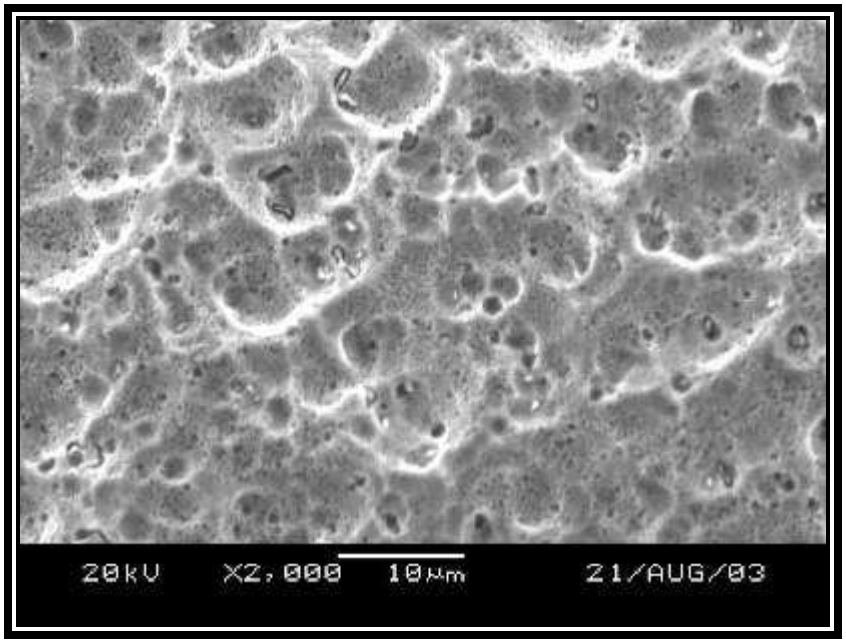

Figure 131: SEM photograph of type 625 weld filler material surface, after 214 days of exposure to formic and acetic acids at an operating temperature of approximately 126°C during the distillation of organic acids as indicated in column I of Table 4 and Table 5.

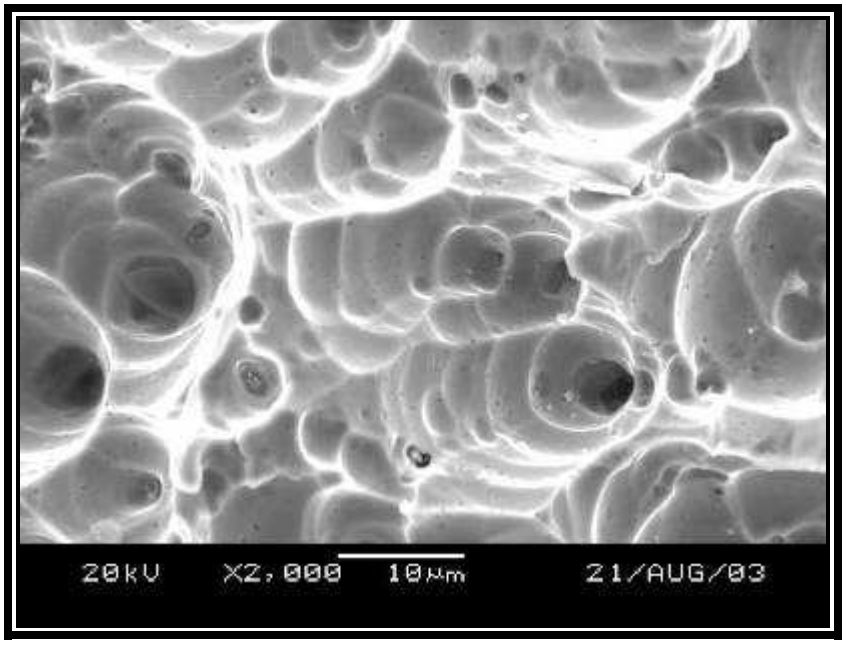

Figure 132: SEM photograph of type 825 weld filler material surface, after 214 days of exposure to formic and acetic acids at an operating temperature of approximately 126°C during the distillation of organic acids as indicated in column I of Table 4 and Table 5.

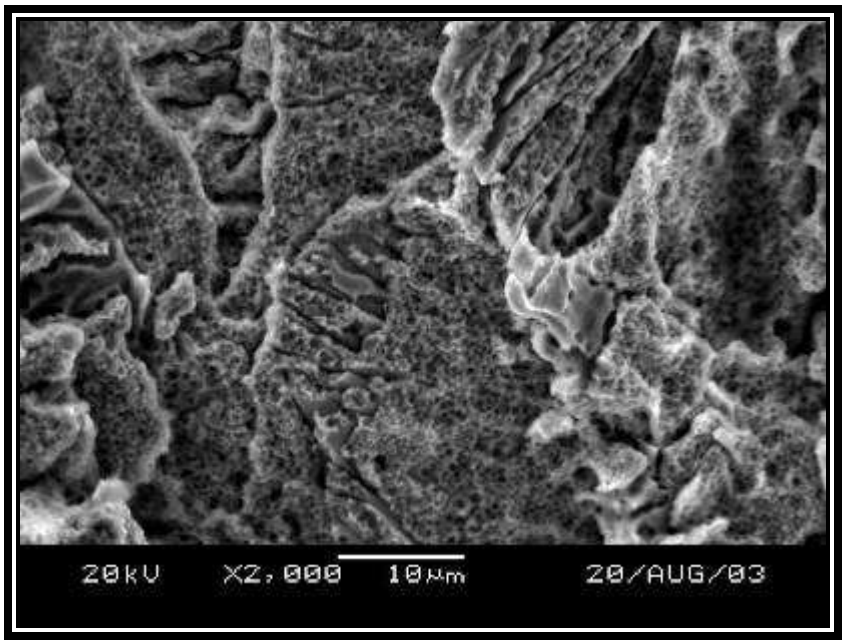

Figure 133: SEM photograph of type 2205 weld filler material surface, after 214 days of exposure to formic and acetic acids at an operating temperature of approximately 126°C during the distillation of organic acids as indicated in column I of Table 4 and Table 5.

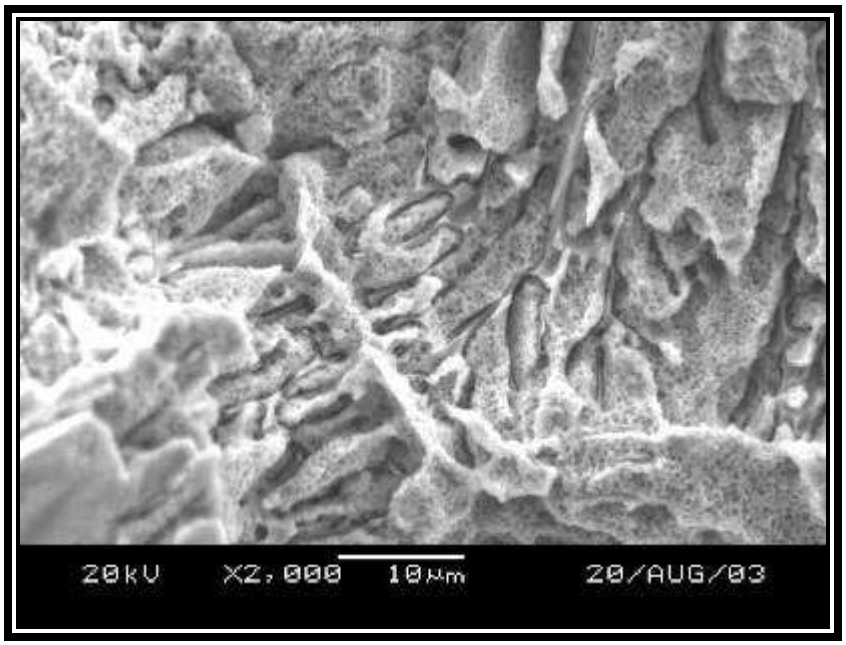

Figure 134: SEM photograph of type 2507 weld filler material surface, after 214 days of exposure to formic and acetic acids at an operating temperature of approximately 126°C during the distillation of organic acids as indicated in column I of Table 4 and Table 5.

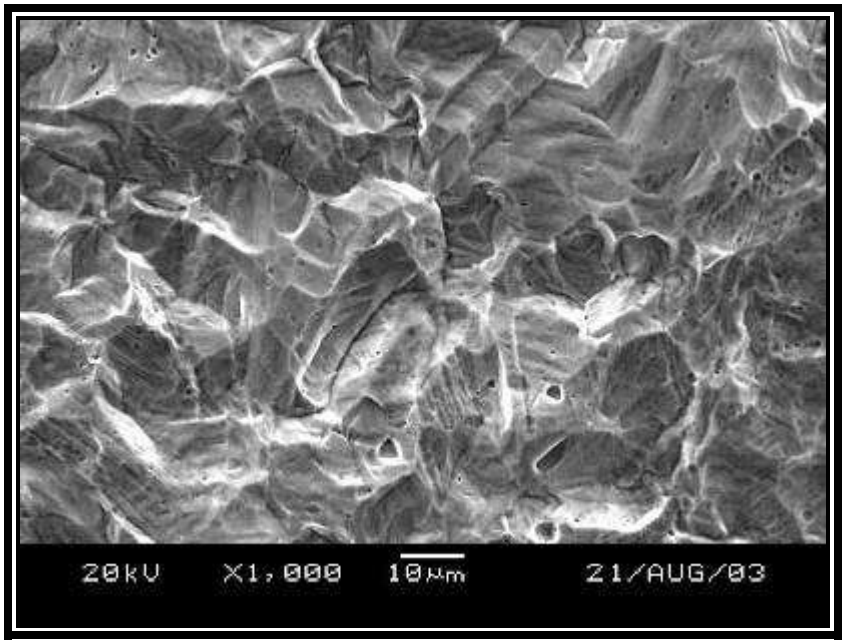

Figure 135: SEM photograph of type 316L plate material surface, after 214 days of exposure to formic and acetic acids at an operating temperature of approximately 126°C during the distillation of organic acids as indicated in column I of Table 4 and Table 5.

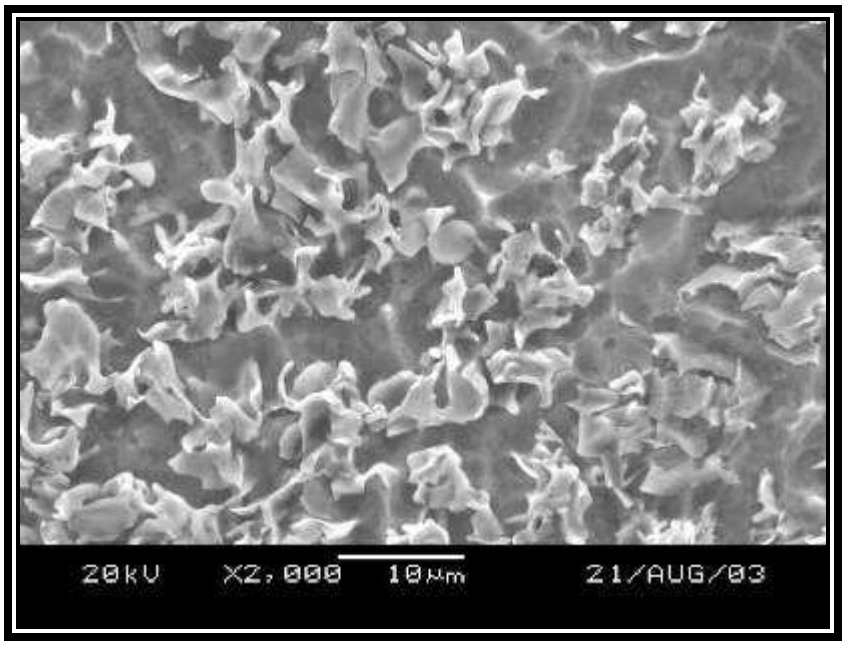

Figure 136: SEM photograph of type 316L weld filler material surface, after 214 days of exposure to formic and acetic acids at an operating temperature of approximately 86°C during the distillation of organic acids as indicated in column J of Table 4 and Table 5.

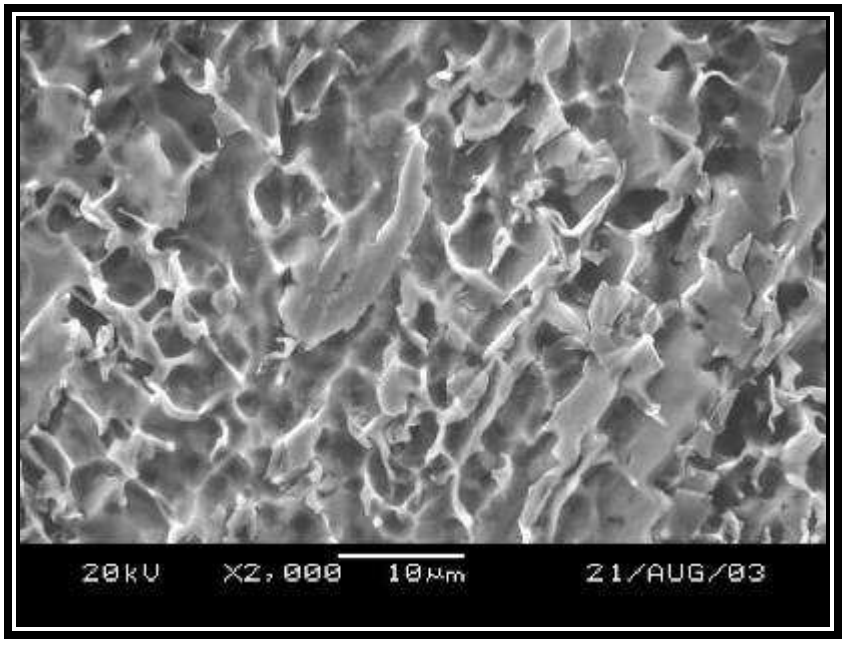

Figure 137: SEM photograph of type 317L weld filler material surface, after 214 days of exposure to formic and acetic acids at an operating temperature of approximately 86°C during the distillation of organic acids as indicated in column J of Table 4 and Table 5.

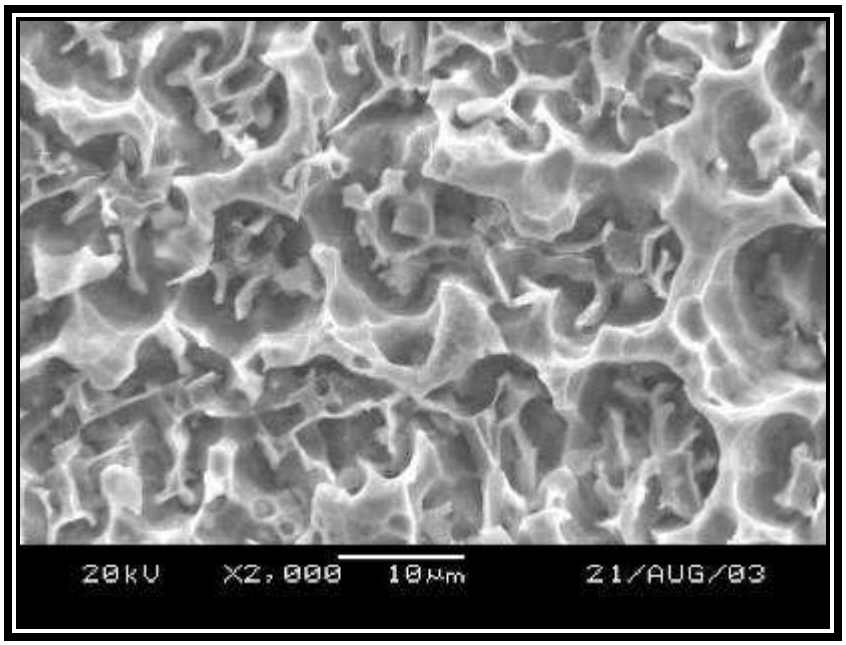

Figure 138: SEM photograph of type 309L weld filler material surface, after 214 days of exposure to formic and acetic acids at an operating temperature of approximately 86°C during the distillation of organic acids as indicated in column J of Table 4 and Table 5.

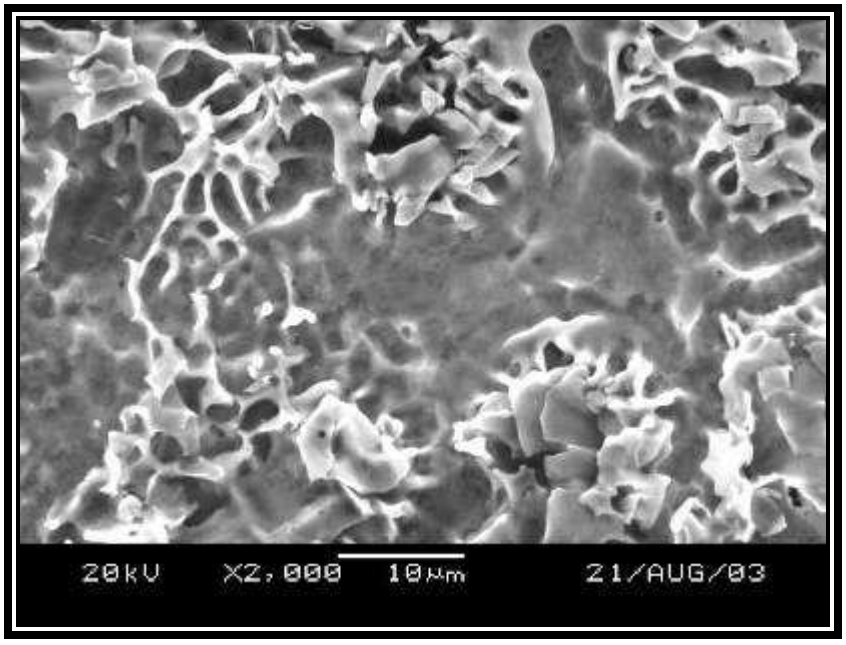

Figure 139: SEM photograph of type 309MoL weld filler material surface, after 214 days of exposure to formic and acetic acids at an operating temperature of approximately 86°C during the distillation of organic acids as indicated in column J of Table 4 and Table 5.

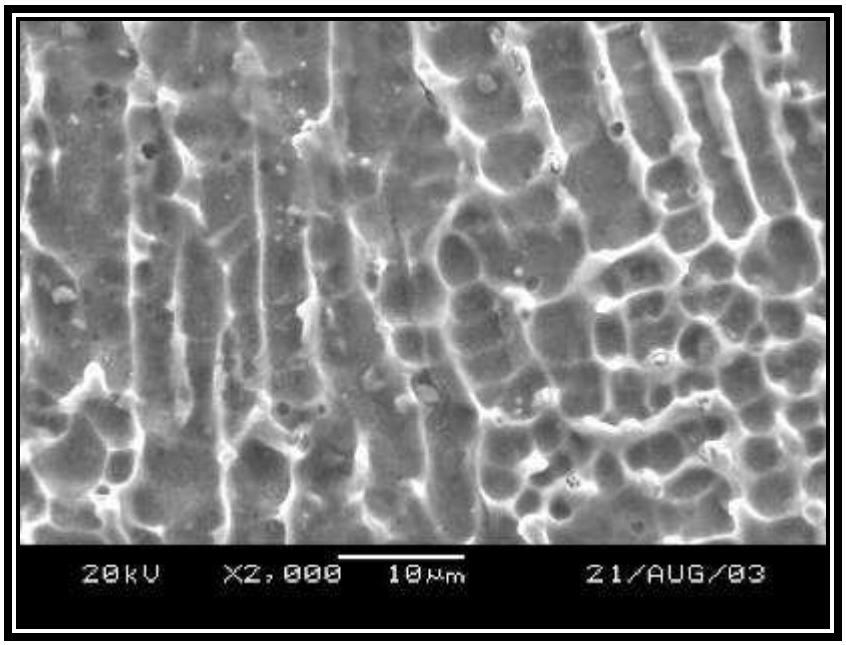

Figure 140: SEM photograph of type 904 weld filler material surface, after 214 days of exposure to formic and acetic acids at an operating temperature of approximately 86°C during the distillation of organic acids as indicated in column J of Table 4 and Table 5.

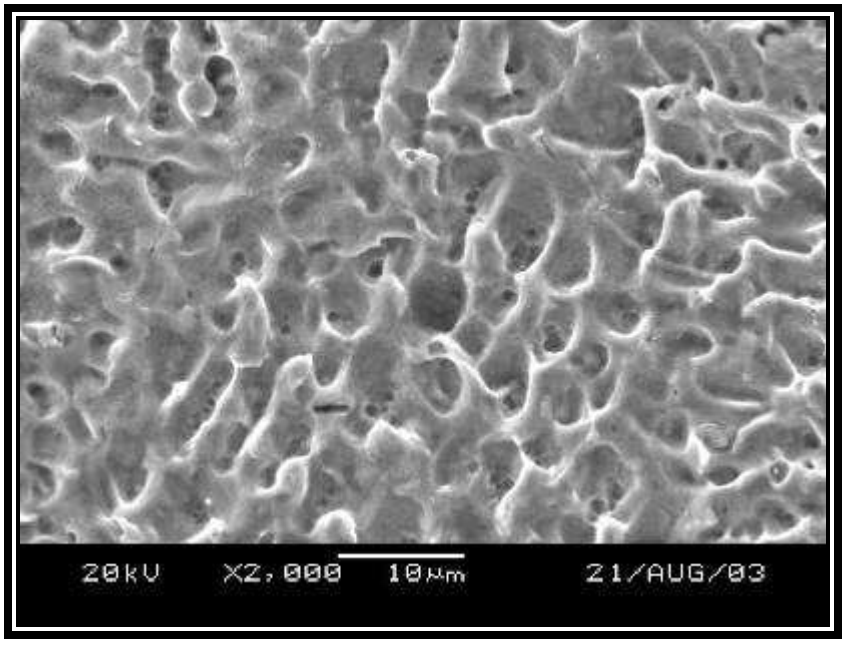

Figure 141: SEM photograph of type 625 weld filler material surface, after 214 days of exposure to formic and acetic acids at an operating temperature of approximately 86°C during the distillation of organic acids as indicated in column J of Table 4 and Table 5.

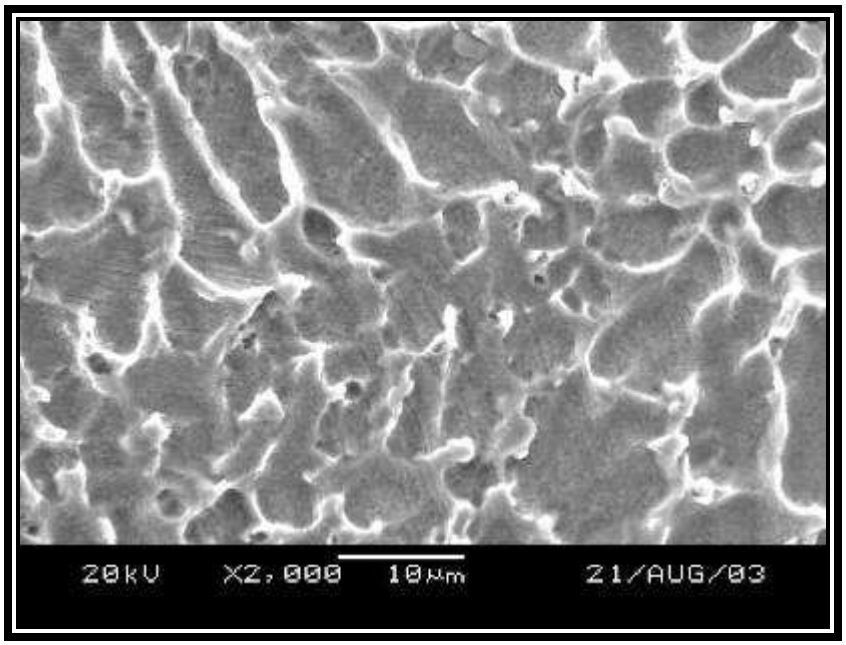

Figure 142: SEM photograph of type 825 weld filler material surface, after 214 days of exposure to formic and acetic acids at an operating temperature of approximately 86°C during the distillation of organic acids as indicated in column J of Table 4 and Table 5.

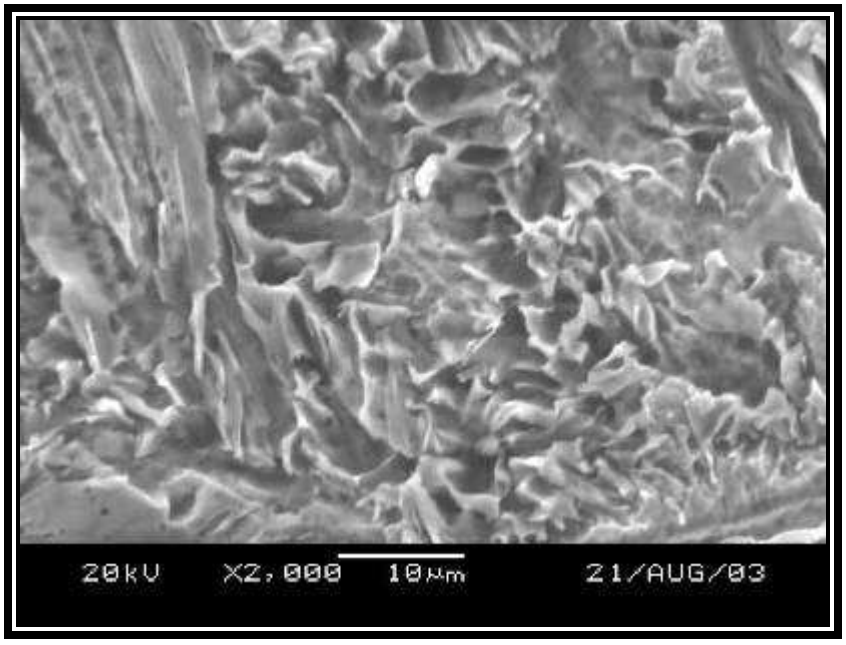

Figure 143: SEM photograph of type 2205 weld filler material surface, after 214 days of exposure to formic and acetic acids at an operating temperature of approximately 86°C during the distillation of organic acids as indicated in column J of Table 4 and Table 5.

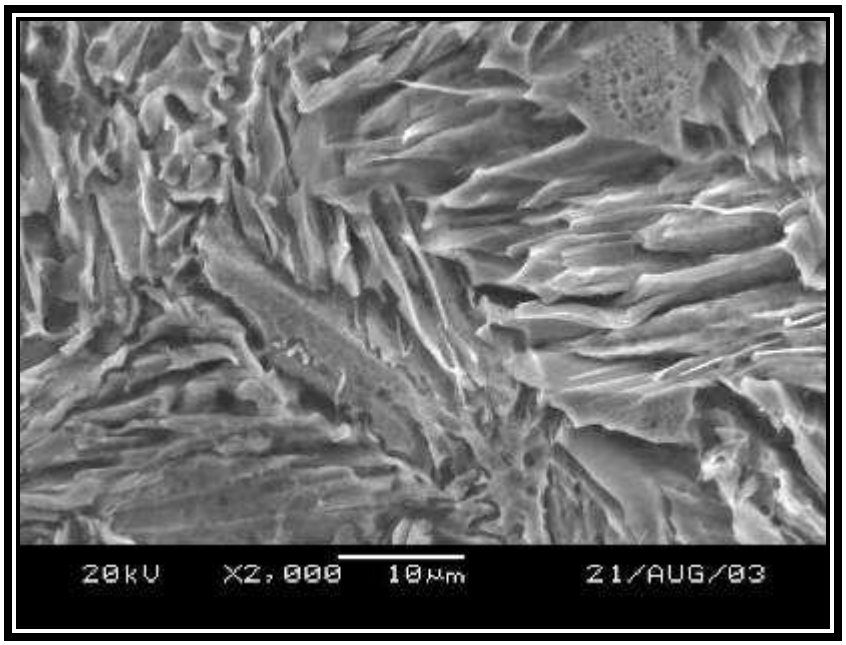

Figure 144: SEM photograph of type 2507 weld filler material surface, after 214 days of exposure to formic and acetic acids at an operating temperature of approximately 86°C during the distillation of organic acids as indicated in column J of Table 4 and Table 5.

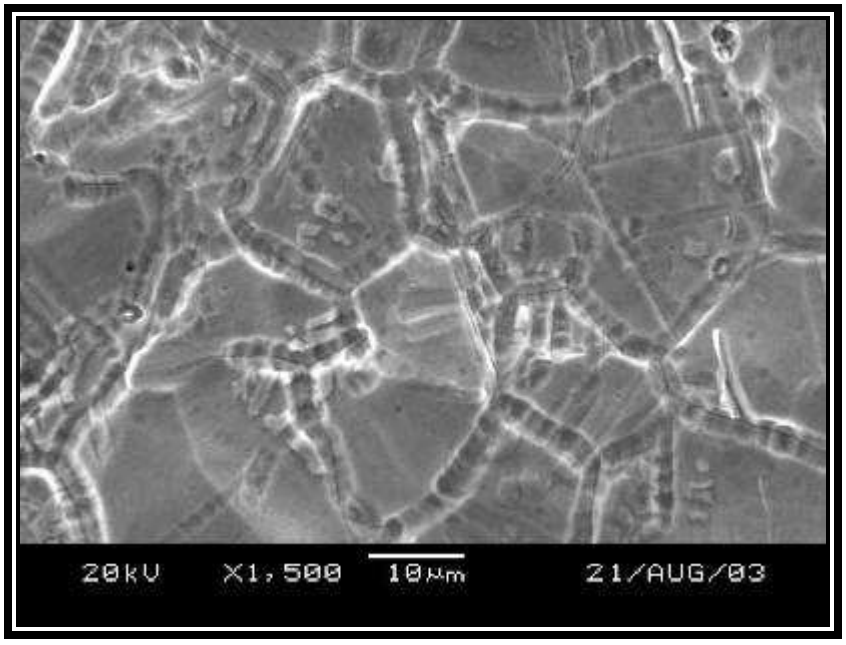

Figure 145: SEM photograph of type 316L plate material surface, after 214 days of exposure to formic and acetic acids at an operating temperature of approximately 86°C during the distillation of organic acids as indicated in column J of Table 4 and Table 5.

As indicated above in Figure 46 to Figure 145 severe corrosion of the less noble filler materials were noted. It was observed that under all the operating conditions the type 309L filler material corroded at a higher rate than the type 316L base material. Type 309L was the only filler material with a low Mo concentration which was tested. It would thus appear that a certain minimal concentration of Mo in the filler material is essential to provide corrosion resistance under these operating conditions. Type 309L filler material should follow the FA mode of solidification. Thus dendrite cores should be rich in ferrite forming elements such as Mo and Cr and the interdendritical cavities rich in austenite forming elements such as Ni, C and Mn. Under all the operating conditions the dendrite cores of the type 309L filler either corrode at the same rate than the rest of the weld material or corrode at an accelerated rate compared to the rest of the weld filler material. It would thus appear that the slight increase in the Cr concentration of the type 309L filler material compared to the lower Cr concentration of the type 316L base material did not compensate for the lower concentration in Mo of this filler material.

Opposite to the above, it would appear that the despite the (slight) increase in the Mo concentration of the type 317L filler material compared to the type 316L filler material and base material Type 317L filler material corroded at similar rates as the type 316L filler materials. The increase in the Mo concentration to the dendrite cores also did not have significant influence in the corrosion resistance of the cores compared to the interdendritical cavities of this filler material.

Increased Cr concentration with similar Mo concentrations compared to the type 316L filler material in the type 309MoL did also not show significant improvement in the corrosion resistance of this filler material. In most of the tested operating conditions,

except conditions E, F and J, did the filler material corrode at a higher rate than the base material.

Corrosion results from the two duplex filler materials, type 2205 and 2507 filler materials, were more variable. Under some of the operating conditions these fillers provided superior corrosion resistance to the operating media than the type 316L base and filler material, but in some cases not. In most of the cases the increased Cr, Mo and Ni concentration of the type 2507 filler material (compared to the 2205 filler material) provided increased corrosion resistance to the operating media.

In all the instances where the type 825 and type 904L filler materials were exposed to the operating conditions pitting of the weld metal was noticed (see Figure 146). The size and the distribution of pits were not constant and varied with exposure condition. However, as with the previous observations, a correlation between the operating medium composition, temperature and corrosion rate could not be established. TEM evaluation of the type 904L filler material did reveal the presence of precipitates within the austenite matrix. Figure 147 presents a TEM photomicrograph illustrating the nature of these precipitates. Using the EDS function of the TEM chemical analyses of these precipitates and 904L matrix next to the precipitates were performed. The analyses results indicated that the precipitates were significantly richer in Mo and Nb and to a small extent richer in Cr as graphically illustrated in Figure 148. The Fe concentration was however lower than the base material. These precipitates are believed to be Mo, Nb-carbides that acted as initiation sites for preferential corrosion resulting in the observed pitting. In most of the cases the type 904L filler material corroded at a lower rate than the type 316L base material.

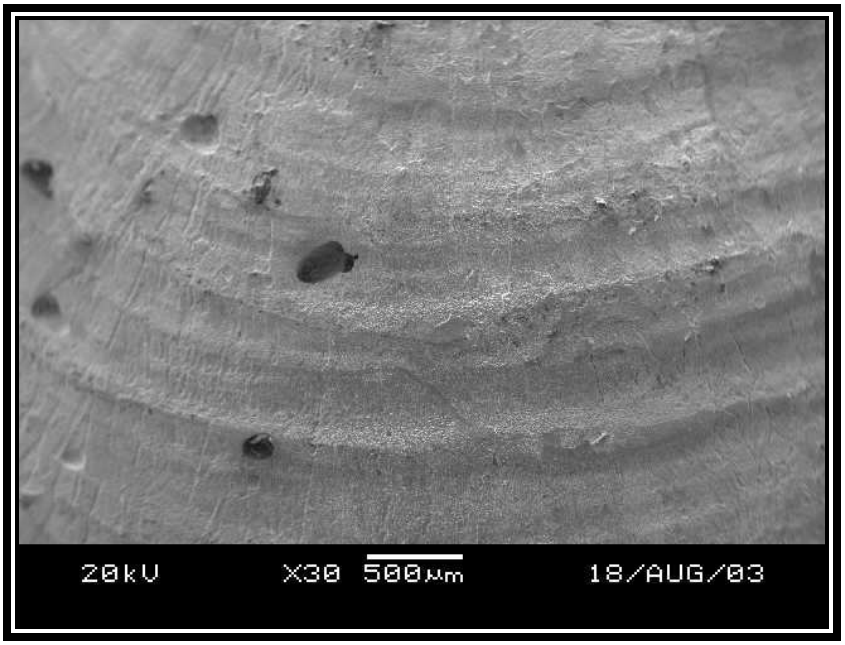

Figure 146: Typical pitting observed on the surfaces of the type 904L and 825 filler materials.

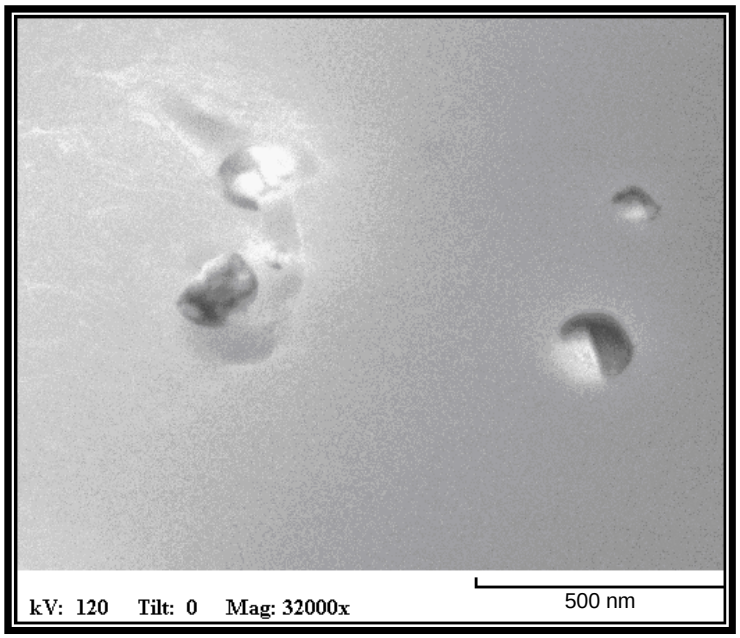

Figure 147: TEM photomicrograph indicating the nature of the precipitates that were observed inside the matrix of the type 904L filler material.

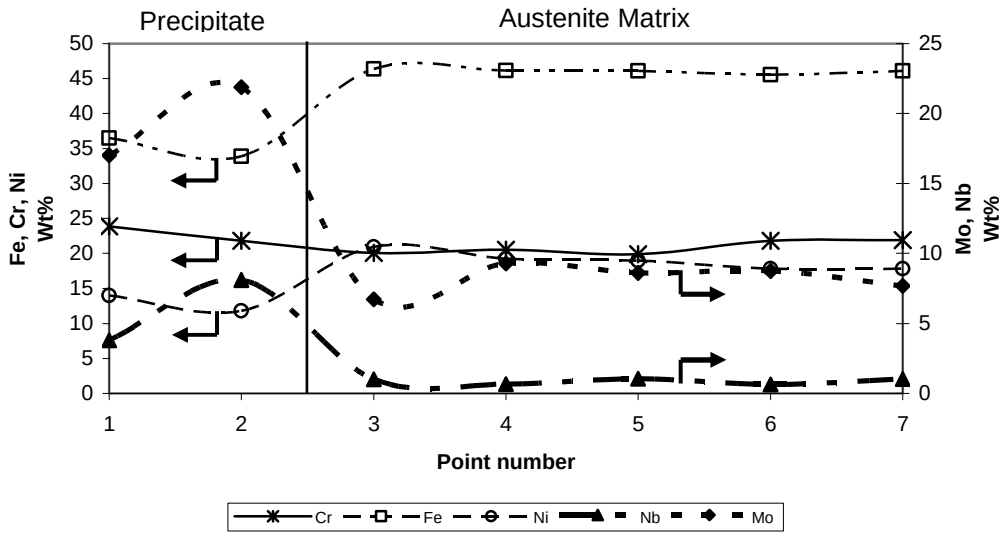

Figure 148: Graphical illustration of the TEM EDX analyses performed on the precipitates observed within the 904L filler material.

Type904L, 625 and 825 filler materials corroded at a lower rate than the type 316L base material. Examination of cross section of these weldments revealed no visual indications of galvanic corrosion in any weldments in these operating media with no preferential corrosion of the HAZ. Although corrosion of the type 625 filler did occur, the extent of this was much less than that of the base material. The nature of the corrosion (faster/slower at the dendrite cores/interdendritic regions) is discussed in more detail chapter 4. Types 625 and type 825 filler materials are expected to follow the A-type of solidification mode. Therefore dendrite cores should be richer in austenite stabling elements i.e. Ni, C, Mn than the interdendritic cavities. Colour etching did reveal that there are cathodic and anodic sites generated between the dendrite cores and the interdendritical cavities of the type 904L filler material. It was therefore expected that the corrosion of one of the two positions would be more significant than illustrated in Table 9.

In most cases, however, the corrosion rate of the dendrite cores was similar to that of the interdendritical cavities, indicating that the increase in the alloying elements within both of these positions were high enough to provide similar corrosion resistance between these positions within the matrix.

4. Discussion and conclusions

- Although all highly alloyed high nickel alloy filler materials (904L, 825 and 625) all corroded at lower rates than the base material, the 625 filler material was the filler material of choice due to the lack of any weld pitting, which was detected in both the 825 and 904L filler materials. The size and the distribution of pits were not constant and varied with exposure condition. In these filler materials, following the austenite mode of solidification, no significant concentration differences were detected within the matrix using the EDS facility of the TEM. In the case of 904L, however, it was possible to get an indication of the chemical composition of the precipitates noticed. These precipitates were rich in molybdenum and niobium and are believed to be molybdenum (Mo) and niobium (Nb) carbonitrides. Since these precipitates are rich in Mo the material adjacent to this precipitates may become depleted in Mo, resulting in selective corrosion of the area next to these precipitates, similar to intergranular corrosion in the case of sensitised materials. These presumably small-scale changes in chemical compositions were not conclusively identified with the EDS analyses during the TEM evaluation of these samples.
- In the case of the 825 filler material where both the quantities of Cr and Ni were significantly higher than the type 316L, 317L, 309MoL, 2205, 2507, but with comparable molybdenum concentrations to the type 317L, type 2205 and 2507 duplex filler materials, the type 825 filler material had significantly superior corrosion resistance to the operating environment than these filler materials. Type 825 filler material had even superior corrosion resistance to the type 316L base material. This suggests that a certain minimum concentration of chrome and nickel is required to improve the corrosion resistance of the filler material. However, available results do not allow any conclusion to be drawn on the individual and joint effects of molybdenum, chromium and nickel, beyond the general conclusion that the filler material needs to be quite highly alloyed to be resistant to these environments.
- In contrast with the conclusion that a substantial alloying content is required to improve corrosion resistance of the filler materials, the difference in composition between ferrite and austenite (and within phases, due to micro segregation) was

quite small, yet appeared to affect the corrosion attack. This is illustrated by the micrographs, which show corrosion to etch out the dendrite structure. The partitioning of alloying elements would be affected by the solidification mode. Types 316L, 317L, 309L and 309MoL fillers should follow the Ferrite-Austenite mode (FA mode) of solidification: $L \rightarrow [L+ \delta] \rightarrow [L + \delta + \gamma] \rightarrow [\delta + \gamma]$.

According to this, the dendrite cores (delta ferrite) of these filler materials should be rich in ferrite forming elements such as Cr and Mo where the interdendritic regions should be rich in austenite stabilising elements such as Ni, N. The semi-quantitative TEM analyses indicate a 4-6% compositional difference in chrome and nickel in the ferrite and austenite phases. The concentration of molybdenum did not differ that much, but were in the same order of magnitude as seen in the filler materials evaluated. It might be expected that the ferrite phase with higher molybdenum and chromium should be more resistant to the operating medium while the austenite should be less resistant. This was, however, not the case for the corrosion of type 309L filler material. In all the cases, except under conditions F, G and J, the ferrite phase was selectively corroded. It would thus appear that in this case the Ni enrichment of the austenite phase had a larger influence on the corrosion resistance of the austenite phase than the chrome enrichment had on the corrosion resistance of the ferrite phase. It would also appear that the lack of significant quantities of molybdenum proves to be very detrimental to the corrosion resistance of this filler material.

- The corrosion rates of type 316L filler material welds were estimated to be an order of magnitude higher than that of the base material. Evaluation of the welds performed on the coupons indicated that the corrosion rate of the plate material relative to the filler materials was not constant for different exposure conditions. This was specifically noticeable for the duplex filler materials where varying results in terms of preferential weld corrosion vs. preferential base material corrosion were noted. Thus, in certain instances the corrosion rate of the duplex filler material was higher than that of the type 316L base material and in other instances the corrosion rate of the type 316L base material was lower than that of the duplex filler materials. Analyses of the operational data in terms of operating temperature and acid concentrations did not reveal any obvious correlation between the differences in operating conditions that could explain the difference in the corrosion behaviour of the filler materials.

- In almost all the cases where the chemical composition of the filler material was comparable with that of the base material (type 309L, type 309MoL, type 316L, type 317L) the corrosion rates of the filler materials were higher than that of the base material. It appears that only under some conditions, i.e. conditions F for type 317L filler material and conditions E, F, and J for type 309MoL, was the Mo concentration high enough to provide similar corrosion resistance to the operating media than the type 316L base material.
- It appears that the major alloying elements that contribute to the corrosion resistance of stainless steels are nickel and molybdenum. Although not tested it is believed that a certain minimum quantity of chromium is also required to provide corrosion resistance to materials in hot organic acid environments as described above. Changes in the nitrogen concentration of the 309L filler material did not have a significant influence on the general corrosion resistance of this filler material, so differences in corrosion behaviour are probably not attributable to variations in nitrogen content. Type 309L and 309MoL also had significant higher Cr concentrations than the comparative 316L and 317L filler materials, but no definite conclusion can be reached on whether these changes in chrome concentration had significant influence on the general corrosion resistance of these filler materials.
- In the case of the duplex filler materials a ferrite mode of solidification is expected. All the liquid is expected to solidify as ferrite followed be a solid-state transformation of ferrite to austenite at lower temperatures. It is, therefore, expected that the ferrite cores will be higher in ferrite stabilising elements while interdendritic regions will be richer in austenite stabilising elements. It is also expected that these regions will be the initiation sites for austenite formation during subsequent cooling. From the TEM EDS analyses performed on the ferrite and austenite phases, it was not possible to detect a concentration difference within the ferrite and austenite phase itself. There were, however, significant differences in the concentration of elements between the ferrite and austenite, with the austenite stabilising elements reporting to the austenite phase and the ferrite stabilising elements reporting to the austenite phase. Since the morphology of the two phases is so similar, it could not be conclusively established which of the two phases was selectively corroded. Cross-sections of these filler materials did also not give any conclusive results. It was however

expected that ferrite, with its higher Mo value, would be more resistant to the operating medium than the austenite. But in some instances, ferrite seems to be selectively corroded, while at other positions, austenite seems to be selectively corroded.

- Experience with current production systems indicate that the corrosion rate of un-welded plate varies between 0.06 mm/y and 0.8mm/y depending on the temperature and organic acid concentration during the distillation process. No correlation between the corrosion rate and analysed chemical composition of the product and operating temperature could be established during the evaluation of this data. It is believed that the influence of unmeasured components, such as formic acid, could have a significant influence on the corrosion rate of the operating columns. At the time of the study it was still unclear how much formic acid can be present in the organic acid mixtures. This was due to the fact that the analysis method used to determine the relative acid concentrations did not distinguish between acetic acid and formic acid and both these acids were reported as acetic acid. Subsequent testing of these medium did indicate the presence of formic acid in the operating media. As indicated in paragraph 1.1, of all the carboxylic acids, formic acid is reported to be the most active and can influence the corrosion rate in is medium significantly. This might also explain the higher than expected corrosion rates of the type 316L materials under these operating conditions.
- In all the instances the corrosion rate of the highly alloyed type 625 filler material was lower than that of the type 316L base material. Galvanic corrosion was no noted at any of the weld/HAZ interfaces: in no case did the parent metal adjacent to the weld corrode preferentially to the material further away of the weld.

5. Reference:

1. G. Elsner, edited by D. Behrens, Dechema corrosion handbook, Volume 6 (1990), pp. 1-175.
2. B.D. Craig, D.B. Anderson. Handbook of corrosion data, ASM international (1997), pp. 88 -110.
3. A.J. Invernizzi, E. Sivieri, S.P. Trasatti, Corrosion behaviour of Duplex stainless steel in organic acid aqueous solutions, Materials science and Engineering, Volume 485 (June 2008), pp. 234-242.
4 . A. Turnbull, M. Ryan, A. Willetts, S. Zhou, Corrosion and electrochemical behaviour of 316L stainless steel in acetic acid solutions, Corrosion Science, vol. 45 (2003), pp.1051–1072
5. Schillmoller C.M., Selection and use of stainless steels and nickel bearing alloys in organic acids, Nickel development institute, NiDI technical series No 10 063 (June 1992), pp. 1-7.
6 . M. Sephton, P.C. Pistorius, Localized Corrosion of Carbon Steel Weldments, Corrosion, volume 56, number 12 (2000), pp. 1272-1279.
7. E. Otero, A. Pardo, M.V. Utrilla, F.J. Perez, C. Merino, The corrosion behaviour of AISI 304L and 316L stainless steels prepared by powder metallurgy in the presence of organic acids, Corrosion science, Vol. 39 No. 3 (1997), pp. 453-463.
8. E. Folkhard, G. Rabensteiner, E. Perteneder, H. Schabereiter, J. Tösch, Welding metallurgy of stainless steels, Springer (1988), pp. 1-279
9. O. Kubaschewski, Iron Binary phase diagrams. Berlin-Heidelburg-New York: Springer; Dusseldorf: Verslag Stahleisen m.b.H. (1982), pp. 152-156.
10 C. Grobler, Weldability studies on 12% and 14% chromium steels, PhD thesis. University of Pretoria, South Africa (1987).
11. H, Kohl, Austenitishe korrosionsbestandige Stahle mit hoher Festigkeit im losungsgegluhten Zustand. Huttenm. Mh. 113 (1968), pp. 377-388.
12. M. du Toit and P. C. Pistorius, Welding journal. Part 1, 82(8), pp. 219-s to 224-s and Part 2 (2003), pp 231-s to 237-s.
13. A. Gruszczyk, The kinetics of nitrogen absorption by arc-melted Fe-C-Mn-type filler metals, Welding journal, Vol. 83 (2004), pp. 94-s to 101-s.
14. A. Schaeffler, Constitution Diagram for Stainless Steel Weld Metal. Metals Progress 56 (1949), pp. 680-680B.
15. V. Shankar, T.P.S. Gill, S.L. Mannan, S, Sundaresan; Solidification cracking in austenitic stainless steel welds, Sadhana Vol. 28, Parts 3 & 4, (2003), pp. 359–382.
16. W.R. Oates, A.M. Saitta, AWS Welding handbook, eighth edition, Volume 4, part 2 (1998), pp. 233-314.
17. K. Rajasekhar; C.S. Harendranath; R. Raman, S.D. Kulkarni; Microstructural evolution during solidification of austenitic stainless steel welds: A colour metallographic and electron microprobe analysis study; Materials Characterization 38 (1997), pp. 53-65.
18. D.E. Nelson, W.A. Baeslack III; J.C. Lippold; Characterization of the weld structure in a duplex stainless steel using colour metallography. Materials Characterization 39 (1997), pp. 467-477.

19. P.I. Marshall; T.S. Gooch; Effect of composition on corrosion resistance of high-alloy austenitic stainless steel weld metals. Corrosion, Vol. 49(6) (1993), pp. 514-526.
20. S.J. Bullard, B.S. Covino Jr, Pitting corrosion of low chrome austenitic stainless steels, NACE corrosion conference 96, paper nr. 431 (1996), pp. 431/1-431/9.
21 . P. Kangas, M. Newman, Performance of duplex stainless steels in organic acids., Anti-Corrosion Methods and Materials, Volume 45, Number 4 (1998), pp. 233–242.
22. E. Schmidt-Rieder, M. Ashworth, J.P.G Farr; The effect of nitrogen on the stability of the passive film on a Zeron 100 super duplex stainless steel., Electrochemical and Solid-State Letters, 2(1) (1999), pp. 19-21.
23. V.S. Raja, S.K. Varshney, R. Raman, S.D. Kulkarni; Influence of Nitrogen on the pitting behaviour of 904 weld clad. Corrosion science, vol. 40 no. 10 (1998) pp. 1609 – 1625.
24. L. Weber, P.J. Uggowitzer; Partitioning of chromium and molybdenum in super duplex stainless steels with respect to nitrogen and nickel content. Material science and engineering, A242 (1998), pp. 222-229.
25 N.J. Zaluzec, Quantitative X-ray microanalysis. Introduction to Analytical Electron Microscopy, J.J. Hren, D.C. Joy, & J.I. Goldstein, (Eds.), pp. 121–167. New York: Plenum Press, 1979.
26. R.C. Newman, T, Shahrabi, The effect of alloyed nitrogen or dissolved nitrate ions on the anodic behaviour of austenitic stainless steel in hydrochloric acid; Corrosion Science 27(1987), pp. 827-838.